

## Chapter 5. Stage-1 Components

### 5.1 Magnets

#### 5.1.1 Introduction

The magnet system of the 20 TeV Stage-1 VLHC is the main component of the collider, and has a strong influence on the total cost of machine. The general design goal is to reduce the complexity and cost per Tesla-meter of the collider. The arcs of the Stage-1 VLHC are based on a 2-in-1 warm-iron, combined function gradient dipole magnet [1,2,3], excited by a single turn 100 kA superconducting transmission line. A cross-section of the magnet, including the cryogenic service line and return bus, is shown in Figure 5.1. The flux lines surrounding the transmission line are shaped by an iron yoke, and two gaps in the yoke provide the apertures for the two beams. The 20 TeV bending field is 1.966 T at the nominal current of 87.5 kA. The magnets have a field gradient of  $\pm 4.73$  %/cm which provides focusing and eliminates the need for separate quadrupoles. The 135.5-m long half-cell is made of two 65.75-m long gradient magnets.

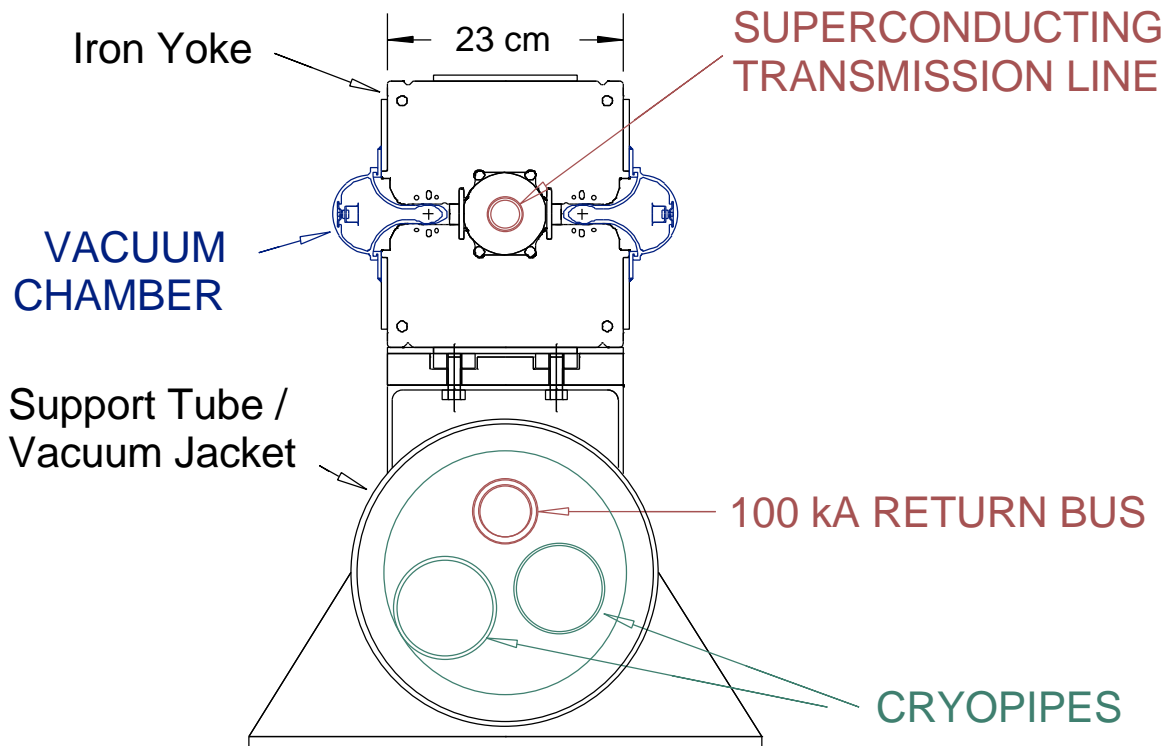


Figure 5.1. Cross-section of the gradient dipole magnet used in the arcs and dispersion suppressor of the Stage-1 VLHC.

At the end of each half-cell, where the beta function is at a maximum in one plane and a minimum in the other, a 3.5-m long space is left open for correction magnets. The transmission line is diverted into the cryogenic service pipe, near the return bus, allowing the use of conventional, room temperature, air cooled iron corrector magnets, as shown in Figure 5.2. Three correctors are installed at each location: a vertically or horizontally steering dipole, a quadrupole and a sextupole. The strength of these correctors is sufficient to accommodate alignment errors, ground motion, and iron saturation effects at full field (Section 3.2).

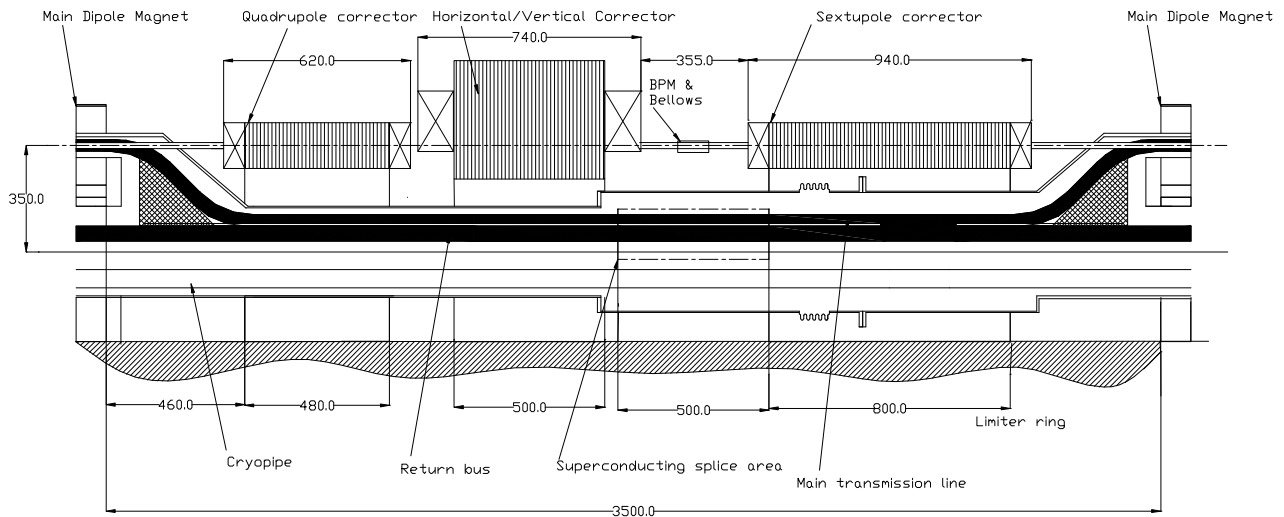


Figure 5.2. Correction magnets placed at each half-cell boundary (135-m spacing). The transmission line is diverted down near the current return bus to provide a field-free region for the correctors.

The dispersion suppressor sections are similar. Here the 101.6-m long half-cell is made of two 48.81-m long dipoles with correctors. The gradient is increased to  $\pm 9.449$  %/cm and the bend field reduced to 1.766 T to match the footprint of the Stage-2 machine (see Section 3.1.2).

Conventional water-cooled quadrupoles are used in the straight sections. Two 6.1-m long, 70-T/m quadrupoles are used in a typical 135-m half-cell. Special optics for the machine utilities— injection, abort, the RF system, beam cleaning, and the matching sections of the interaction regions—are constructed using quadrupoles of the same design but with various lengths. The low-beta triplets utilize superconducting 300-T/m  $\cos 2\theta$  quadrupoles made from  $\text{Nb}_3\text{Sn}$  cable. Special dipole magnets, similar in concept to the arc gradient magnets and excited by the transmission line, are used to bring the beams into collision at the interaction regions, to separate the beams to make room for RF cavities, and at the beam cross-over regions.

Table 5.1 summarizes the main parameters of the magnets used in the Stage-1 VLHC design.

Table 5.1. Main parameters of magnets in the Stage-1 VLHC.

Magnet Type	$B_{\text{nom}}$ (T)	$G_{\text{nom}}$ (T/m)	$L_{\text{mag}}$ (m)	Number of elements	Notes
Gradient dipole (arc)	1.97	9.73	67.75	3136	Main Arc Magnets
Gradient dipole (DS)	1.80	16.88	48.81	160	Dispersion Suppressors
Straight sect quads		70	4.8 - 6.8	464	Room temp. conventional
Low $\beta$ quadrupoles		300	9.2 - 10.9	16	Supercond. IR Quads
Special dipoles	1.95		25 - 35	52	Separation, recombination, and cross-over
Correctors					Air-cooled Iron/Copper
Dipole (horiz.)	1.0		0.50	1648	Every "F" location
Dipole (vert.)	1.0		0.50	1648	Every "D" location
Quadrupole		25	0.50	3296	Every F&D location
Sextupole		1750 T/m <sup>2</sup>	0.80	3296	Every F&D location

During the past three years, most of the R&D effort has concentrated on the dipole design, with considerable attention focused on the 100-kA superconducting transmission line cable and cryogenic system. Conductors meeting all requirements have been developed and successfully tested at a 17-m length 100-kA superconducting test stand [4]. This design study is based on cables and splicing methods identical to those tested. A low heat-leak cold mass shielded support system was developed (Section 5.1.2.2). A 100-kA power supply and current leads (Figure 5.42) are being built for extended system tests. A 50-m Invar pipe was thermally cycled 1000 times to verify cryogenic weld reliability in the "zero-contraction" mode [5]. The parameters of the cryogenic system including pipe sizes, pressure drops, and refrigeration process flows have been calculated. Quench behavior has been calculated with a detailed magneto-hydrodynamic simulation [6], and results were in adequate agreement with observations in the 17-m test loop. The magnetic and mechanical design was refined and several configurations tested using a room temperature magnetic test stand [7]. Two 6-m magnet prototypes with the parameters of this design study are now being manufactured to confirm the main technical decisions.

Section 5.1.2 describes the combined function arc and dispersion suppressor magnets in detail, including magnetic design, design of the 100-kA transmission line, and the mechanical and thermal designs. The correctors are described in Section 5.1.3 and the interaction region magnets in Section 5.1.4. Section 5.1.5 presents the various special magnets, including straight section quadrupoles; beam separation, recombination and cross-over dipoles; and injection and abort system magnets. Production of the 66-m long gradient dipoles and the testing and measuring of them are described in Sections 5.1.6 and 5.1.7 respectively. Transport, installation and alignment methods are summarized in Section 5.1.8.

## 5.1.2 Combined Function Arc Magnets

The twin-aperture superconducting transmission line magnets [1-4,7-9] are shown in Figures 5.1 and 2.6. All bending magnets share a common single turn excitation transmission line winding. The return bus, located within the cryogenic service pipe, is 290 mm below the drive bus. There are several advantages of this single turn warm iron magnet: simple construction, low parts cost, low inductance, small cold mass, low field in the superconductor area, absence of turn to turn insulation, low magnetic forces and heat leak, high stability against beam losses and simple quench protection. Nevertheless there are some negative effects associated with the external return bus: a non-negligible fringe field, asymmetric saturation of the lower and upper iron half-cores, and partially uncompensated magnetic forces on the drive and return buses.

Table 5.2 shows the main parameters of the dipole magnets. Section 5.1.2.1 describes the magnetic design. The transmission line design is presented in Section 5.1.2.2. The mechanical and thermal designs are described in Section 5.1.2.3, including the magnet structure, the transmission line, the cryogenic service pipe and cryostat, and the beam pipe. The magnet ends, where space is provided for the correction magnets and interconnections from one magnet to the next are made, are described in Section 5.1.2.4.

Table 5.2. Main parameters of the dipole magnets.

		<i>Main Arc Dipole</i>	<i>Dispersion Suppressor</i>
Magnet air gap in the orbit center		20 mm	22.26 mm
Beam Pipe Inner Dimensions		18 mm x 28 mm (elliptical)	
Separation Between Beams		150 mm	
Magnet length		65.75 m	48.81 m
Half-cell length		135.5 m	101.6 m
Sagitta in Magnet		1.6 cm	0.6 cm
Gradient		$\pm 4.73$ %/cm	$\pm 9.449$ %/cm
Magnetic field:	injection	0.1 T	0.09 T
	maximum	1.966 T	1.766 T
Good field diameter (< 0.02%):	injection	20 mm	
	maximum	10 mm	
Transmission Line Design Current		100 kA	
Current at 20 TeV		87.5 kA	
Magnetic field energy @ 100 kA		790 kJ (12 kJ/m)	473 kJ (10 kJ/m)
Superconducting cable		braided NbTi with braided Cu stabilizer	
Specified Max. Temp of Conductor		6.5-6.7 K	
Nominal Max Temp of Cryo System		6.0 K	
Iron Core		1-mm laminated low carbon steel (AISI 1008 or better)	

Figure 5.3 shows a detailed cross-section of the magnet, with an inset showing the dimensions and placement of the saturation control holes. The laminated core consists of upper and lower iron half cores, which are stamped from 1-mm thick low carbon steel. The upper and lower laminations are stacked and welded into 6-m long yoke blocks, which are then assembled into the complete yoke structure. The precise spacing between the two yoke halves is set by

non-magnetic 316L stainless steel spacer bars, and the two halves are welded together with non-magnetic steel plates at the inner radius. The weld is done inside a press, and the weld shrinkage provides the preload necessary to assure precise and stable contact between all of the laminations and the spacer bar. The yoke blocks are mounted on the support tube, which also serves as the cryogenic service pipe for the magnet. The 12-m long yoke and support tube assemblies are shipped to Fermilab from outside vendors. Final assembly into 65-m magnets, including insertion of the transmission line cryostat, beam pipes, and cryo service pipes, is performed in final assembly buildings on site as described in Section 5.1.6.

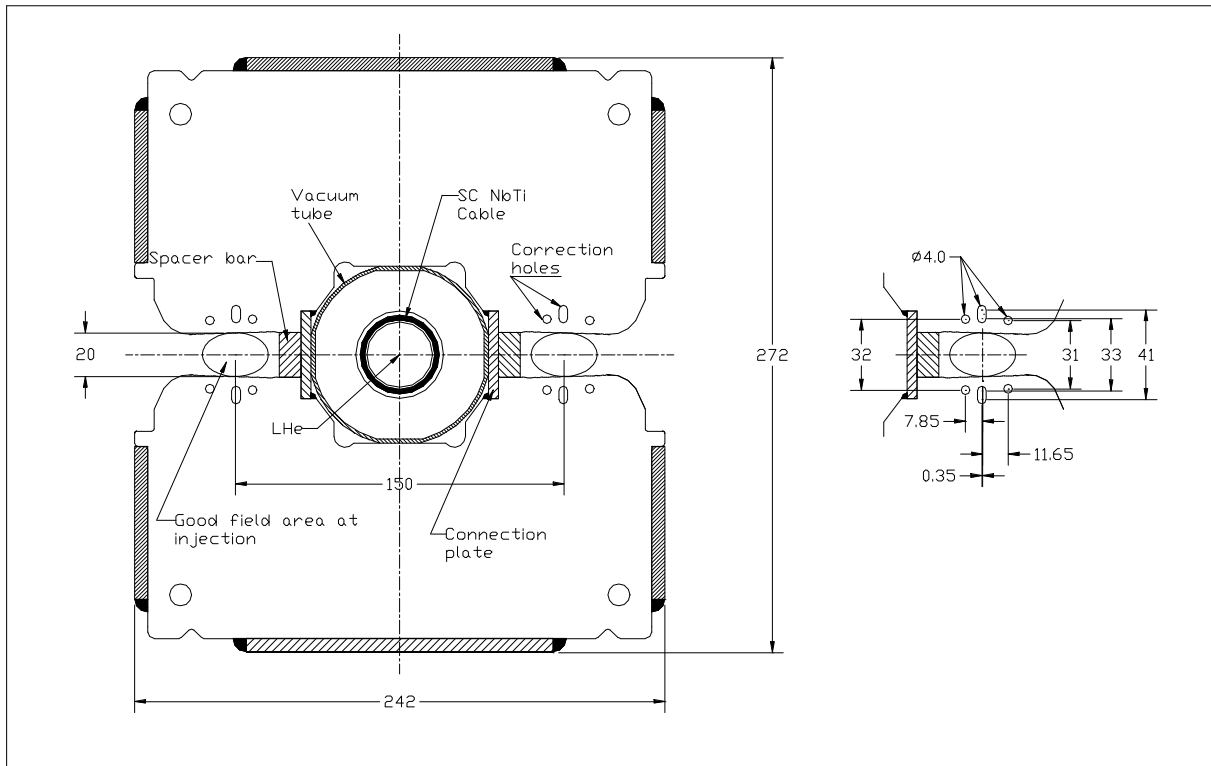


Figure 5.3. Cross-section of the transmission line magnet yoke. Inset shows holes used to control field defects from iron saturation. The vacuum system is installed after magnetic measurements are complete. Not shown are the vacuum antechambers shown in detail in Figure 5.52.

### 5.1.2.1 Magnetic design

The combined function gradient dipole is an iron-dominated magnet, in which the field quality is determined mainly by the shape of the pole tips and the properties of the iron from which they are made. The field quality is insensitive to conductor placement errors as large as 1 mm. The magnet must maintain a high quality field over a 20:1 dynamic range.

#### Field Quality at Injection

Field quality requirements are most severe at injection where the beams are largest. The injection field of 0.1 T is above the range where hysteretic field defects cause difficulties. Recent experience building several hundred iron magnets for the Fermilab Main Injector and

Recycler projects has shown that achieving the required  $10^{-4}$  field quality in production is straightforward at this field level.

Mechanical tolerances on the pole tip shape will be tighter for the 2-cm magnet gap of the VLHC than for magnets with larger gaps. (Field error modeling is discussed in Section 3.2.2.) Relatively thin 1-mm steel laminations are chosen to improve this tolerance. If necessary, end shimming techniques similar to those used in Recycler production [10] can be used to reduce systematic and random multipoles at injection to a level limited by magnet measurement errors. Finally, a technique has been tested to put inexpensive multipole correctors in the body of the magnets by running wires down the saturation-control holes in the pole laminations [11]. It is unlikely that these measures will be needed.

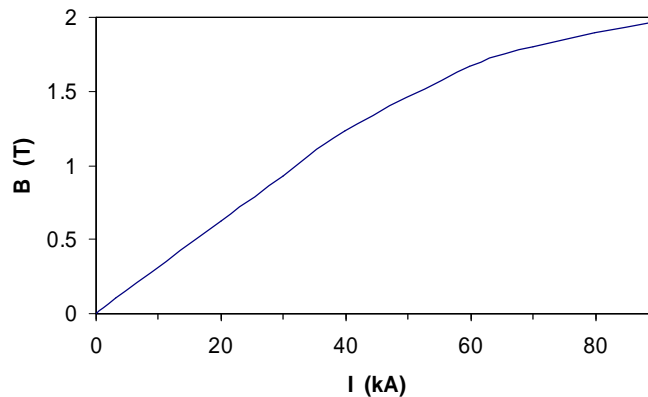


Figure 5.4. Magnetic field strength as a function of transmission line current. The 20 TeV bend field of 1.966 Tesla occurs at 87.5 kA. The design current of the transmission line is 100 kA.

#### *Saturation Control and Maximum Dipole Field*

The main design challenge is dealing with field distortions induced by saturation of the iron at fields from 1.7 to 2 T. Both sextupole and gradient shift are important. The sextupole defect is caused by early saturation of the corners of the pole tips, since they carry more flux than the centers of the pole. Gradient shifts are caused by asymmetric saturation on the high-field (narrow gap) side of the gradient magnet. Both of these saturation effects are controlled in the current design with a set of holes placed in the iron near the poles (see Figure 5.3 inset). At the highest fields, where the holes are insufficient, quadrupole and sextupole corrector magnets in each half-cell are needed to regulate tune and chromaticity. No significant loss of dynamic aperture results from this as discussed in Section 3.2.2.3.

There is a tradeoff between the maximum bend field (beam energy) and the strength of the corrector system required to compensate saturation effects. The present system allocates 1.2% of the ring circumference to sextupole and gradient corrector magnets. These allow a peak field  $\sim 15\%$  higher than would be possible without these strong correctors. This is worthwhile, even considering the larger cost-per-meter of the corrector magnets. On the other hand, doubling the current corrector strengths would increase the peak field by less than 5% (see Figure 5.6). Thus the chosen corrector strengths seem to be roughly optimized.

Saturation control with “holes in the poles” proceeds as follows. Best results are obtained with a large number of holes, whereas field strength and mechanical considerations favor a

smaller number of holes. The combined optimum was found to be three holes per pole, as shown in Figure 5.3. The field optimization objective function was the integral field homogeneity around a circular aperture. The optimization process was carried out simultaneously for three field levels (1 T, 1.7 T and 2.0 T). The optimization was done using an ANSYS Sub-problem Optimizer, and a large number of local minima were investigated. The best solution was tested by OPERA 2D and had  $\pm 0.02\%$  field quality within a 20 mm diameter aperture for  $0.1 = B = 0.8$  T, 15 mm for  $0.8 < B = 1.5$  T, and 10 mm for  $1.5 \text{ T} < B < 2.0$  T. This shrinkage of good field region is acceptable, since the beam is  $\sim 4x$  smaller ( $\sigma = 0.2$  mm) at full energy than at injection.

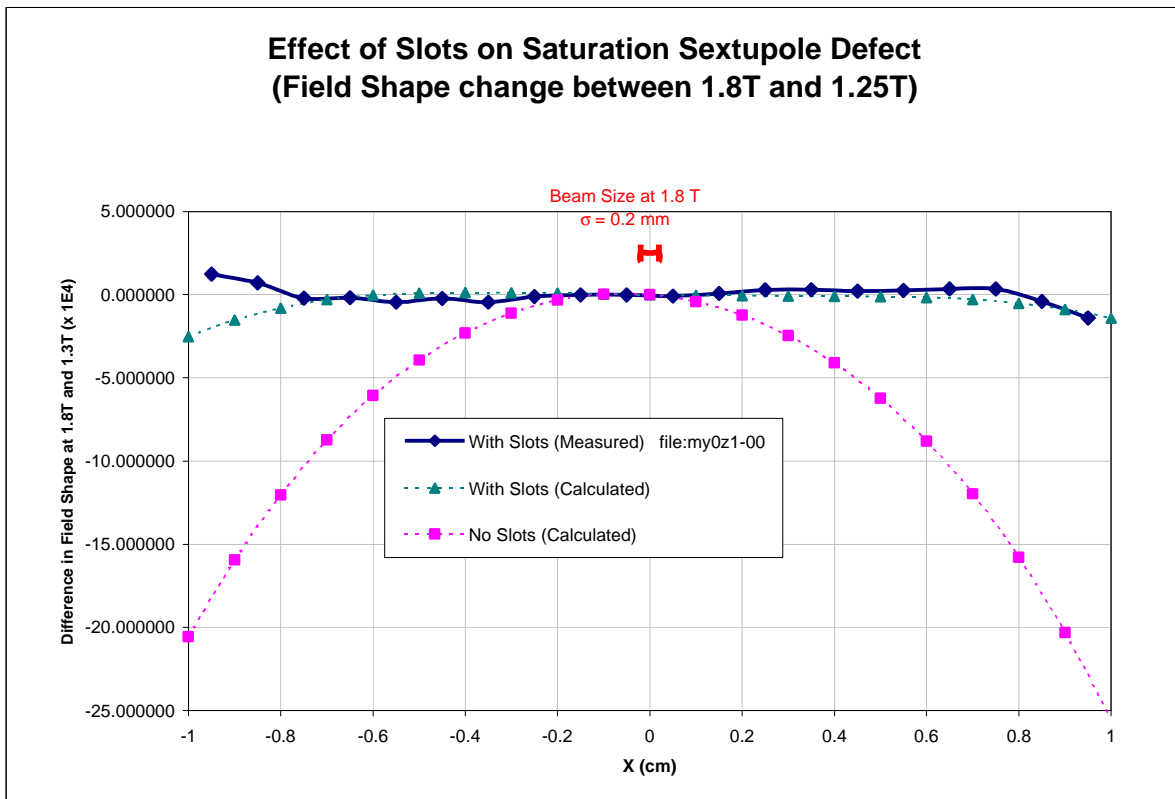


Figure 5.5. Measured effect of “Holes in the Poles” on the saturation sextupole defect as a function of transverse position in the transmission line magnet.

Both the Main Arc and Dispersion Suppressor magnets are excited by the common transmission line. The Dispersion Suppressor magnets operate at a higher gradient and reduced bend field to match the footprint of the Stage-2 dispersion suppressors. This results in similar pole tip fields and saturation characteristics for both magnet types.

We have not re-optimized the pole tip designs for the current design study parameters. The results shown below [6] correspond to an earlier parameter set with a smaller gradient of  $\pm 3$  %/cm, corresponding to a lattice with  $60^\circ$ /cell phase advance and 150-m halfcell length, and a smaller spacing of 140 mm between beam apertures than the current value of 150 mm. It is anticipated that performance similar to that described here will be achieved for the current designs when their optimization is complete.

Figure 5.5 shows the measured effects of putting the correction holes in the pole laminations on the saturation sextupole defect at 1.8 T. The measured results agree well with the 2-D calculation, and demonstrate a large improvement with respect to the field shape without holes. Figure 5.6 compares the calculated and measured shift in the quadrupole moment as a function of excitation for a prototype yoke stack. The quadrupole and sextupole errors are  $\pm 2$  units in the field range 0.1 T - 1.85 T and both are about -8 units at 1.95 T.

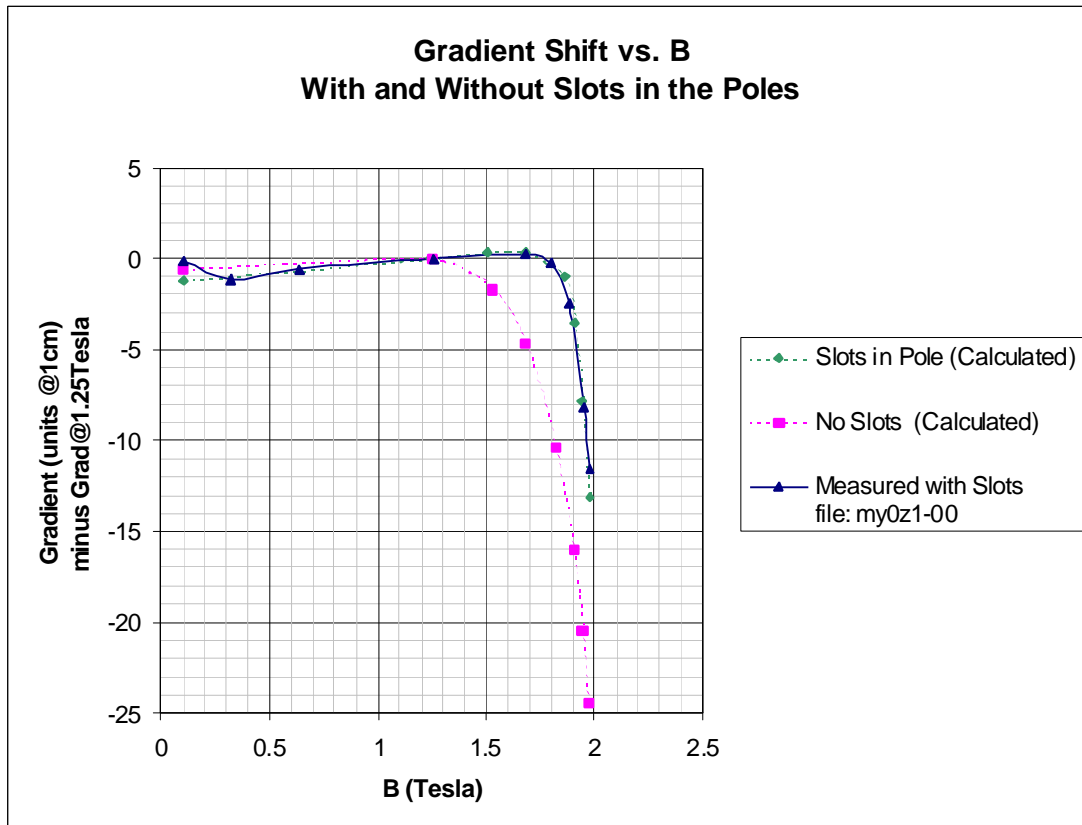


Figure 5.6. Effect of “Holes in the Poles” on the gradient shift in the transmission line magnet.

### *Magnetic Forces and Asymmetric Saturation*

In order to suppress distant magnetic fringe fields and minimize the system inductance, a return conductor is placed outside the magnet laminations. At the midpoint of the accelerator, the drive conductor returns back through the first half of the magnets (but outside the lamination stack). At the points where the beams cross each other—at the interaction regions and the beam cross-over insertions—the drive and return buses trade places. See Figure 5.40.

The drive conductor is centered in the iron yoke and the return conductor is placed 290 mm below the drive conductor. The return conductor generates a fringing field that saturates the lower core more than the upper, which decreases the field quality in the gaps and increases the magnetic force on the drive conductor. This can be countered by increasing the thickness of the lower half core and adjusting the spacing of the return conductor. With these two adjustable parameters it is possible to adjust the magnetic force to zero on both the drive and return

conductors when they are at their nominal position at full current. This same optimization largely eliminates the asymmetric (skew) multipoles in the magnet gap.

Although the force on the drive conductor in its nominal position is zero, it experiences a force gradient of about 200 kg per meter of magnet per mm of displacement. The force is horizontally stabilizing and vertically destabilizing (negative spring constant). The force gradient on the return conductor is 20 times smaller. The mechanical implications of this are discussed in Section 5.1.3.

### 5.1.2.2 Superconducting Transmission Line

The transmission line is a cylindrical superconducting braid inside a pipe cooled by supercritical 4.5-6.0 K helium, placed inside a co-axial cryostat, which in turn is placed at the center of the room temperature iron yoke. The transmission line (Figure 5.7) consists of (from inside out) a 2.5 cm helium flow space, a perforated Invar tube, a copper stabilizer braid, the braided superconductor cable, an Invar pipe to contain the helium, the cold pipe support, a cryoshield, the superinsulation blanket, and the vacuum jacket. The cold pipe support centers the conductor cable in the vacuum jacket, which in turn is placed centrally inside the magnet lamination. It also supports the cryoshield pipe, which in turn supports the superinsulation blanket.

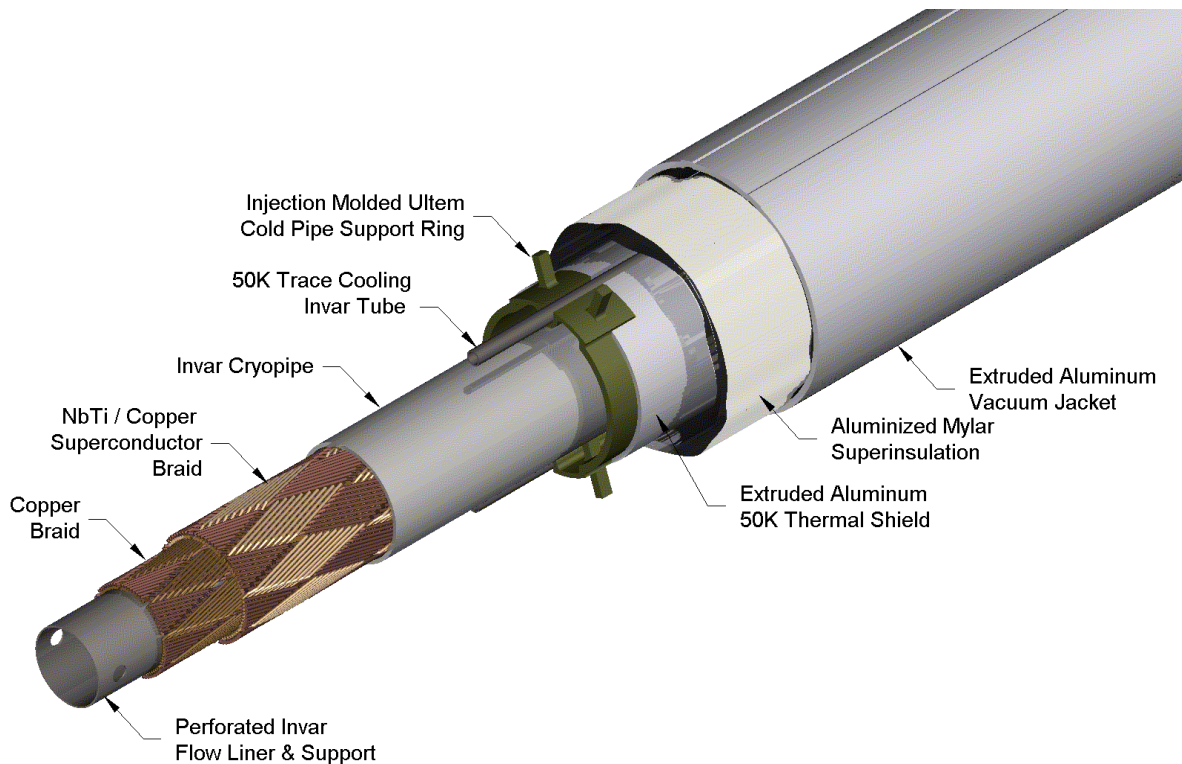


Figure 5.7. Transmission line drive conductor.

The main design requirements for the transmission line are as follows. First, it must contain enough superconductor to carry the specified current of 100 kA at 6.5 K. This includes a significant margin since the peak temperature of the cryogenic system is specified at 6.0 K (Section 5.2.1) and the required current for 20 TeV is 87.5 kA. It must maintain a 2.5-cm clear bore for the helium flow in a 10-km loop. It must contain enough copper stabilizer and thermal

mass to carry the full current in the non-superconducting state during a 1-second shutdown following a quench. The cold pipe must handle the maximum pressure transient of ~35 Bar which occurs during a quench. The cold mass supports must center the conductor with an accuracy of 0.5 mm and resist magnetic decentering forces while maintaining a low heat leak consistent with the cryogenic design. Finally, it must survive hundreds of temperature cycles *with its ends constrained*, since the transmission line forms a loop around the accelerator which cannot be allowed to shrink during cool down. This mandates the use of Invar (36% Nickel steel) for the cold pipes.

### Conductor Design

Three distinct conductor designs are utilized (see Table 5.3). The main drive bus that excites the dipole is optimized for minimum size consistent with operation at 100 kA in a ~1 T self-field. The current return bus in the cryogenic service pipe is identical to the drive bus but enlarged to increase flow area. A special type of conductor is required at the half-cell boundaries where the drive conductor is diverted downward to make space for the correction magnets (see Figure 5.2).

Table 5.3. Main parameters of the three types of transmission line conductors.

	Drive Bus	Return Bus	Bus in Corr. Space
Cu/SC ratio in strand	1.8	1.8	1.3
Diameter (mm)	0.648	0.648	0.808
Cond. Type	Braid	Braid	9 Rutherford Cables
Number of strands	288	288	270
Cu Wire dia. (mm)	0.64	0.64	0.64
Number of wires	240	288	288
Inner Pipe ID (mm)	25.3	36.8	36.8
Outer Pipe OD (mm)	38.1	47.1	50.1
Max working Pressure (bar)	40	40	40

A braided conductor is used for the main drive and return buses. The superconductor braids are sandwiched between an inner perforated Invar pipe, which serves as a liquid helium channel, and an outer Invar pressure pipe that closes the helium space. The braid consists of 288 NbTi strands arranged in a pattern of two sets of 24 crossing bundles with opposite pitch angle about the tube. It uses strands of the dimension of the SSC dipole outer layer design; current prototypes use actual SSC strand. For the Stage-1 VLHC it is planned to use a more cost effective wire optimized for the lower fields and without the constraint of small filament size. There is also a copper braid placed inside the superconductor to provide additional copper for carrying current during a quench. The conductor braid is secured in position by swaging the inner pipe against the outer one by drawing a series of carbide steel balls through the pipe. This provides adequate clamping and preload against the radial compressive forces of the magnetic self-fields, as evidenced by the fact that all of our test cables built this way achieved ~100% of the theoretical current at quench. No training or degradation has been observed during the few quenches per sample tested.

The bus in the 3.5-m long corrector magnet region uses a spiral wrap of nine SSC inner dipole Rutherford cables in place of the braid. Here, due to the proximity of the two currents, the peak field rises to 1.5 T, requiring more superconductor to carry the 100 kA current. Cables are

used here rather than braid to allow openings to be made in the superconductor assembly for pressure relief ports placed at every 4th half-cell (542 m). The Rutherford cables have less void space, which may help reduce conductor motion in the presence of azimuthal forces in this region.

Both braided and spiral-wrapped conductors (and the 10 cm long splice between them) have been successfully tested in the 100 kA test facility. Power dissipation was  $<0.2$  W per splice at 100 kA.

The critical temperature vs. current for the braided conductor is shown in Figure 5.8. The data point is the measured performance of the conductor used in the prototype, and the diagonal line is the computed performance using the properties of NbTi and the self-field as a function of current. This slope has been measured on various transmission line samples and agrees with predictions derived from short sample parameters. At 90 kA current the critical temperature is 6.8 K. The temperature margin of 0.8 K with respect to the maximum helium temperature of 6.0 K (see Section 5.2.1) is sufficient both for stability of the superconductor and for operational “head room.” The margin for the braided conductor, normalized to its higher self-field in the space between dipoles, is slightly larger than for the main conductor.

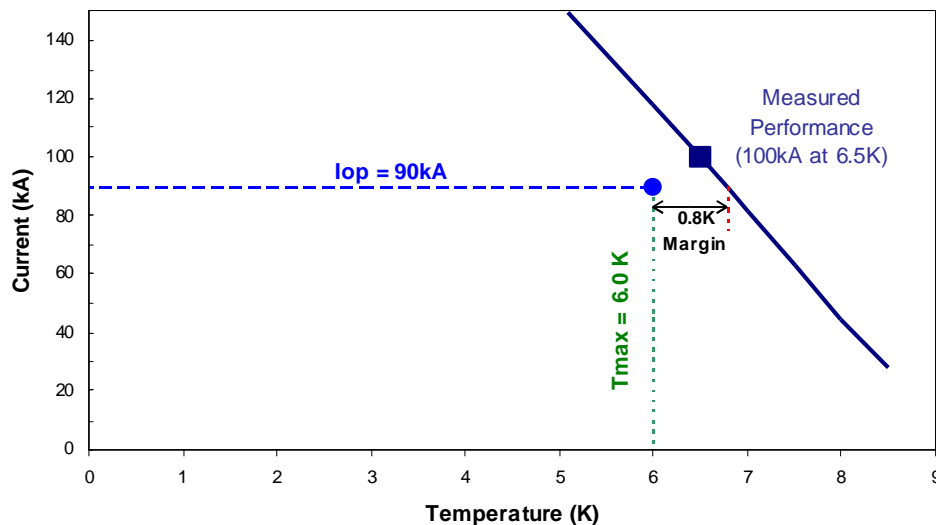


Figure 5.8. The critical temperature vs. current for main drive and return conductors. The design has a temperature margin of 0.8 K at 90 kA, or a current margin of 28 kA at nominal temperature.

Detailed thermohydraulic simulations [8] have been performed on many quench scenarios with a number of different configurations of the transmission line. The simulations use a 1 V quench detection threshold and a 1 second decay time constant (see Section 5.2.2.3). The calculations demonstrate that, for conceivable worst-case scenarios, the peak temperature remains low ( $<60$  K) and, with relief valves spaced every four half-cells, the peak pressure is below the 40 bar maximum for which the Invar pipe is rated without taking credit for its increased strength at low temperature. The simulations also show that the additional copper stabilizer braid is essential. Without it the peak temperature can reach 250 K, and the higher temperature can result in peak pressure above 40 bar.

The quench propagation velocities were measured in a 17 m long conductor loop [4]. Although the properties of the conductor in the 17 m loop are not identical to the final design, the

general behavior should be similar. It was found that in a forced quench by a local heating of  $\sim 10$  K, quench propagation velocity rises linearly with current, and it reaches about (10-12) m/s at  $\sim 80$  kA. Above this current, it rises exponentially reaching about (30-40) m/s at 100 kA. This indicates that by applying a current dump circuit of a time constant of 1 second, the quench zone would be at most half the length of a dipole magnet (34 m). Repeating these tests with long lengths of the final transmission line is an important goal of the R&D program.

### Cryostat Design

A cross-section of the drive conductor cryostat is shown in Figure 5.9. The support spider consists of an injection molded ULTEM ring with two pairs of pegs pointing up and down, the direction of the magnetic force. The inner pair of pegs support the cold pipe, while the outer pegs contact the vacuum shell. The conductor must be placed precisely on the central line of the magnet to minimize the de-centering force. Offsets of the order of 0.5 mm, in excess of what can be expected due to part tolerances, lead to de-centering forces on the order of 100 kg/m. The supports are specified to withstand 100,000 mechanical cycles during the accelerator lifetime, or 10 ramps/day for 30 years. Laboratory tests on these supports withstood 100,000 mechanical cycles of 300-kg/m force, three times that of the design requirement. Further design development, however, may be required to optimize the spider design with respect to axial motion, expected under thermal cycling. (See Section 5.1.2.3.)

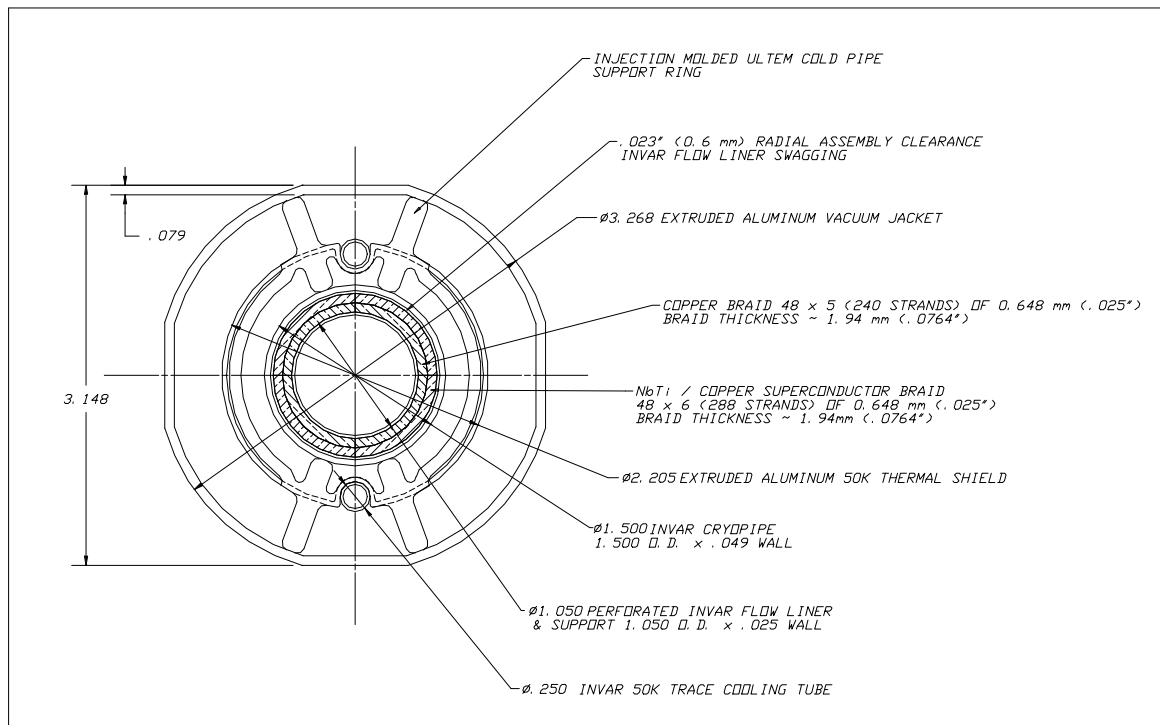


Figure 5.9. The drive conductor cryostat.

The cryo-shield is made of extruded aluminum pipe segments  $\sim 50$  cm long, which slide over opposite ends of each support spider. The 6.4-mm diameter Invar pipe that is used to provide the 50 K pressurized helium is “snapped in” to the cavities at the top and the bottom of

both the shield and the supports once a magnet's length of shield has been assembled. The shield pipe is wrapped with 40 layers of a dimpled superinsulation blanket. The vacuum jacket is made of extruded aluminum, and it is of a "squared" shape to firmly fix its position inside the iron laminations. This also helps to prevent potential rotation (and/or twist) of the cold pipe supports.

### 5.1.2.3 *Mechanical and Thermal Design of Transmission Line Magnet*

#### *Magnet Length*

Many considerations entered into the 67.75 m magnet length chosen for this study. There appear to be no hard technological or financial limits to considering magnets either twice as long or half as long. The weight of 33 tonnes is slightly less than an LHC dipole so that considerations of floor loading, transportation power, etc. will be comparable. A magnet of this length can be picked up at two points and transported using a lifting fixture (load spreader bar) which weighs 1/3 as much as the magnet and is small enough (2 m height) to fit into the tunnel. This greatly simplifies handling. With the electronics modules located at half-cell boundaries, all instrumentation and cables can be factory-installed and tested on our ¼ cell long magnets, but this is not true of shorter magnets. Cryogenic heat load from transmission line splices is about 0.4 W per magnet end or <10% of the total 5 K heat load. Labor estimated for in-situ magnet splicing is ~60 person-hours per magnet, which corresponds to <\$10 M for 3000 magnets. This sets the scale for possible savings of in-tunnel labor from longer magnets. Doubling the magnet length would increase the floor space of the factory by about 50%.

#### *Distance Between Support Posts and Gravitational Sag*

The main structural element of the magnet assembly is the 300 mm steel pipe which serves as the vacuum jacket for the cryogenic service lines and current return. The magnet cores act mainly as a dead weight on this pipe. The support pipe is made from A36 carbon steel 5 mm thick. The magnet core is welded to the tube every 0.5 m to increase the vertical stiffness of the assembly and to reduce system deflection.

The magnet is installed on vertical support/adjusters every 6 m. This distance was chosen [12] to limit deflections due to gravity to 1–2 mm depending on assumptions about the connections between the cores and service pipe. As is common for long laminated magnets, this deflection will be precompensated by assembly tooling so the magnet sags into alignment. The present design also allows for a final shimming of the core position if needed. The maximum stress does not exceed 50 – 60 MPa.

#### *Force Needed to Introduce Alignment Bumps*

The force needed to introduce the 1.6-cm global sagitta into the 67-m magnet assembly is very small (<10 kg). Large forces may be generated, however, on individual support/adjusters from gravity and friction, or if they are driven in opposing directions during magnet alignment in the tunnel. To estimate forces and deformations of the straight magnet structure during alignment, 3D numerical simulations were performed using a 12-m section model [13]. Forces were applied on a single support/adjuster connected to the vacuum tube at the center of the model, and the model ends were restricted from motion or rotation. The model also had a distributed

weight load from the laminations in addition to the horizontal force applied by the adjuster. The force needed for 1-mm motion is 450 kg. The result shows the magnet twists slightly because the force is not applied along the neutral axis of the magnet assembly. The block moves about 0.9 mm for a 1-mm movement of the vacuum tube. The difference in relative movement of the iron halves of the magnet can reach 30  $\mu\text{m}$ .

### *Yoke Deflection and Gap Stability under Magnetic Forces*

The magnetic force acting between the yokes rises quadratically from 6 kg/m at injection to 2500 kg/m at the maximum field of 2 T. The outside of the gaps must remain open for magnetic measurements and vacuum chamber installation. Thus this force is taken across support spacers in the relatively small  $\sim 1$  cm distance between the transmission line vacuum jacket and the beam pipe. The yoke and gap spacer assembly must be rigid enough to keep the air gap stable within  $\sim 20$   $\mu\text{m}$ . Several prototypes were built before identifying a viable and economical design.

The laminated magnet yoke (Figure 5.3) consists of upper and lower iron half cores. Core laminations are stamped from 1-mm thick low carbon steel. The stack of laminations is pressed and welded into a block. Two blocks, upper and lower, separated by two nonmagnetic 316L stainless steel spacer bars and are welded together by stainless steel strips from the inside of the central hole. The weld contraction provides a preload greater than 5 tons/m which removes all clearances between the spacer bars and half-cores.

Tests of the final short mechanical model showed that under full load, the left gap shrank vertically by 12  $\mu\text{m}$  and the right gap by 6  $\mu\text{m}$ . The horizontal change was less than 4  $\mu\text{m}$ . These changes were reproducible indicating elastic deformation. In full magnetic testing a 1 m model with outer spacer bars was successfully tested and no gradient shift was observed (Figure 5.6) aside from that expected from iron saturation [14]. These measurements will be repeated with better statistics on longer magnets currently in production.

### *Magnetic Forces on the Transmission Line and Cold-Mass Support Spider*

Loads from transmission line magnetic forces are transmitted from the drive conductor to the pipe, through the supports (spiders) to the vacuum jacket, and to the magnet core. In the ideal case, the magnetic forces are zero on both the drive and return conductors as described in Section 5.1.2.1. Nevertheless, iron saturation effects and assembly tolerances in the position of superconducting cable will cause uncompensated magnetic forces [15]. At a current of 100 kA, each meter of the transmission line experiences a decentering force gradient of 228 kg per mm of vertical displacement and a stabilizing force gradient of 100 kg/mm in the horizontal direction. The vertical force gradient gives rise to an instability [16] in which the current-carrying pipe bends into a sinuous curve with a period of twice the support distance. This instability sets the maximum support interval of 0.5 m.

Spiders made of ULTEM [17] centrally position the conductor. Pegs are nominally under pure compression inside the cryostat. The compression depends on the leg over-sizing and on the variation in pipe diameter. A 0.5 mm tolerance is required on the combined tolerance stackup of the cryopipe diameter, spider leg lengths, vacuum jacket wall thickness, and lamination geometry. See Section 5.1.6.3. The pressure range is 20-40 kg. These numbers increase up to 70-100 kg in cold conditions and under the action of magnetic forces.

Prototype injection-molded supports were exposed to 100,000 mechanical cycles with a load force of 300 kg/m (three times that expected) [18]. This test indicates that in principle the transmission line supports would function with every second spider missing or destroyed.

The relative axial motion of the cold conductor line and the warm vacuum jacket tube requires the spiders to slide along the pipes to avoid a high stress in the spider material [19]. The sliding behavior needs to be carefully verified in system tests. If it is insufficient, other rolling or sliding support systems can be used [20,21,22].

#### *Magnetic Forces on the Current Return Conductor*

The return conductor is at a force null in the main body of the magnet, and experiences a force gradient 20 times smaller than the drive conductor. However in the corrector region where the buses are not shielded from each other, the magnetic forces are 700 kg/m at the standard separation of 0.29 m, increasing to ~4000 kg/m at the 10 mm separation in the corrector region. This force is handled by mechanically connecting the two buses together in this region (see Figure 5.11) with an insulating cold-to-cold support that does not generate a heat leak.

#### *Longitudinal Forces from Thermal Contraction of Invar Pipes*

The conductors in the transmission line magnet form a continuous loop around the ring circumference that can not be allowed to contract as the pipes cool down. Most materials will be damaged if they are cooled down to cryogenic temperatures but not allowed to contract (Table 5.4). Expansion bellows can be used for normal cryogenic piping but not with the transmission line conductor. The best solution for the conductor is to use materials such as Invar that will go into tension but will not be destroyed as they are cooled down with their ends constrained.

*Table 5.4. Stress in pipe materials after cool down from 300 K to 5 K with ends constrained.*

<i>Material</i>	$\dot{\alpha}dt$ , <i>mm/m</i>	$E(5\text{ K})$ <i>GPa</i>	$s=E*\dot{\alpha}dt$ <i>MPa</i>	$s_{yield}$ <i>MPa</i>	$s_{yield}/s$	$DL(mm)$ $L=135\text{ m}$
304 Stainless Steel	3	220	660	600-1200	0.9-1.8	405.0
6061 Aluminum	4.1	80	328	380	1.15	553.5
Invar (36% Ni Steel)	0.48	140	67	700-1000	10.4-14.9	64.8

As the table above indicates, Invar will survive cooldown with 67 MPa of thermal stress, corresponding to ~1400 kg tension in our conductor (independent of length) at 5 K. The hoop tension on the Invar pipe is provided by a radially outward force of ~0.06 kg on each spider.

A test of the cryogenic reliability of Invar pipe welds was performed [5] as part of the VLHC R&D program. A 50 m Invar tube containing 128 automatic girth welds was thermally cycled 1000 times from 300 K to 77 K with the ends constrained. No leaks were detected at a sensitivity of  $10^{-10}$  std cc/sec.

#### *Longitudinal Anchoring for Magnet and Cryogenic Pipes*

The magnet anchor system consists of the vacuum barriers, the force-anchors, the transportation locks and the vacuum jacket anchors, as shown in Figure 5.10.

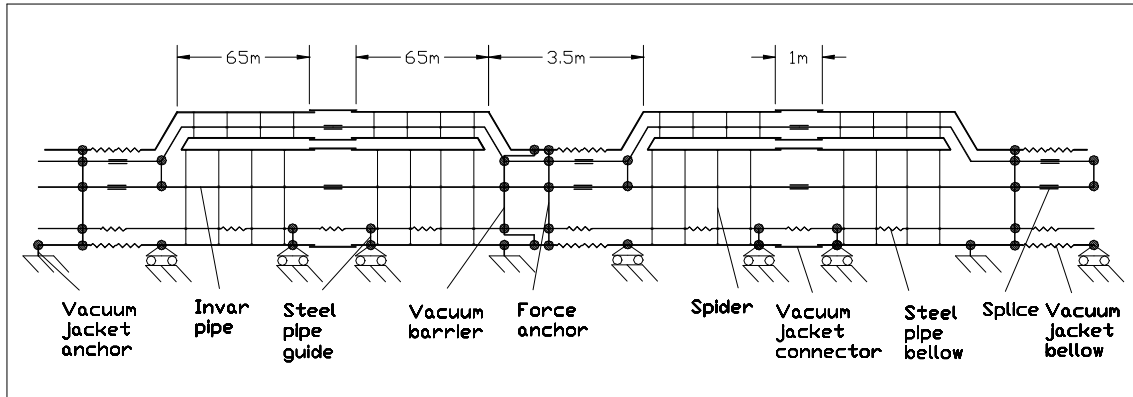


Figure 5.10. Longitudinal anchor schematic. The vacuum jacket and all pipes are anchored every 135 m.

The basic philosophy is to longitudinally anchor the vacuum jacket and all piping at a single point near the corrector location at the half-cell boundary (every 135 m). Two 67-m magnets will be hard-welded together into a single 135-m assembly. The vacuum jacket is also connected to the ground every 135 m at the anchor point. These points define an immovable magnet cross-section in case of accidental vacuum loss and jacket thermal contraction from a cool down to about 250 K [23]. There will be expansion joints in the vacuum jacket and beam pipes on one side of this anchor. Magnet adjusters will permit 2-3 cm of longitudinal motion for normal tunnel temperature variations.

Cryogenic piping will be anchored at the 135-m locations, and will have sliding supports in places where it is not anchored. Either Invar or stainless steel piping can be used for the normal cryogenic piping. Stainless pipes will need compensation bellows every  $\sim 33$  m to reduce shrinkage to the level of  $\sim 100$  mm. The convoluted length of the bellow is  $100/0.25 = 400$  mm. The force to expand the bellows by 50 mm is 300 kg for the bellows' spring constant 6 kg/mm. The bellows' stability problem is solved by using an internal tube liner and an outer protecting skin.

Vacuum barriers and quench pressure reliefs occur at the anchor location in every 8<sup>th</sup> magnet (540 m). The vacuum breaks are used to isolate vacuum sectors in order to facilitate installation, troubleshooting, and repair. They provide a good vacuum in the transmission line ring section [24,25]. The vacuum barriers are designed to withstand a differential pressure of 0.15 MPa and to minimize the heat in-leak [26]. They are made of an all-welded construction of thin-wall stainless steel tubes. The vacuum barrier is located close to the pipe longitudinal anchor to prevent damage to the ceramic insulators that electrically isolate the Invar conductors.

The longitudinal anchor restrains thermal forces from Invar pipe shrinkage and stainless steel bellows expansion ( $\sim 3000$  kg) during cool-down and warm-up. This anchor consists of graphite fiber composite tie rods and a G-10 spider, and connects all the pipes to the vacuum jacket.

The transportation lock is located on the opposite end of the magnet from the vacuum break. It is mounted in place during production and removed after magnet installation in the tunnel.

### Cryostat Interconnection

After magnet alignment, interconnection activities will take place. The magnet and the cryo-service line must be connected every 67.75 m at the 3.5-m and 1-m interconnection regions, as shown in Figure 5.11.

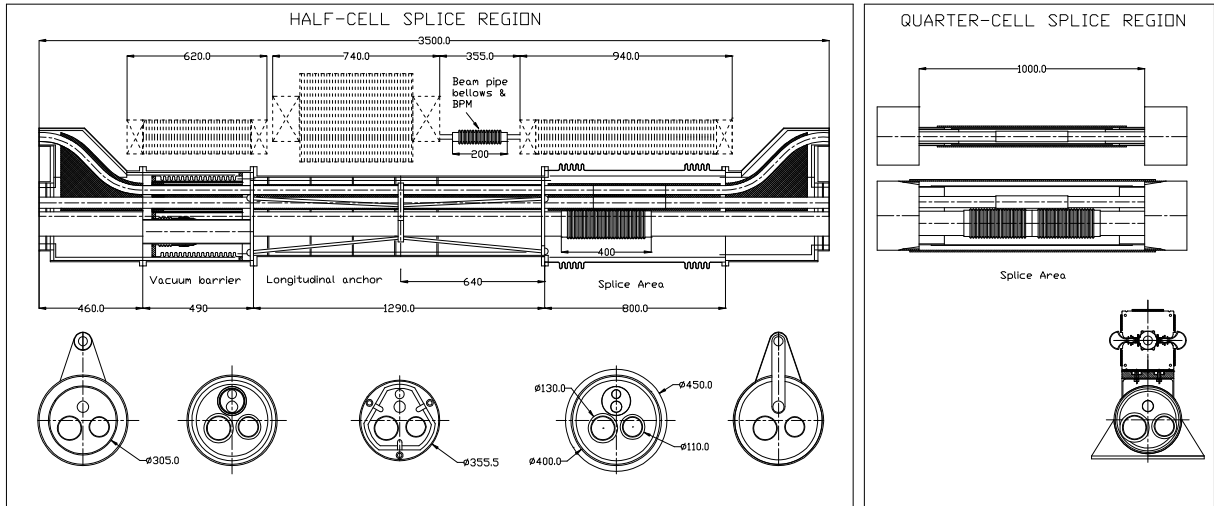


Figure 5.11. Magnet interconnections with bellows and correctors at the half-cell boundaries (left), and the hard-welded connection at the quarter-cell boundary (right).

Both conductors will be spliced at these areas. To compensate magnetic, thermal and hydraulic forces in the region where the transmission line conductors make a loop and are located close to each other, an additional set of special spacers and clamps will be used. The weld on the conductor line pipes can take place directly over the copper/superconductor structure without damaging it. A picture of the splicing operation is shown in Figure 5.33.

Three cryo-service pipes having bellows will be orbital welded automatically. An aluminum thermal shield made from two pieces will cover all the pipeline connections [27]. Multi-layer insulation blankets are mounted around the shield to reduce radiation heat load. The vacuum jacket is connected by a bellows in the 3.5 m region and by a thin steel skin in the 1 m region.

Beam pipes are connected by bellows every 135 m in the space between corrector magnets to compensate  $\sim 25$  mm motion of the magnets from expected temperature excursions in the tunnel.

### 5.1.3 Corrector Magnets

In Stage-1 there are independently powered dipole, quadrupole and sextupole correctors in the 3.5 m free space at the boundary of each 135 m half-cell. See Figure 5.2. Horizontal or vertical dipole correctors occur at each horizontally focusing or defocusing location. The specified strength of 0.5 T-m is sufficient to control closed orbit errors due to misalignments, dipole strength errors, and ground settling (Section 3.2.3). Dipole correctors can perform a full aperture scan at energies up to 7 TeV and can produce a 3-mm “3-bump” in the closed orbit at full energy. Quadrupole correctors have sufficient strength to overcome the gradient shift from

magnet saturation (Figure 5.6) and can be used to diagnose and correct  $\beta$ -waves in the lattice (Section 3.2.3.2). Sextupole correctors have the strength to overcome dipole saturation effects at full energy (Figure 5.5) as well as regulation of chromatic effects (Section 3.2.2.3).

Table 5.5. Corrector parameters.

Corrector type	Horizontal Dipole	Vertical Dipole	Quadru-pole	Sextupole
Quantity	1720	1720	3136	3136
Maximum magnet strength	1.0 T	1.0 T	25 T/m	1750 T/m <sup>2</sup>
Field quality, 18 mm diameter area, %	1.0	1.0	1.0	1.0
Effective magnet field length, m	0.5	0.5	0.5	0.8
Integrated field at r = 1 cm, T-m	0.5	0.5	0.125	0.14
Magnet core length, m	0.48	0.48	0.5	0.8
Current, A	25	25	1.0	1.0
Voltage, V	23	23	140	175
Power, W	600	600	150	200
Number of coils per magnet	1	1	4	6
Number of turns per coil	640	640	1240	633
Copper conductor dimensions, mm	5 x 5 sq.	5 x 5 sq.	1 mm Ø	1 mm Ø
Copper weight, kg	250	250	40	50
Core weight, kg	300	220	30	50

Higher multipole correctors have not yet been specified. In addition to the 3.5 m space at half-cell boundaries, the accelerator lattice design includes an unallocated 1 m space at the ¼ cell point that could be used for a Neuffer-Simpson type multipole corrector scheme.

The main design issue for the correction system is the fringing field generated by the two 100 kA conductors in the drift space between dipole magnets. This field is 0.3 T in an unshielded beam pipe and causes magnetic forces of 700 kg/m on the superconducting cable. The distance between the outer shell of the superconducting transmission line and the vacuum chamber center is only 30 mm; it is a nontrivial task to form the needed correction field in this area. Several options were considered to solve this problem:

1. Compact superconducting correctors with cold ferromagnetic screen [28]
2. Room temperature correctors with iron core as a ferromagnetic screen
3. Room temperature correctors with the transmission line deflected downwards and out of the way in the corrector region
4. Pole tip windings on the main dipoles (effective at injection, less useful at high fields)
5. Iron-dominated mechanical correctors (stepping motor drive, low power)
6. Permanent magnet correctors (rotational multipoles, stepping motor drive)

Option 3 (warm correctors with out-of-the-way transmission line) was chosen for this Design Study on the basis of lowest overall design risk and predictable costs.

The six correctors in the 3.5 m space at each half-cell will be pre-aligned and transported on a common skid. See Section 5.1.8.6. All the correctors can be installed and removed without breaking the beam pipe vacuum.

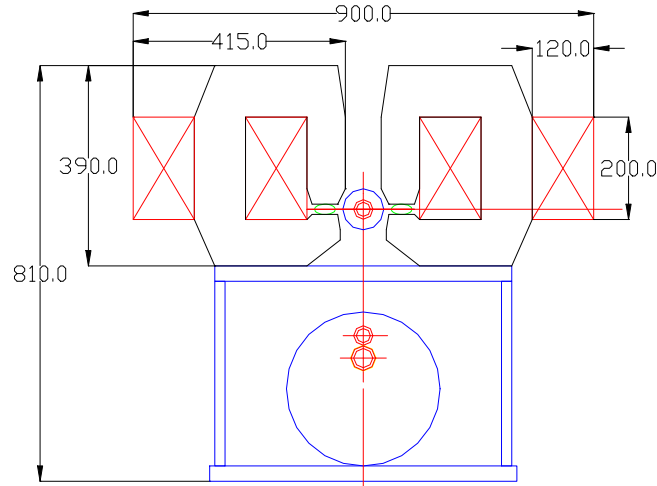


Figure 5.12. Horizontal dipole correctors.

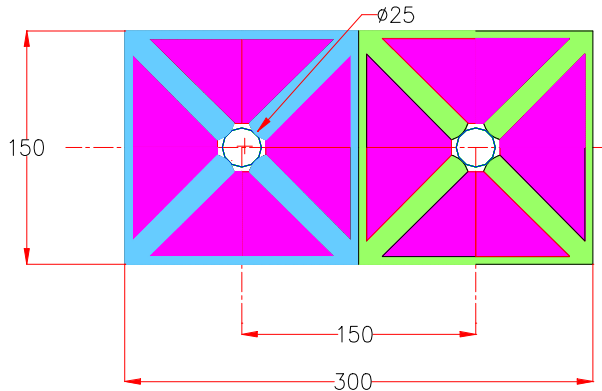


Figure 5.13. Quadrupole correctors.

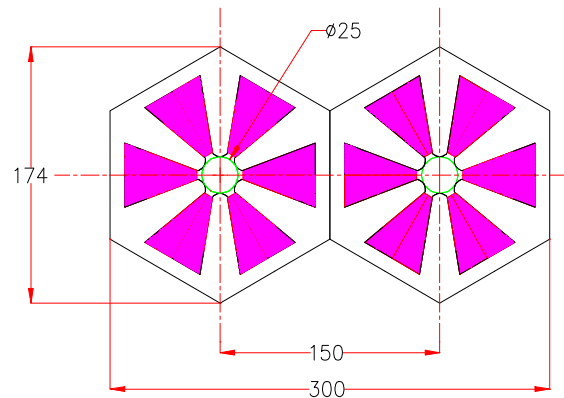


Figure 5.14. Sextupole correctors.

The powering scheme for the correctors is discussed in Section 5.2.3. All correctors are independently powered so that if necessary they can be programmed to overcome both random and systematic errors in the saturation characteristics of the magnets.

There is significant scope for reduction of corrector strengths. One rather promising approach is to optimize pole profiles for low field and saturation correction hole positions for maximum field. In this case, correctors will work at full power for only a short period of time during the acceleration cycle and will return to near zero at full field. This will reduce the operational cost of the corrector power supplies and simplify cooling.

### 5.1.4 Interaction Regions

The VLHC has provisions for two large colliding experiments located on the present Fermilab site. A system of magnets on each side of the interaction regions is required to bring the beams into collision. With these magnets come additional requirements for the accelerator including power supplies, beam absorbers to protect the magnets and prevent activation of the tunnel, and

an alignment system for the magnetic elements. For the superconducting magnets there are quench protection systems, cryogenics, current leads, and warm-to-cold transitions for instrumentation and beam vacuum.

Figure 5.15 shows a schematic of the interaction region magnetic elements. Each interaction region spans a space of 6 half cells, from  $\pm 21$  meters to approximately  $\pm 810$  meters from the interaction points. The interaction region consists of eight high gradient “inner triplet” quadrupoles, four beam separation/recombination warm dipole elements, and an outer system of lower gradient quadrupoles. There will also be orbit and local field corrector magnets. The separation dipoles, “outer” quadrupoles and correctors are warm-iron magnets identical to those used elsewhere (Section 5.1.5).

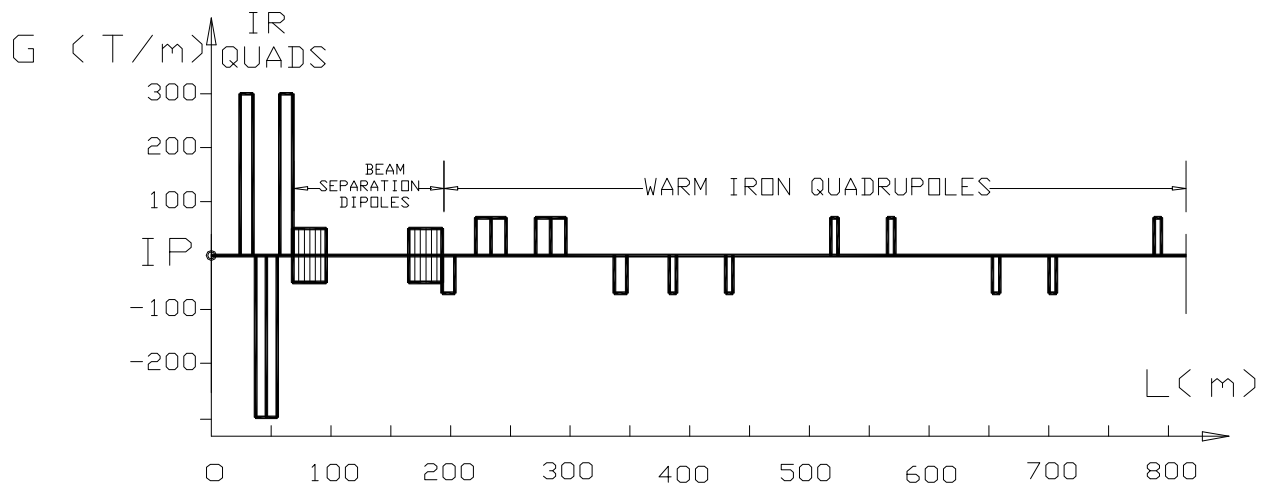


Figure 5.15. Principal magnetic elements for the VLHC-1 interaction region.

#### 5.1.4.1 Low-beta IR Quadrupoles

These magnets form the final focus at the two collision points. The required gradient is 300 T/m with a length of 10 meters and a single aperture of  $\sim 80$  mm. The field quality must be very good because the beams could be separated by as much as 12.5 mm due to the crossing angle.

A design developed by INFN-LASA for a possible upgrade of the LHC low- $\beta$  quadrupoles, with an aperture of 85 mm [29], can be used as a starting point to meet these requirements. The basic design as shown in Figure 5.16 has two  $\text{Nb}_3\text{Sn}$  layers in a  $\cos(2\theta)$  geometry, wound using the cable described in Table 5.6. The cable has a target critical current density of  $3000 \text{ A/mm}^2$  at 4.2 K, 12 T [30]. Internal splices can be avoided using the double pancake technique. The main characteristics of the magnetic design are shown in Table 5.7. The field quality of the basic design (aperture = 85 mm) gives acceptably low values for the allowed harmonics. The value of the  $b_6$ ,  $b_{10}$  and  $b_{14}$  multipoles, normalized to the gradient and using a 10 mm reference radius are respectively  $1.5 \times 10^{-6}$ ,  $1.6 \times 10^{-8}$  and  $<1.0 \times 10^{-9}$ . The relative field error is lower than  $1.1 \times 10^{-5}$ , at 12.5 mm from the center on the midplane. Iron saturation effects remain to be studied.

Table 5.6. Conductor characteristics for LHC upgrade low-beta quadrupoles.

Superconductor	Nb <sub>3</sub> Sn
Critical current non Cu (@ 4.2 K 12 T)	3000 A/mm <sup>2</sup>
Strand diameter	0.825 mm
$\alpha = \text{Cu/nonCu}$	1.3
Number of strands	36
Cable dimension	(1.34 $\leftrightarrow$ 1.60) x 15.0 mm <sup>2</sup>
Effective filament diameter	< 40 $\mu\text{m}$

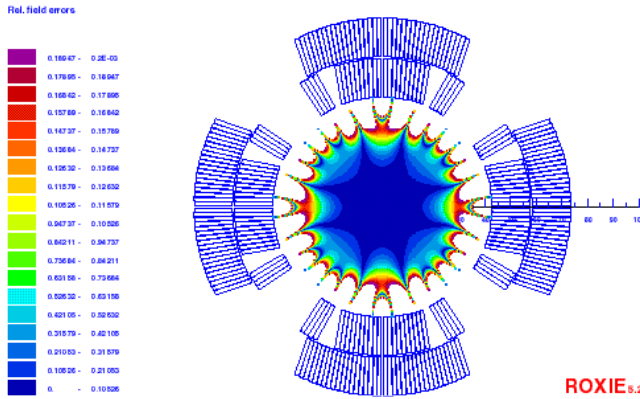


Figure 5.16. Basic design cross section with field quality at maximum gradient.

Table 5.7. Magnetic design characteristics at short sample limit.

Aperture	85 mm
Gradient	300 T/m
Current	20218 A
Self inductance	4 mH/m
Stored energy	820 KJ/m
Horizontal Magnetic force (per octant)	2.78 MN/m
Vertical Magnetic force (per octant)	3.43 MN/m
Number of turns	10 + 4 + 19
Collars thickness	20 mm
Iron inner radius	93.5 mm

Quench protection has been studied at an operating current corresponding to 93% of the short sample limit. Simulations were performed using a version of the QLASA code [31] modified at Fermilab [32] for the study of FNAL Nb<sub>3</sub>Sn high field magnets. These studies show that full coil coverage by heaters on both layers is required, and the delay time between the spontaneous quench start and the beginning of the heater-induced quench must be very short. This solution has an impact on magnet technology, because if the insulation of the heaters between the inner and outer layers can not withstand the conductor heat treatment, the double pancake technique must be abandoned. Furthermore, protection redundancy will not be possible (or at least very complicated) and fault scenarios have to be addressed. The short time delay necessary to avoid excessive hot spot temperature and the lack of protection redundancy should be the object of an appropriate R&D program.

A possible solution for the mechanical design is the one proposed for the upgraded version of the LHC IR low-beta quadrupoles presented in [33]. It uses 20 mm thick stainless steel collars, which can provide part of the required prestress and magnetic force containment. The rest of prestress and support are provided by a thick skin. The yoke is only in contact with the collars close to the midplanes, in order to transfer the stress from the skin to the coils where it is most necessary. The effectiveness of this design for the higher forces developed in the VLHC IR quadrupoles is still under investigation. A finite element analysis of coils and collars, simulating the rest of the mechanical structure by use of an external load, showed that the maximum stress in the coil can be kept below 160 MPa. The design of yoke, skin and contact regions must still be optimized to provide the required support on the coils.

In summary, it can be concluded that a two layer design using Nb<sub>3</sub>Sn at 4.2 K is a good candidate to meet the requirements for these magnets, if the critical current target is reached. Optimization will be required for the quench protection and mechanical design.

#### 5.1.4.2 *Interaction Region Subsystems*

Most of the 1600 meters of the interaction straight section will be in the standard VLHC tunnel. Since the IR magnetic elements need to be “tunable” they require a special gallery to house their power supply and electronics. There will likely be a global alignment system that connects the experiments to the final focussing elements. Finally, the tunnel will need to be wider near the IP to accommodate the extra shielding and vacuum connections and instrumentation associated with the detectors and IP interconnect.

Four independent power systems are required for each side of an interaction region: one for the inner triplet, one for each separation dipole and one for the outer quadrupoles. Additional quadrupoles in the IR region will likely be powered in series with other straight section quadrupoles in the accelerator and are not included here. The high gradient quadrupoles require a 25 kA, 10 Volt supply, the conventional separation dipoles require 1 kA, 100 Volt supplies while the conventional outer quadrupoles need a 7 kA, 10 volt supply. Superconducting correctors will be powered independently with supplies comparable to the outer quadrupole conventional correctors except that quench and lead protection systems will be required.

Superconducting circuits will rely on quench heaters for protection. With the relatively small amount of stored energy (50 MJ) and small number of magnets/circuit (4 or less), an energy extraction circuit and bypass diodes are unnecessary. Instead, in the event of a detected quench, protection heaters on all the magnets in a circuit will be energized and the circuit power converter will be phased off.

As stated, inner triplet quadrupoles will likely need protection levels comparable to or greater than a similarly sized LHC IR quadrupole magnet. Thus 4-8 quench heater circuits plus the requisite electronics are required for each magnet. The total space for power supplies and electronics required for each quench heater circuit is approximately two 6U VME crates. Thus a space of approximately 70 6U crates are required for each side/IR.

The IR quadrupoles are cooled by 4.5 K helium. Since the operating temperature and pressure differs from the transmission lines, they will require separate transfer lines and cryogenic systems. The dynamic heat load is approximately 600 Watts/side/IP or 2.4 kW for both interaction regions [34]. This heat load, if taken directly by the 4.5 K helium, will require approximately ½ of a VLHC-1 cryo plant. This heat load does not occur at the same time as ramping losses in the Tevatron injector, and thus might be provided for by load shifting from Fermilab’s existing Central Helium Liquefier. Impact on the cryogenic system is discussed in 5.2.1. Local heating in the quadrupoles could be quite large due to the strong focusing elements (GL ~ 3000 T-m/m) which sweep charged particles into the cold mass. The helium requirements might be reduced by carrying away some of the heat load by actively cooled absorbers in the 80 mm beam tubes.

A distribution box will be required in order to make a connection between the room temperature and cryogenic electrical elements, as well as to supply the cryogens to the magnetic elements. This will include voltage taps, strip heater leads, thermometry and other cryogenic instrumentation. 25-30 kA HTS leads would be used to supply the excitation currents.

LCW and electrical power will be required for the power supplies and conventional magnets. The LCW system will be required to deliver several hundred liters/minute per IR and are included in the totals in Section 5.2.2.4.

A particle absorber system will be required to protect the IR magnets from the excessive radiation from particles produced from the interaction region. Using the LHC as a guide, the system will require a hadron and neutral particle absorber. The primary hadron absorber will be located on the IP side of the inner triplets. The size of the absorber will be comparable to the LHC absorber but will have significantly larger heat loads, estimated to be 2 kW per IR [35]. Thus an actively cooled absorber will likely be necessary. The neutral absorber, located between the separation dipoles would be necessary to protect the outer quadrupoles, possibly the transmission line magnets and the walls of the tunnel from activation. It, too, will likely need to be actively cooled. If water cooled the requirements would be modest and would be parasitic to the magnet and power supply LCW system.

Alignment tolerances are likely to be comparable to those of the LHC interaction region. Transverse alignment tolerances will thus need to be on the order of 100-300 microns over both sides of the IP. Thus an alignment system will be required to tie together the two sides of the IR and the detector.

### 5.1.5 Special Collider Ring Magnets

This section describes several different magnets installed in the straight sections of the ring. There are a total of 10 straight sections, 5 in each half of the ring. On the Fermilab site there are two Interaction Region straight sections, two Utility straight sections and one Beam Crossing straight section. The straight sections on the opposite side of the collider are basically the mirror reflection of what is on the Fermilab site, except that there are no IRs and minimal utility equipment installed in this area.

Beam focusing in the standard straight sections is provided using a classical FODO cell made of four quadrupoles. The cell half-length is 135 m. The basic lattice is modified for special insertions as described in Section 3.2.1.

Both superconducting [36] and conventional quadrupoles were considered for the straight sections. Conventional water-cooled copper magnets are preferred because of their lower cost and ease of system integration. Warm magnets are more tolerant than superconducting magnets of the beam losses that occur in beam transfer and beam cleaning insertions. No warm-to-cold transitions, gate valves, etc. are required between the quadrupoles and the ~100 m of warm beam pipe between quads. The compact quadrupoles in both rings can be installed side-by-side at the basic beam-beam spacing of 150 mm (Figure 5.17), or at non-standard beam spacings as required by special insertions. It is easy for extracted beam lines to miss the warm quads due to their low profile and absence of a cryostat. The cooling water system needed for warm quadrupoles is absent in the arcs but is already present in the straight sections to service other systems.

#### 5.1.5.1 Straight Section Quadrupole

This quadrupole uses water-cooled windings and has been designed so that a pair of them can be installed side-by-side in both rings. The 150 mm beam spacing and the required beam pipe

size of 22 mm implies certain restrictions on the achievable quadrupole field gradient. The chosen gradient of 69.3 T/m results in the basic quadrupole length of 6.1 m. The preliminary magnetic design indicates that field quality is not going to be a problem since there is plenty of space to make the needed pole shaping. The magnetic field in the steel is acceptable, reaching 1.9 T at the pole base, but there are regions where the field exceeds 2.0 T at 70 T/m, so good quality low carbon steel must be used. Table 5.8 summarizes the quadrupole features.

*Table 5.8. Straight section quadrupole parameter list.*

Number Required	456
Gradient, T/m	70
Pole diameter mm	22
Length, m (typical)	6.1
Width, mm	148
Height, mm	168
Number of coils per winding	4
Number of turns per coil	12
Conductor cross section area, mm <sup>2</sup>	61.5
Resistance, $\Omega$	0.18
Rated current, A	285
Voltage drop, V	53
Power consumption, kW	15
Conductor hole diameter, mm	5
Water temperature rise at 1 MPa (deg. C)	12
Water flow per quadrupole (l/min)	17

### 5.1.5.2 *Beam Cross-Over Section*

Two beam cross-over regions (Section 3.2.1.3) are needed to equalize the circumference of the two side-by-side rings. To accommodate the magnets in the cross-over region, a short straight section is used that consists of a focusing cell that differs from the standard focusing cell. At the entrance to the cross-over region, the two beams are in the horizontal plane, separated by 150 mm. To make a cross-over, it is necessary to bring the beams together horizontally, separate them vertically before the crossing, and make the opposite transformation after the crossing. The vertical shift of each beam required to eliminate beam-beam interaction effects is 4.5 mm, which results in a beam-beam separation of 9 mm, more than  $18 \sigma$ . To reduce the number of magnets required for beam manipulation, tilted dipoles are used to bend beams both horizontally and vertically. The cell layout is shown schematically in Figure 5.18.

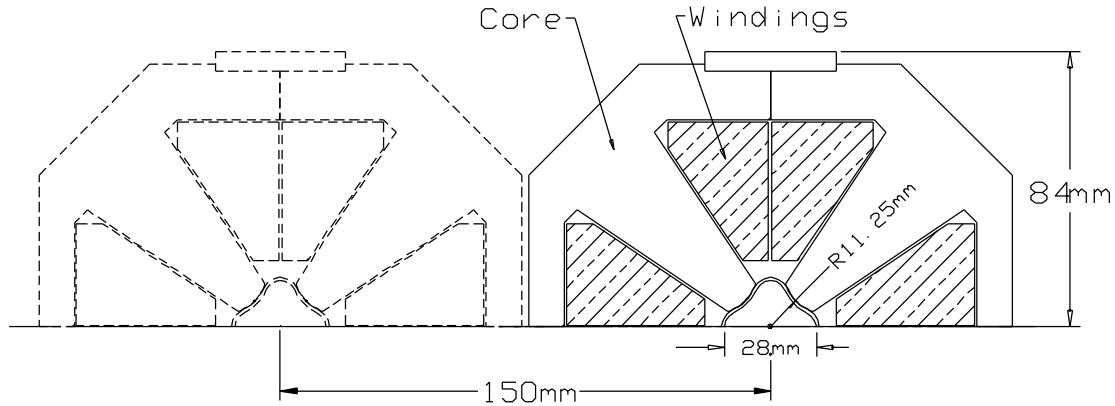


Figure 5.17. The straight section quadrupole is a conventional water-cooled copper design that allows two magnets to be mounted side-by-side with the standard beam separation of 150 mm or larger.

The magnet length  $L_m$  and tilt angle  $\theta$  can be found based on nominal magnetic field and length of gaps between the magnets in the string. As in the arc dipoles, the transmission line is used for magnet excitation. Moreover, because of the large required pole width of the magnet, the return line is also used as an active part of the magnet excitation winding. To minimize iron core saturation effects, a magnetic field of  $B_m=1.95$  T was chosen, as it was for the arc dipoles. With two-meter gaps introduced between the magnets to allow some space for repositioning of the transmission line, this results in a magnet length of  $\sim 35$  m and a tilt angle of  $\theta \approx \pm 7^\circ$ .

The total length of the beam cross-over magnetic system is about 150 m. The magnet cross-section is shown in Figure 5.19. The dipole gap is 44 mm to accommodate (while tilted) the two beams with their vacuum pipes. The pole width provides a good field region for beams separated by 150 mm. Because of the big difference in gap thickness for the pole and flux return regions, the force applied to the cable is significant, up to 2000 kg/m for this magnet. Special measures must be taken to strengthen the cable "spider" to the needed level at this location.

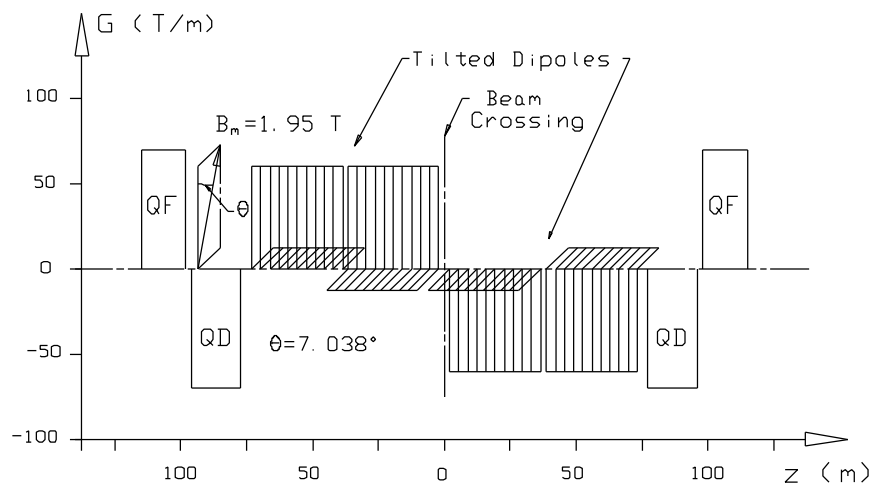


Figure 5.18. Beam cross-over region layout. See also Section 3.2.1.3.

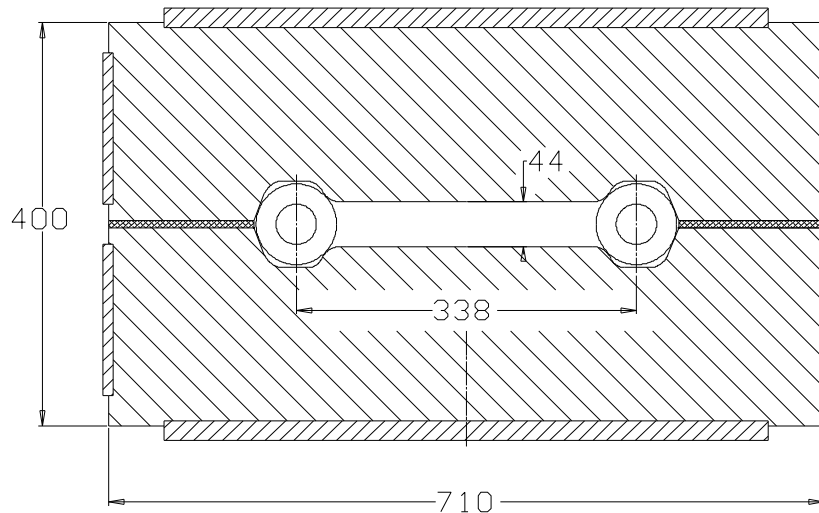


Figure 5.19. Beam crossing dipole. This is energized by the 100 kA transmission line.

To allow a 150-m gap for the tilted magnet installation, the cell focusing was modified using different lengths of standard cell quadrupoles. Quadrupole lengths were limited to 6 m by water cooling considerations. The total length of quadrupoles installed in both rings for each of the two cross-over sections is 143.6 m.

### 5.1.5.3 Warm-Iron Magnets in the Interaction Region

As described in Section 5.1.4, the IR straight section requires horizontal beam manipulations to collide the beams at the IP. For this purpose, so called “separation/ recombination” dipoles, as shown in Figure 5.15, are used that bring the two beams together within the low-beta lens string region and place the beams onto the nominal orbits before they go into the regular part of the straight section.

The main transmission line cable is used for excitation of these magnets, and a 1.95 T maximum magnetic field in the dipoles has been chosen. As it follows from Section 2.1.1, the gap available for installation of the bending magnets is about 125 meters. Leaving some space for the transfer line position manipulation, a magnet length of 28 m was chosen to insure that a 75-mm beam shift within the 120-m gap in the lattice. Beam displacement inside this dipole is about 12 mm. This displacement must be taken into account when the good field region of the dipoles is being specified.

The two beams, initially separated by 150 mm, are simultaneously bent together by the recombination dipole, whose cross section is similar to the one shown in Figure 5.19. The separation dipole separates beams moving in the opposite directions. Final beam separation at the outer edge of the magnet is 24 mm. To reduce the force applied to the transmission line and to avoid field asymmetry, a symmetrical iron core configuration was chosen. The magnet cross-section is shown in Figure 5.20. The good field region area for this dipole is 35 x 20 mm, which is enough to accommodate the two shifted beams.

The double-channel separation dipole makes use of both the arc dipole transmission line and current return. The gap height is 26 mm. The maximum force applied to the superconducting cable is about 65 kg/m at full field. The magnet cross-section is similar to shown in Figure 5.19 above, except the pole gap and pole width are smaller resulting in a more compact magnet

with  $650 \times 350 \text{ mm}^2$  cross-section. The good field area of the dipole is  $185 \times 20 \text{ mm}^2$ , which is slightly larger than necessary for this dipole location. This allows using the same dipole in the utility straight section where a larger beam separation is required.

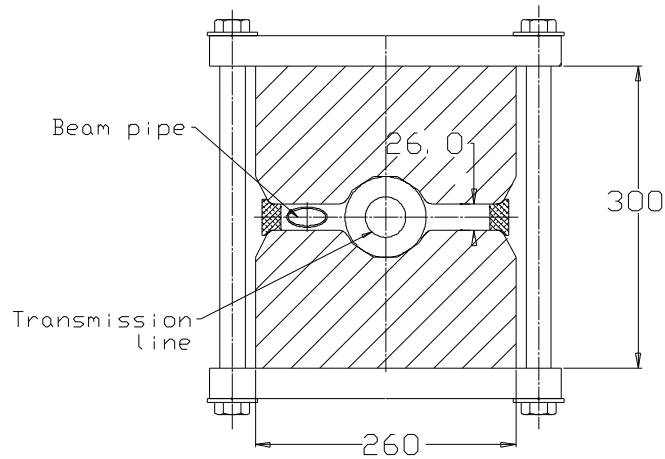


Figure 5.20. Separation/recombination dipole used for the utility straight sections and IRs.

Besides the separation/recombination dipoles, each of the two IR sections requires a set of focusing quadrupoles similar to that described in Section 5.1.5.1. The required strength of these quadrupoles can be found in Table 5.7. The total length of quadrupoles in each of the two FNAL-site IR sections is 445.1 m. Quadrupoles with lengths longer than 6.1 m will be segmented into two magnets to limit water cooling requirements.

#### 5.1.5.4 Utility Section Conventional Magnets

The utility straight section is introduced into the ring lattice to provide the space needed for various accelerator systems including RF cavities, instrumentation, injection, extraction and abort systems. At the RF cavities the required beam separation is 460 mm. This is accomplished with separation dipoles similar to those used in the IR sections. At the input and the output of the section, these dipoles have an air gap width that accommodates both beams. In the middle of the section, individual separation dipoles are installed side-by-side in both rings. The cross-section of the dipole can be found above (Figure 5.20). The length of the dipoles in the utility section is 25 m, which allows shifting each beam by 155 mm within the 242-m space as is shown in Figure 5.21 below.

Two types of quadrupoles are used in the Utility section. Most of the quadrupoles are identical to the 70 T/m straight section quadrupoles described earlier. The total length of this type of quadrupole used in each of the two FNAL-site utility sections is 208 m. The quadrupole triplet installed between the abort system kicker and Lambertson requires more radial space to accommodate the beam deflected by the kicker. In each of the two FNAL-site utility sections, 58.9 meters of these quadrupoles, described below, are needed.

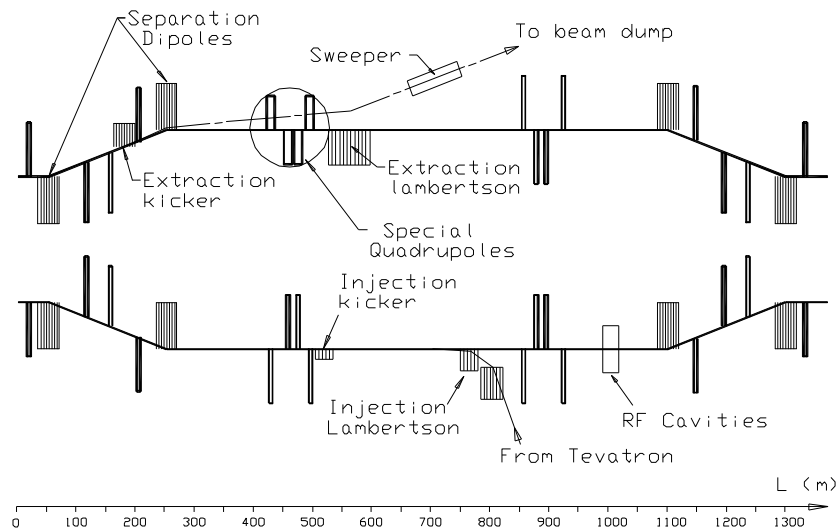


Figure 5.21. Utility straight section including injection, abort, and RF cavities.

#### 5.1.5.4.1 Injection System

The overall injection/extraction scheme of the machine is shown in Figure 5.22. As described in Chapter 4, the Tevatron is run bipolar and is used to inject protons both directions into the collider rings. Beams for both collider rings are extracted using two extraction systems as described in Section 4.3.3. Two identical 3-km transfer lines slope downward at 3% and end at the corresponding collider downstream utility section where Lambertsons and kickers inject the beam into the VLHC. In both utility sections the beam is injected into the radially inside ring, with the outboard ring reserved for extraction and abort.

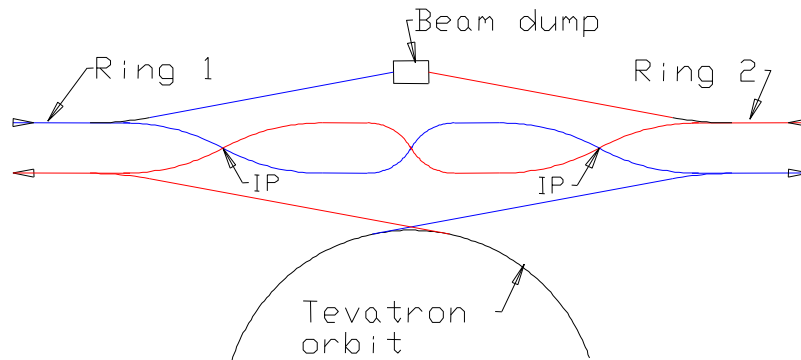


Figure 5.22. Injection and beam abort system scheme.

Downstream of the injection point it will be convenient to have an internal beam absorber for transfer line commissioning and tests which do not involve the arc magnets. The injected beam, after passing through two quad locations to measure position and steering errors, will be deflected 5-10 cm onto the absorber by a standard corrector magnet. The scope of absorber will be comparable to the Tevatron collider-mode abort. With reasonable intensity limits, air-

cooling should be sufficient. A few bunches of  $10^9$  protons are sufficient for a good BPM measurement.

The injection optics fit comfortably into the long 350-m drift in the utility region. The injection uses a full-aperture kick so that the Lambertsons do not restrict the circulating aperture. The layout, working backwards from the injection point, is as follows: six meters of pulsed kicker magnets with a magnetic field of 0.05 T provide the horizontal angular kick of 0.1 mrad to the injected beam. The horizontal separation between the injected and circulating beams is 25 mm at the nearest Lambertson 250 meters away. A total of 6 m of Lambertsons operating at 0.8 T provide a vertical angular kick of 1.6 mrad. The Lambertsons are short enough that an asymmetric design is not needed. The clearance at the nearest quad (100 m away) is 160 mm, large enough to allow unobstructed placement of standard quadrupoles on both the injected and circulating beam lines. The vertical clearance at the RF station (300 m from the Lambertsons) is 480 mm. If desired this separation can be increased using normal dipoles to begin part of the 30-mrad up-bend needed for the slope of the transfer line ramp.

**The injection kicker** parameters are listed in Table 5.9. The system is composed of six separate modules, each 1-m long. A field strength of 0.05 T is used for this study, close to that used for SSC injection system [37] and similar kicker magnets at Fermilab. The duration of the kick provided to the injected beam is  $\sim 20$   $\mu$ sec and is defined by the length of the beam pulse extracted from the Tevatron. The injection kicker requires a magnetic field switching time of 150 ns. This determines the minimum time separation between successive injected batches.

*Table 5.9. Injection kicker system parameters.*

Number of modules	6
Length of Module (m)	1
Maximum field (T)	0.05
Rise time (0 to 100%) (nsec)	150
Fall time (100 to 0%) (nsec)	150
Impedance ( $\Omega$ )	16.6
Maximum current (kA)	2.1
Maximum PFN voltage (kV)	70

Each module is fed by an individual pulse-forming network (PFN). A C-shaped magnet is made from ferrite blocks and with additional capacitors forms a twelve-cell lumped delay line with a characteristic impedance of 16.6 Ohm. The ceramic beam pipe has thin resistive coating on the inside surface, and conductive strips for image current on the outside.

Fast timing on both the rising and falling edges is required. This permits “box-car stacking” of a Tevatron batch in between two filled batches. This gives the freedom needed to produce a “smoothed” filling pattern (i.e. one without large low-frequency components that would produce a time-dependent Laslett tune shift). See Section 3.2.5.2. This will require a more complicated pulser than a Thyatron PFN, and will probably require a second Thyatron for the trailing edge. Ripple requirements after the trailing edge will probably require a cleanup kicker similar to one recently installed in the Tevatron.

**The injection Lambertson** (Figure 5.23) steers the injected beam into the vicinity of the circulating beam without affecting the circulating orbit. Only a symmetric version is required due to the small length and sagitta. The magnet pole with the field free region is made of a solid piece of annealed, low carbon steel to reduce magnetic field in the field free region. To obtain good vacuum the pole is enclosed in a thin-wall stainless steel shell. The pole gap is fixed with the use of stainless steel spacers. For magnet excitation, conventional copper wire coils are used. Water-cooling can be omitted due to the low duty cycle (4-second flat top with a 40-second cycle time). The main parameters of the injection Lambertson are summarized in Table 5.10.

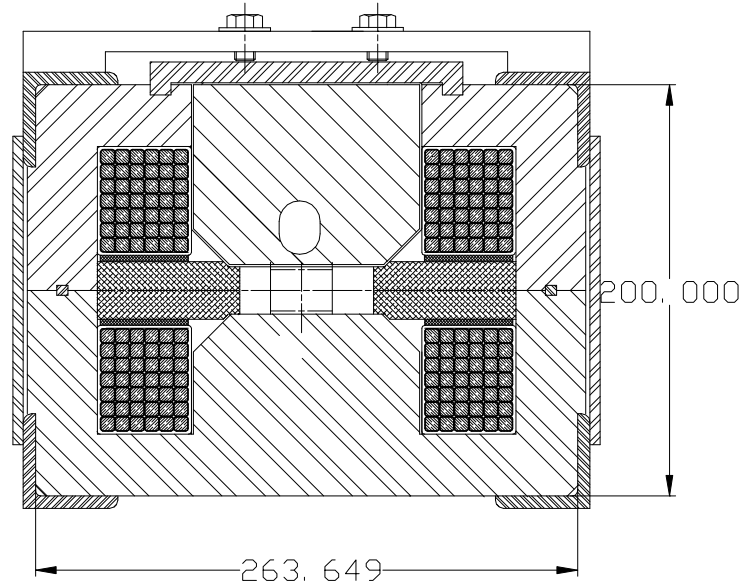


Figure 5.23. Injection Lambertson magnet.

Table 5.10. Parameter list for the injection Lambertson magnet.

Magnetic field, T	0.8
Pole spacing, mm	25
Length, m	4
Width, mm	288
Height, mm	260
Number of coils per winding	2
Number of turns per coil	42
Conductor cross section area, mm <sup>2</sup>	42
Resistance, $\Omega$	0.32
Rated current, A	208
Voltage drop, V	70
Peak power consumption, kW	15
Average power consumption, kW	1.25
Magnet surface temperature rise, °C	20

Transfer line dipole magnets, similar to the Lambertsons but without the field free region, have been designed. The coil cross-section is the same. Because the pole width can be made

significantly smaller, and because no vacuum shell is required for this magnet, it is even more compact: 180 x 180 mm<sup>2</sup> in cross-section with pole gap of 25 mm. The rest of the magnet parameters are very close to those shown in Table 5.10.

In addition to vertically bending magnets, the transfer line may require horizontal bending with an estimated total angle of 80 mrad (depending on siting details). This bend can be made using the same type of magnets. The total dipole length required for this bend in both transfer lines is about 300 m.

There are 86 quadrupoles installed in the transfer line. Most of them have a gradient of 40 T/m and a length of 1 m. Using a design similar to described in Section 5.1.5.1, and intermittent powering of about 0.8 kW peak power per lens, we can employ air cooling. This results in about 10 °C temperature rise at the surface of the magnet.

For this study, conventional magnets have been chosen to establish a reference point for future research work with the goal of building the transfer channel using only permanent magnet based equipment. Although this technique was well studied during fabrication of the Fermilab Recycler Ring, the requirement of having adjustable bending and focusing strength makes it difficult to scale the system cost without making first a thorough design study of this approach. An encouraging start to this study has been undertaken in [38].

#### 5.1.5.4.2 *Beam Abort Magnets*

The abort magnet system (Figure 5.55) consists of a kicker magnet, a Lambertson, a beam sweeper magnet and defocusing quadrupoles. The beam absorber design and other system issues are discussed in Section 5.3.2. The circulating beam goes through the field free area of the Lambertson magnet. The beam is kicked radially outward into the bend channel of the Lambertson magnet, which deflects it vertically upward into the beam dump channel. The abort channel is equipped with a beam sweeper magnet to spread the energy on the graphite absorber.

As the machine ramps, the magnetic field of the abort kicker, Lambertson and sweeper magnet must track the beam energy. For the Lambertson this is accomplished automatically by energizing it with the transmission line current. The abort kicker and sweeper systems must rely on active systems to monitor the capacitor charging voltage and force an abort if it starts to go out of tolerance.

**Abort Kicker Magnets** switch the beam between the circulating orbit and the abort channel. Their strength is chosen to provide the needed beam separation of 17 mm at the entrance to the abort Lambertson located 300 m downstream. Assuming a kicker field strength of 0.2 T, the required length is 30 m. The cross-section of the kicker is shown in Figure 5.24.

The current rise time in the extraction kicker is about 3 μsec, so a beam abort gap of about 3 μsec is needed. This requirement results in using a medium-high frequency magnetic material for magnet core fabrication. Mn-Zn MN8CX (Ceramic Magnetics) ferrite was chosen for this study. The core is made of ferrite blocks and assembled using epoxy bonding after the windings and ceramic vacuum pipe are installed inside. At nominal field of 0.2 T the current is 2410 A. Maximum field in the core is about 0.45 T, which is below the material saturation level. Pole width was optimized using pole profiling by attaching 1-mm ferrite stripes near the pole wedges. With this shaping, field uniformity in the entire vacuum pipe region is within 0.1 %, more than good enough for this device. In the configuration shown, the magnet inductance is

2.5  $\mu\text{H}/\text{m}$ . Ten 3-m sections are used, installed one following another, with each section having 7.5  $\mu\text{H}$  inductance and 2.5 ohm impedance. Each section is fed independently by its own pulser.

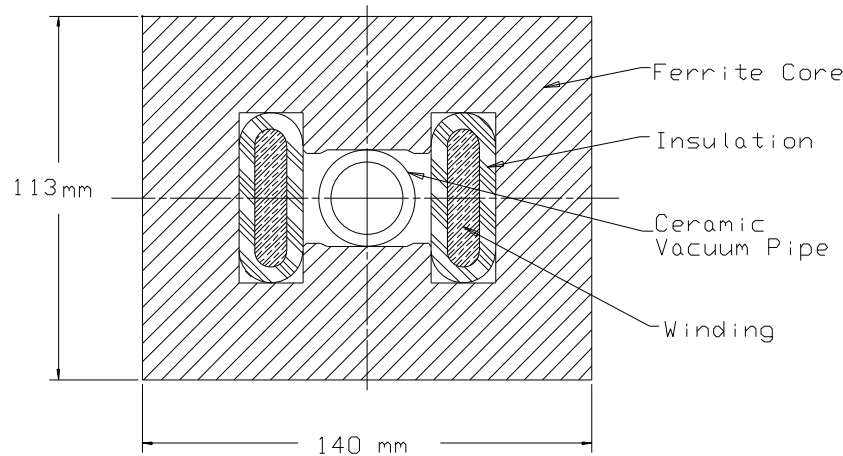


Figure 5.24. Abort system kicker magnet.

The abort kicker pulser uses a two-stage scheme. The first stage delivers high voltage for a fast current rise time. Capacitor discharge is used at this stage. Then, in the second stage, a long SCR-generated pulse with much lower voltage is used to support the flat top level. For the three-meter section, a discharge capacitor with  $C = 0.5 \mu\text{F}$  provides the needed current rise time. This results in maximum voltage at the first stage of 9600 V. Energy stored in the capacitor bank or in the magnetic field is about 25 J. The flat top length for the abort kicker magnet is defined by the ring circumference and is about 800  $\mu\text{sec}$ . To have this long pulse shape, a separate power source must be switched on when current in the primary circuit starts to decay. This is a typical long-pulse pulser implementation (see, for example, [37]).

**Large Aperture Quadrupoles** are required between the Abort Kicker and the Lambertson to allow for the 17-mm radial displacement at the Lambertson (see Figure 5.21). This larger aperture means that a lower field gradient of about 45 T/m can be achieved, and longer quadrupole lengths are required for focusing. A longer quadrupole results in higher power consumption and cooling water temperature rise. Using two 5-meter quadrupoles instead of one 10-meter, it is possible to have a lower water temperature rise at the expense of higher total water flux. Table 5.11 summarizes the large aperture quadrupole parameters.

**Abort Lambertson Magnets** use the superconducting transmission line as an excitation winding. This ensures that at each moment the magnetic field is proportional to the beam energy. The magnet cross-section is shown in Figure 5.25, and its main parameters are listed in Table 5.12. The magnet part that includes field free beam channels is placed inside a stainless steel vacuum box. Only one field free channel is used in this device; another channel has been added to obtain needed symmetry. The tolerable magnetic field in the field free area limits the maximum field in Lambertson magnet. The deflecting gap field value of 0.8 T was chosen to have field in the field free region on the level of 20 Gauss. The 67-m total length of the Lambertson gives the beam a kick of 0.8 mrad that results in more than 200 mm of beam separation at the downstream quadrupole and horizontal dipole. Magnetic forces on the transmission line

conductor are about 25 kg/m. This force can be handled by the standard transmission line support spider.

Table 5.11. Large aperture quadrupole parameters.

Number Required (total both rings)	8
Aperture radius, mm	20
Gradient, T/m	45
Length, m	5
Quadrupole width, mm	260
Quadrupole height, mm	260
Number of coils per winding	4
Number of turns per coil	12
Conductor size, mm	11.7 x 11.7
Conductor cross section area, mm <sup>2</sup>	104
Resistance, $\Omega$	0.091
Rated current, A	625
Voltage drop, V	61
Power consumption, kW	38
Water Hole diameter, mm	6.35
Water pressure drop, MPa	1
Cooling circuits per winding	8
Water temperature rise ( $^{\circ}\text{C}$ )	16
Water flow per magnet (liter/min)	35

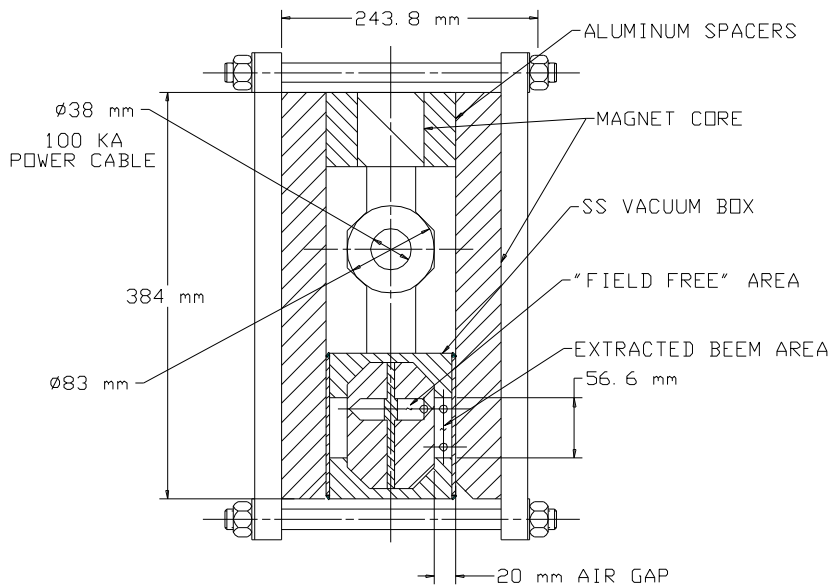


Figure 5.25. The abort Lambertson magnet. This is energized by the transmission line so that it automatically tracks the beam energy.

Table 5.12. Main parameters of the abort system Lambertson magnet

Maximum field, T	0.8
Total length, m	67
Air gap, mm	20
Field homogeneity, %	0.1
Maximum field in the hole, Gauss	20
Maximum current, kA	100
Weight, kg/m	330

**Abort Sweeping Magnets** are introduced to reduce heating of the graphite absorber block by distributing the beam energy across a larger dump surface area. See Section 5.3.2. Although reliability of this sweeping system must be high, the field quality requirements for sweeping magnets can be quite modest, allowing about 10% field nonuniformity in the sweeping magnets. Sweeping magnets deflect the beam in the X and Y directions with amplitudes that correspond to the beam striking the dump block at a location close to its radial dimension. If the phase difference between X and Y oscillations is  $90^\circ$ , the beam projection on the dump surface will move along a circular path. The velocity of this movement must be high enough to allow beam circling around the block at least twice during the extraction time,  $\sim 800 \mu\text{sec}$ . This requires a beam oscillation frequency of  $\sim 2 \text{ kHz}$ . The integrated strength of the sweeping magnets must be about  $12 \text{ T}\cdot\text{m}$  in each coordinate. A field strength of  $0.3 \text{ T}$  was chosen for this device, resulting in a  $40 \text{ m}$  magnet. The required aperture is about  $50 \text{ mm}$  after taking into account possible steering mistakes due to kicker malfunction and unpredictable beam position in cases of emergency extraction. To make the system simple and reliable, the two steering magnets are combined in a single unit, as shown in Figure 5.26. Field uniformity in this magnet is at an acceptable level of about 5% at reference radius of  $15 \text{ mm}$ . A positive sextupole component in the whole aperture results in additional beam defocusing on the target. The magnet yoke is made of standard toroidal iron powder cores (e.g. T520-40D by Micrometals). Core effective permeability is 60 to 150 in the frequency range up to  $100 \text{ kHz}$  and in the flux density ranges up to  $1 \text{ T}$ . The main parameters of the magnet are summarized in Table 5.13.

Table 5.13. Parameters of the sweeping magnet.

<i>Parameter</i>	<i>Unit</i>	<i>Value</i>
Magnetic field	T	0.3
Magnet length (total)	m	40
Maximum field in the core	T	0.45
Stored energy / meter	J/m	160
Number of turns		2 x 8
Wire diameter	mm	5
Maximum current	A	2000
Inductance	$\mu\text{H}$	2 x 80

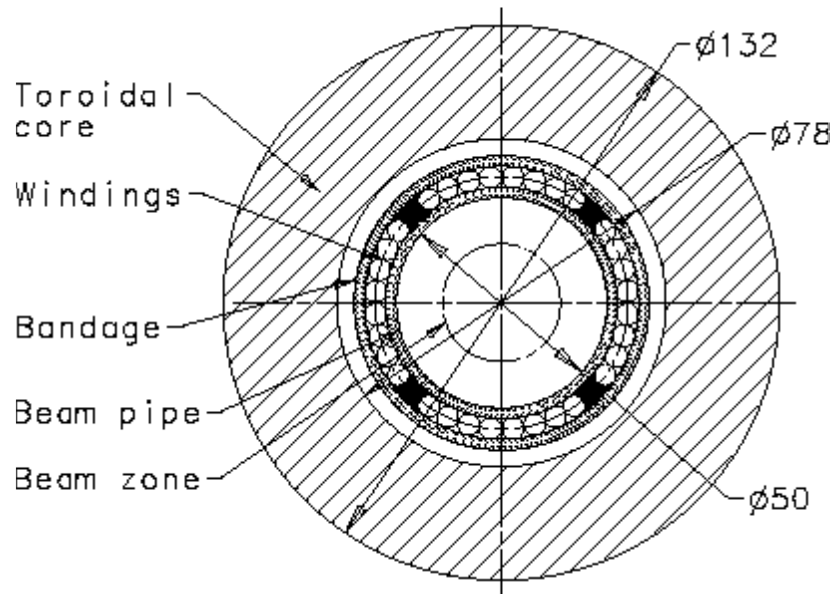


Figure 5.26. Sweeping magnet cross-section.

For equipment safety reasons the sweeping magnet is made of 10 separate 4-m sections powered by independent pulsers. The simultaneous failure of two sections, which is a very low probability event, will not compromise the safety of the absorber core. For each section, the current in the magnet windings is supplied by a simple pulser that discharges a capacitor bank into the windings. For each 4-meter section, the capacitance required to have an oscillation frequency of 2000 Hz is about 20  $\mu\text{F}$ . With a circuit impedance of 4  $\Omega$  and resistance of windings at 2 kHz of about 0.1  $\Omega$ , one can expect periodic oscillations with a rather low rate of current decay. If desired, it is possible to increase the decay rate by adding some resistance to the circuit to ensure a better beam energy distribution across the dump block surface. Peak voltage is about 8 kV, requiring at least a 12 kV rating on the windings and capacitor bank to ensure high reliability of the system. SCRs with conservative ratings can be used at these values of voltage, current, and repetition rate.

### 5.1.6 Magnet Production

Construction of the Stage-1 VLHC will require the fabrication of several thousand magnets. The largest and most numerous of these are the combined function arc magnets. They, along with the dispersion suppressor dipoles, represent the majority of magnet costs. They are also the most technically challenging as they are a significant departure from existing magnet technology, and because of their extreme length they require unique assembly procedures and facilities. All of the other required magnets are variations of magnets previously produced for other accelerators. They do not present any significant technical challenge, as fabrication methods are well understood and a broad experience base exists at various facilities within the labs and in private industry. A breakdown of magnet type and quantities is shown in Table 5.14.

Table 5.14. Magnets required for the Stage-1 VLHC.

Magnet Type	Physical Length, m	Quantity Required
Main Arc Dipole	67.75	3136
Dispersion Suppressor Dipole	48.8	160
Straight Section Quadrupole	6.0 typ.	456
Quadrupole, Large Aperture	10.0	8
Low Beta Quadrupole	10.0	16
Special Warm-Bore Magnets	Various	~20
Dipole Corrector	0.5	3296
Quadrupole Corrector	0.5	3296
Sextupole Corrector	0.8	3296

The extreme length of the combined function and dispersion suppressor dipole magnets makes the fabrication process unique. The obvious problems associated with the transport of these long devices make it necessary for the final assembly of the magnets to occur in a building strategically located to facilitate delivery of the completed and tested magnets directly to the accelerator tunnel. Two production facilities are envisioned. One facility will be located adjacent to the injection transfer line with the other remotely located on the opposite side of the ring. Magnet fabrication is projected to take place over approximately six years.

The facilities are considered assembly centers rather than manufacturing sites. The magnet components will be fabricated at subcontractor facilities off site to the highest level of completeness (value added) possible, considering that the components will need to be transported to the final assembly site. Constraints have been applied to the maximum length of component parts and subassemblies so as not to prohibit fabrication at remote locations around the country or overseas. Twelve meters was chosen, as it is the standard for shipboard containers and can easily be trucked over roadways without the need for special permits and vehicles. The on site assembly facilities will do only that work that cannot be done off site given the above constraints.

In any large-scale production program, a thorough quality assurance program must be carried out during all stages of manufacture. Inspection of parts upon receipt, testing of components where needed, and statistical sampling techniques will be employed to ensure that specifications are met. Warm magnetic measurements will be performed on all magnets as part of the QA program. Cold tests will be performed on all of the initial, low rate arc dipole production magnets and will continue during full production at rates determined by the test capacity. A discussion of magnet measurement and testing can be found in Section 5.1.7.

In this section we will concentrate on fabrication of the arc dipoles; they are a cost driver and present some unique requirements, including the superconducting transmission line. The facilities design, dominated by the 65-m length of the final magnet assemblies, is discussed first. Factory throughput, labor required, and fabrication details associated with the arc dipole magnet are then proposed. Fabrication of the iron and structural assembly is discussed as well. Costs and schedules are covered elsewhere.

### 5.1.6.1 Production Facilities

The fabrication of the transmission line magnets (combined function and dispersion suppressor dipole) takes place in two separate custom facilities each with an approximate size of 210 meters by 140 meters. A floor plan of the building is shown in Figure 5.27. Each facility has three distinct areas: 1) component storage, 2) assembly and test, 3) storage and staging into the tunnel.

**Component storage.** The facility will be used as the terminus for components fabricated off site. These components range from 12-m long iron core subassemblies to individual small parts. The space is sufficient to house stock for at least three months of production. The actual amount of storage needed will depend on vendor location and capabilities. In addition to bulk storage, space is allocated for staging (kitting) components at the various assembly area stations.

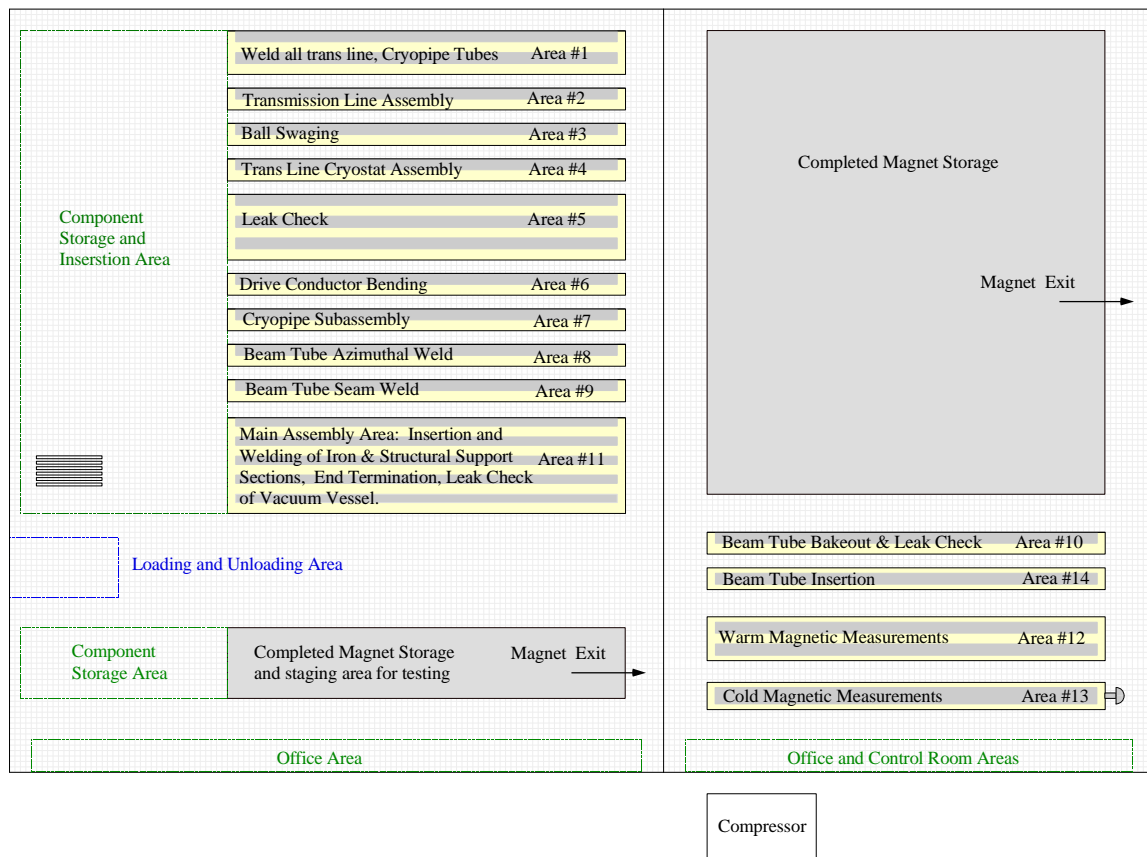


Figure 5.27. Transmission line magnet assembly factory floor plan.

**Assembly and test area.** The bulk of the facility is dedicated to magnet assembly. There are fourteen “areas,” each devoted to a specific step in the fabrication process. Each fabrication area includes one or more stations needed to achieve the required throughput for a specific operation. Each area will work autonomously and have the capability of locally storing one week’s production, so that glitches in one manufacturing step do not immediately halt the production pipeline. The facility will be manned 24 hours per day (three shifts) five days per week.

Two shifts (shifts 2 and 3) will do production at the assembly stations. One shift (shift 1) will be used exclusively to move product between the various stations, stage components at the stations and provide routine maintenance. The output of each facility is one magnet per day. Table 5.15 lists each area, its function, number of stations required, and a list of the tooling necessary to accomplish the stated function. A more detailed description of the tooling necessary is included in reference [39].

Table 5.15. Assembly area and tooling summary.

Assy Area	Stations Req'd	Function	Special Tooling Required
Area 1	2	Tube subassembly: Weld 12m tubes segments together to make a 68m tube: eight varieties, trim ends six varieties to final length	(1) storage rack, (2) welding machines, (40) welding heads, (1) part staging table, (22) support stands, (2) cutoff saws.
Area 2	1	Transmission line subassembly: Install copper braid over inner tube, install SC braid over copper braid, install outer tube segments over cable braid	(1) storage rack, (44) support stands, (1) part staging table, (1) conductor spooler, (1) outer swage
Area 3	1	Transmission line subassembly: Expand inner tube using ball swaging,	(1) storage rack, (44) support stands, (1) ball swage
Area 4	1	Transmission line drive conductor cryostat subassembly: using transmission line produced at station 3, install suspension spiders, install shield segments, install shield cooling tubes, install superinsulation, install vacuum tube segments.	(1) storage rack, (44) support stands, (1) 70K tube straightened, (1) MLI applicator, (1) part staging table, (1) tube installer
Area 5	3	Leak check of welded tubes produced at station 1	(6) leak check carts, (1) storage rack, (1) manifold and adapters.
Area 6	1	Drive conductor bender: bend end of conductor into dogleg shape	(1) storage rack, (1) support stand, (2) bending frames
Area 7	1	Cryopipe subassembly: merge cryo pipes, return transmission line subassembly, support spiders, shield segments, MLI blankets	(1) storage rack, (44) support stands, (1) blanket handler
Area 8	1	Vacuum tube subassembly: weld 12m extrusion pieces together to make 68m lengths	(1) storage rack, (1) staging table, (5) welding machines, (44) support/alignment stands.
Area 9	1	Vacuum tube seam welding: install getter pumps, seam weld together half tubes produced at station 12, weld end adapters	(1) storage rack, (1) assembly table, (1) seam welder, (2) end welder, (2) cut off saws
Area 10	1	Leak check station: bake out and leak check completed vacuum pipe	(1) storage rack, (2) leak check carts, (1) bake out insulator, (44) support stands
Area 11	5	Main assembly station: a) merge drive and return transmission line subassemblies, iron subassemblies, cryo subassembly; align and weld vacuum vessel. b) end assembly, connect primary transmission line shield cooling line to 70K header, assemble end components, fit and weld end vacuum vessel. c) leak check of completed vacuum vessel.	a): (1) iron staging and transport, (44) support stands, (5) welding machines, (15) temporary end supports b): (1) support stand, (1) welding machine, (1) alignment jig c): (1) leak check cart, (1) adapter fitting
Area 12	2	Warm measurement stand: install probe assembly and power magnet, measure and record field	(2) probe insertion alignment fixtures, (1) power supply, (1) DAC system
Area 13	1	Cold measurement stand: install cryo lines to feed and return boxes, install probe assemble, power magnet, measure and record field	(1) feed box, (1) return box, (2) probe insertion alignment fixtures, (1) power supply, (1) DAC system, (1) refrigeration system
Area 14	1	install beam tube assemblies: compress beam tube and insert in pole gap, secure in place	(1) storage rack, (2) compression insertion fixtures

The factory will have special handling requirements. Since the magnets and their subassemblies are 65 m long, and will need to be transported laterally between areas, no columns can be located within the primary assembly area. A custom hoist system is required to lift and transport the long subassemblies between the various assembly area stations. Storage areas, associated with each assembly area, will be needed to house finished subassemblies before

moving to the next higher-level assembly area. Most stations will require a staging area where the various component parts for the day's production are marshaled. Figure 5.28 shows, schematically, an elevation of a section of the plant, showing the workstations in nine areas.

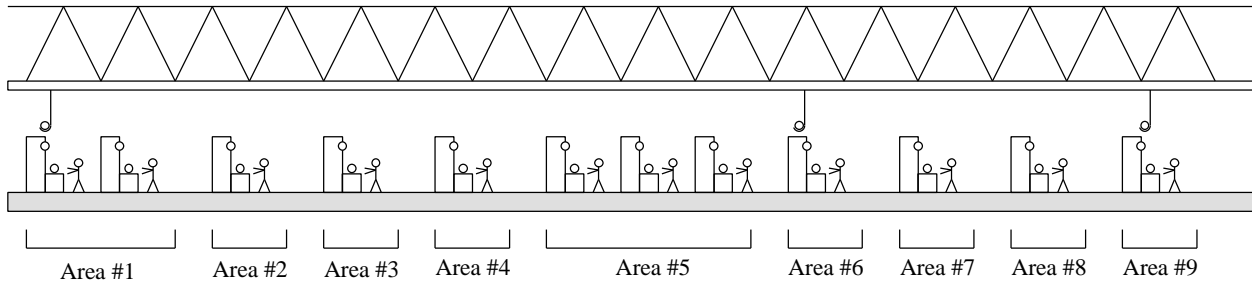


Figure 5.28. Transmission line magnet assembly factory elevation.

**Storing and staging into tunnel.** The completed and tested magnets will be stored until they need to be transported into the tunnel. Installation is not expected to begin until some time after magnet production is underway. Consequently, space has been allocated to allow a sufficient number of completed magnets to be stored in preparation for installation. Support stands will allow the magnets to be stacked vertically. A custom hoist system (described previously under assembly and test area) will move the magnets from the test stand to the storage space. An area is provided to allow transfer from the storage area to a specially built transporter rig (see Section 5.1.8). Magnet installation in the tunnel is expected to take place at a peak rate of 4 magnets per day, significantly faster rate than the production rate.

### 5.1.6.2 Factory Throughput

Each magnet construction factory is designed to produce one magnet per day, accomplished in approximately 2 shifts. As with any normal production scenario, initial throughput would be much lower than one magnet per day, with the schedule eventually increasing to reach the peak production levels.

Table 5.16 lists, for each area, the number of technicians and times necessary to accomplish each operation, the number of technician-hours required per day to manufacture one magnet, and the number of stations needed in each area to complete the required tasks. All activities shown in Table 5.16 are accomplished in two, 8 hour shifts per day.

Reference [40] shows detailed schedules for each sub-assembly manufactured for the transmission line magnet, with a breakdown of elapsed time for each individual operation described in Section 5.1.6.3. “Throughput” schedules for each work area are also shown.

At the end of each day, enough components or subassemblies are completed in each area to produce one magnet. The subassemblies are stored on a rack near each station after they are completed. A third shift is used to move the components to the appropriate area of operation for the next day's work. Maintenance of tooling is also done on the third shift or weekends. Table 5.16 does not include these third shift activities.

Table 5.16. Technician resources required to produce one magnet per day.

Area	Operation	Techs per operation	Tech time used per operation (hrs)	Number of operations per day	Total Tech hours per day	Techs assigned to area	Stations in area
1	Tube Welding	2	3	8	48	4	2
2	Transmission Line Subassembly	2	4	2	16	2	1
3	Ball Swaging of Lines	2	4	2	16	2	1
4	Cryostat Assembly	2	16	1	32	2	1
5	Leak Checking of Components	2	2.7	6	32	2	3
6	Drive Line Bending	2	8	1	16	2	1
7	Cryopipe Subassembly	3	16	1	48	3	1
8	BT/Vac Cham Azimuthal Weld	2	4	4	32	2	1
9	BT/Vac Cham Seam Welding	2	4	2	16	2	1
10	BT/Vac Cham Bakeout & Lk Chk	2	4	2	16	2	1
11	Iron & Struct Support Installation, End Assembly, Leak Check Vac Vessel	3	56	1	168	12	5
12	Warm Magnet Measurements	2	32	1	64	4	2
13	Cold Magnet Measurements	2	80	0.1	16	2	1
14	Beam Tube/Vac Cham Install	2	4	2	16	2	1
Total					536	43	22

### 5.1.6.3 Magnet Assembly

Assembly of the arc dipole magnet for the VLHC Stage-1 accelerator is summarized in this section. It is described in more detail in reference [39].

#### A. Assembly of drive transmission line for Stage-1 VLHC

The transmission line consists of four components made by outside vendors: inner tube sections, a superconducting braid, a copper braid, and outer tube sections.

Mount six 12-meter long Invar pipes together into one continuous section at Area #1. Weld using automatic rotary welding heads, and inspect mechanically. Tooling pulls the copper and superconducting braids over the Invar tube at Area #2. The outer tube is fed, in 12-meter sections, over the assembly, then returned to Area #1 to be welded, then leak checked at Area #5. The welded transmission line is moved to Area #3 for ball swaging. 3 carbide balls, each of increasing diameter, are pulled through the inner tube, swaging out the diameter and compressing the braid between the two tubes. The line is moved to Area #4 for the cryostat assembly. Support rings and aluminum thermal shield sections are automatically fed onto the transmission line from the end. Trace tubes for 60 K helium are installed on the sides. 30 layers of superinsulation are individually spiral wrapped onto the shield, while the cryostat rotates on the assembly table. Tooling punches holes in the insulation as it is being wrapped, to accept the penetrations from the support rings. The extruded aluminum vacuum jacket is then fed over the insulated assembly in 12-meter sections, returned to Area #1 and welded, then leak checked at Area #5. The end of the drive conductor is bent into a dogleg shape at Area #6. It is then moved to storage to wait for installation into the iron at Area #11.

Assembly of the transmission line will require somewhat complex tooling, which must perform seven types of automatic processes: automatic rotary welding, feeding parts longitudinally onto pipes, pulling copper and superconducting braid onto pipes, installing trace tubes, wrapping superinsulation, pulling carbide balls through the assembly to swage the inside diameter, and bending the line into the dogleg shape. Pictorial representations of each of these processes are shown in reference [39].

*B. Assembly of the return transmission line*

The return transmission line design is similar to the drive transmission line, except a slightly larger size. The return transmission line is not surrounded by an individual cryostat, as was the drive line. Instead, it is included in the cryopipe assembly. The fabrication scenario is identical to that given for the drive assembly, excluding the cryostat.

*C. Fabrication of cryopipe assembly*

Weld the 6.5 K flow return pipes, the 40 K shield supply header, and the 70 K shield return header pipes together longitudinally in Area #1, and leak check in Area #5. Transport the three pipes, together with the Return Transmission line, to the assembly station Area #7 [39]. Mount and align the four pipes. Feed 34 spiders over the pipes, spaced every two meters. Attach shield sections. They are each two meters long, and will clip on between each spider. Attach braids to intercepts from 4.5 K with connection to 6.5 K. Apply superinsulation. Inspect, and transport to storage area.

*D. Installation of iron and structural support over the cryopipe assembly and transmission lines.*

At Area #11 the Transport Drive Transmission Line and Cryopipe Assembly are positioned in space using special tooling. The 12-m long Iron and Structural support subassemblies slide over the prepositioned drive line and cryopipe assemblies, are positioned and attached.

When installed, the transmission line, complete with cryostat, needs to be positioned with an accuracy of  $\pm 0.5$  mm with respect to the iron laminations. This will be accomplished by using a series of steel balls, which will contact the outside surface of the transmission line cryostat and fit into pockets stamped into the iron laminations. The balls, cryostat, and iron laminations can easily be manufactured to a tolerance acceptable to accomplish the accuracy necessary between the transmission line and the iron. The specific tooling and procedure still need to be developed, since this process was not used on the initial prototype.

Welds are then made at each junction between the magnet support tubes (vacuum vessel). The vacuum vessel is leak checked, and the entire assembly is inspected.

It is presumed that the iron and structural support subassembly, including vacuum vessel, will be prefabricated in 12-m sections in industry and supplied to the final assembly site for assembly in the 65-m long magnet. As the accuracy of lamination profile and stackup are paramount in achieving the design parameters some discussion is warranted.

The pole tip profile is required to be reproducible to within 20 microns. While this tolerance is not achievable globally for all features of the stamped laminations, manufacturing experience indicates that it is possible for the limited range over which the pole surface is defined. The

laminations are to be stacked directly on the base datum feature for the profile. This minimizes the tolerance buildup due to the stacking operation. The design of the core assembly tie bars and welding of the spacer bars to the laminations draw the laminations toward the reference datum from which the profile is defined, assuring that the basic dimension is maintained accurately.

The internal welding of the spacer bars to the laminations poses some unique problems associated with physically fitting the required automated welding equipment within the small space. Equipment will need to be designed that fits within the limited space. A properly designed apparatus will produce very repeatable results.

#### *E. End assembly*

Still at Area #11, connect drive transmission line shield cooling line to 70 K header. Assemble end components. Fit up and weld end vacuum vessel. Leak check completed vacuum vessel.

#### *F. Assembly of the beam tube and vacuum pumping chamber*

Start at Area #8. Beam Tube sections are received in 12-m long extrusions. Two pieces must be seam welded together to make the final assembly [39]. Inner and outer pieces are butt welded together into 68-meter long sections. Welds and interior surface quality is inspected, while the assembly is still in two pieces. Getter pumps are installed into outer piece. Then beam tube halves are connected and seam welded longitudinally at Area #9. Leak check and beam tube bake out takes place at Area #10.

#### *G. Measurement of the magnetic field of the assembly*

All magnets are measured warm, either magnetically or with mechanical measurements of the pole tip profile and alignment. Cold testing will be performed on a limited fraction of the total production. Measurements must be done before the beam tube and vacuum pumping chamber is installed, because the test probe must be placed in the area occupied by the beam tube. Separate stations are used for warm and cold testing and appropriate space has been allocated in the facilities layout. A key concern is isolation of the measurement area from sources of electrical noise, which are typically from welding, electric motors, etc. The testing operation is estimated to take 30 hours for a warm test and 70-80 hours for a cold test, although this might be speeded up. More details on measurements and testing follow in Section 5.1.7.

#### *H. Installation of the beam tube and vacuum pumping chamber*

Beam Tube Assemblies are mounted onto the Structural Support and installed from the sides at Area #14. On half of the assemblies, the beam tube must be “sprung” into position, but then will stay in position after being installed. On the other half, they will slide into position easily, but will need to be secured afterward. See Figure 5.1 and Section 5.2.4.1. The completed magnet is then transported to the storage area to await installation into the tunnel.

### **5.1.7 Magnetic Measurements and Testing**

We focus discussion on testing of the combined function magnets during production since these magnets are the dominant element of the Stage-1 machine. Because of their length and small bore, these combined function C-magnets are also the most difficult to measure. Measurement

and testing of other magnetic elements in the ring are can be accommodated by existing equipment and approaches.

Unlike conventional superconducting magnets, the conductor of the combined function magnets (transmission line) is not in a high field region and quench training is not a significant issue for magnet performance. Thus magnetic field measurements dominate the magnet testing process, both as a quality control measure and as characterization necessary for machine operation.

Warm measurements will be performed on all magnets. This must be done before the beam tube and vacuum pumping chamber is installed, because the test probe must be placed in the area occupied by the beam tube. Roughly 10% of magnets will be measured with the transmission line cooled to cryogenic temperatures allowing characterization of the field to full current. The remainder will be measured with the transmission line at room temperature. During initial stages of production when the fabrication rate is lower, we will cold test all magnets. As rates approach one magnet per day, the fraction of total magnets cold tested will be determined by test facility capacity and test needs as indicated by initial results.

We first discuss a conceptual design for a magnetic measurement system to be used for the combined function magnets. We then follow with a brief overview of the approach to cold testing and conclude with a few remarks on other test and measurement considerations.

### 5.1.7.1 *Measurement System*

As described above, magnetic measurements are the primary concern of the test program. While one would expect to perform an extensive series of measurements, possibly using several measurement techniques, during the R&D phase of magnet development, we have chosen to present here one concept for measurements of production magnets. This concept utilizes a rotating coil. We define the most important issues related to this concept and examine the consequences. A brief discussion of other approaches follows.

The main parameters of the arc dipole magnets are ~2 T field,  $\leq 12\%$  horizontal gradient, 65 m length, and 20 mm gap. Measurement of the integrated dipole field is needed with an accuracy of a few parts in  $10^4$ . Desired measurement accuracy for the higher order harmonics is 0.1 units.<sup>1</sup> We begin by examining the implications of requirements for field strength measurements. Based on this discussion we present a concept for a measurement system. Given this system we then address the issue of measurement of field harmonics.

With respect to measurement of the integrated field strength, there are two issues. The fractional accuracy of the measured field goes as  $\Delta R/R$  where  $R$  is the radius of the rotating coil [39]. This requires that the radius of the probe be known with high accuracy. Typical manufacturing and measurement uncertainty for coil placement in magnetic measurement apparatus is ~0.001 inch (25  $\mu\text{m}$ ) which translates into a field error of 0.3% for a probe of 10 mm maximum radius. At least an order of magnitude greater precision (0.03% strength error) is required. This level of precision can only be achieved using a calibration magnet in which the strength is known at least as well as one need know it in the subject magnets.<sup>2</sup> The second issue is unique

<sup>1</sup> One unit of harmonic corresponds to  $10^{-4}$  of the main field, measured at a reference radius (in our case) of 1cm.

<sup>2</sup> Calibration in both a dipole and quadrupole magnet are required due to the large gradient which we want to measure with high accuracy.

to measurement of combined function magnets. Due to the horizontal field gradient, an error in the horizontal position of the probe translates into an error in measured field strength. In a magnet with 10%/cm gradient, measurement of the strength to 5 parts in  $10^4$  requires positioning the probe with 0.05 mm accuracy after averaging over the length of the magnet. Although difficult, this can be achieved using mechanical fixtures referenced to the magnet laminations. Vertical placement of the probe is not as critical.

The main conclusions from the preceding discussion are that (1) a rotating coil of the size we are considering can be calibrated with sufficient precision, and (2) that the horizontal position of the probe can be set to the required accuracy with mechanical fixtures. For reasons we list below, we choose to insert the rotating probe into the aperture from the side rather than from the end. The probe is supported on a frame attached to the magnet as shown in Figure 5.29.

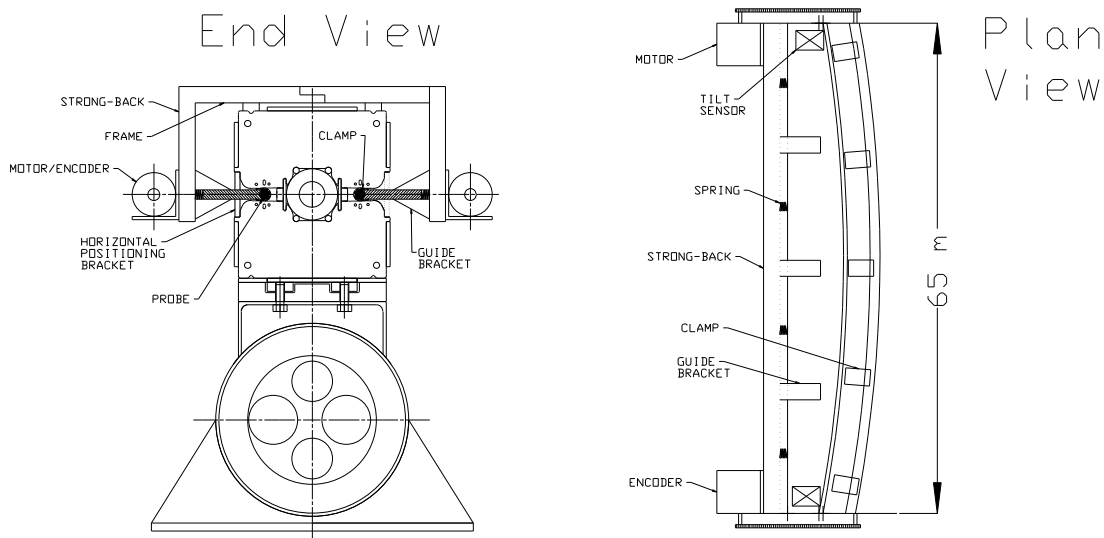


Figure 5.29. Measurement fixture. Note that the magnet sagitta is highly exaggerated.

Principle elements of the design are the following:

- The probe body is clamped to a precisely machined fixture ('strong-back') on an edge which follows the magnet sagitta.
- The strong-back slides horizontally in a series of guide brackets ('jaws') attached to the vertical member of the frame. The strong-back is spring loaded so that it and the probe are forced against the magnet laminations at the edge of the magnet gap, referencing the horizontal probe position with respect to the laminations.
- The vertical position of the probe is defined by the precision with which the frame is attached to the magnet and the precision of the jaws relative to the vertical member of the frame and the horizontal surfaces of the strong-back. A tilt sensor is mounted on the strong-back to monitor its alignment.
- The motor for rotation and encoder for probe angle readout are mounted on the frame and connected to the probe by a mechanism such as a toothed belt or right angle drive. Other drive components could also be mounted outside the magnet bore (e.g. gearboxes).

- Development of slip rings small enough to fit the probe bore is assumed although one might choose to digitize and transmit the signals from inside the bore. A pre-amplifier circuit sized to fit the bore is also assumed allowing a boost in signal size.

A consequence of insertion from the side is that one loses a few extra mm of probe radius due to the reduction in gap at the magnet edge of the focusing magnet. One also needs to allow space for the clamps holding the probe to the strong-back and for clearance during insertion.

Given a probe radius, we need to examine the accuracy of the measurement of field harmonics. From [41] we see that probe calibration matters little in measuring error harmonics. Accuracy of 10% or so is adequate. This requires knowing the probe radius to 0.1%. What is of greater interest is the evaluation of the interplay of signal size with harmonic measurement. This has implications for the required level of excitation current during test. For a reasonable set of probe parameters, pre-amplifier gain of 100, measurement accuracy of 0.1 unit through  $n=9$  requires at least 200 A excitation current [41]. This should be possible for room temperature measurements. We would no doubt increase the gain and run at the highest tolerable current for increased accuracy. Hysteretic effects in the steel may be the limiting factor in the measurement accuracy at this low field ( $\sim 70$  Gauss, or 1/15 of the injection field).

A probe length of 6.5 m was assumed above. Ten measurements are then required to construct the integral field. The time required for measurement is estimated as 2.5 hours with 2 crews of 3 technicians using 4 sets of measurement apparatus [41]. This certainly allows for the required production throughput. Automation and optimization of procedures will reduce the time required. We also note that the apparatus described could be used for either warm or cold measurements. The only special consideration for cold measurements would be to construct the strong-back of a nonmetallic material to prevent the formation of eddy currents during ramping.

We have chosen a probe inserted into the magnet bore from the side and supported by an external frame. An alternative approach would be a “mole.” This probe type, having drive and angular alignment systems built in, was developed for measurements of SSC [42] and LHC magnets [43]. The obvious advantage of this approach is that the probe can be larger by as much as 25% as insertion is from the magnet end rather than the side. A larger probe produces larger signals. However, development of drive apparatus operating in a strong magnetic field is neither trivial nor cheap. We have no doubt that this could be done; however, we have chosen a simpler approach that removes elements of the measurement system other than slip rings and pre-amplifiers from the bore accepting as a consequence somewhat smaller signals.

### 5.1.7.2 *Cold Testing*

As a quality control measure and to characterize the magnetic field of a sample of the magnets to full current, we plan to cold test at least 10% of produced magnets. The peak rate of 2 magnets built per day requires 1 magnet cold test per week. Cooldown and warmup times are short (about an hour) due to the low cold mass, so testing time will be dominated by setup and measurement times. If an accurate measurement of the heat leak is required, it may take a couple of days for the multilayer insulation and vacuum to stabilize.

As discussed in the introduction, quench training is not a significant issue for the superferic design employed. However, it is important to have a full set of field measurements of magnets produced early in the program to check the overall design, iron saturation, yoke

fabrication, and related effects on the field quality and transfer function. This increased testing also produces a statistically significant warm-cold correlation for the field harmonics. As the production rate rises, measurements check mechanical properties of the magnets as well as properties of the materials used to build them; and the set of measurements can be reduced to those necessary for quality assurance.

The cold parts of the magnet are the transmission line and return bus and their relatively small cryostat. Refrigeration requirements are modest; cool down and warm up times, short. The associated test equipment – cryogenic end boxes, transfer lines, pumps, and refrigerators – is simple and inexpensive when compared to facilities developed for testing ‘conventional’ superconducting magnets. Cold testing can be done in a small area in the production facility in conjunction with warm measurements rather than in a large, separate cold test laboratory. The actual time spent in hooking up, cooling down, testing, warming up, and disconnecting the magnet is small when compared with conventional superconducting magnets. A peak production cold test cycle occupying the test stand for one five day week would allocate a two shift day to each of these tasks: installation and connection of the magnet on the stand, cool down, testing, warm up, removal.

### 5.1.7.3 *Other Testing Considerations*

One of the difficult issues in design and construction of a magnet system of the scale proposed is the understanding of its overall reliability. Failure rates for the magnets must be very small if collider availability is to be kept at the level necessary to carry out the physics program. Determining failure rate is itself a difficult task as it is unrealistic to plan for the number of tests necessary to ‘prove’ that the magnets as constructed will meet the lifetime reliability requirements for the collider (even assuming that we could agree on a ‘proof’.) However, since the iron yoke design and peak fields are similar to conventional magnet designs in use for decades, we do not envision reliability problems here. Key components will be subjected to ‘lifetime’ testing – equivalent magnetic and thermal cycles (if appropriate) –to verify that they meet requirements. While it is impossible to argue the statistical validity of a small sample of test magnets, accelerated life testing of a few early magnets will be used to validate design and provide feedback early in production should any degradation in performance be detected.

### 5.1.8 **Magnet Installation**

More than three thousand 67.75 m superferric magnets and their associated subsystems must be installed in the arcs of the 233-km accelerator ring. This installation must be tightly coordinated with tunnel excavation, outfitting, and magnet manufacturing. The scale of this work and the difficulty of subsequent maintenance require techniques that ensure high quality installation resulting in high reliability of the accelerator.

In addition, about 1000 conventional magnets (Section 5.1.5) are to be installed in the local straight sections and two transfer lines. This installation is comparable to existing accelerators, nearby to surface access, and less constrained by schedule.

The baseline assumptions adopted for the arc magnet installations are:

- Beneficial occupancy of the tunnel takes place after the tunnel is dry and safe. Specifically, the excavation, muck removal, roof support, grouting, ventilation, sump installation, emergency egress systems, etc. should be complete.
- The first installation activities complete the safety and transportation infrastructure. These include emergency and work lighting, communication, environmental safety monitoring, and trolley power lines for transport vehicles. At this point the tunnel can be used by workers without extraordinary training.
- The second phase of installation provides infrastructure in advance of actual magnet installation. This includes magnet stands, power cables, local electronics modules, helium gas return header, and a sufficiently accurate survey and alignment network.
- Magnets are transported into the accelerator tunnel one-by-one and installed onto pre-aligned adjustable support stands. The magnets arrive with the majority of subassembly installation and test work completed at the factory. Specifically this includes transmission line and cryogenic pipe assembly and test, hi-pot and vacuum tests, vacuum system bake out, and cable installation and instrumentation checkout on the magnet (Section 5.2).
- Final installation of each magnet into the string involves: 1) rough alignment; 2) making the necessary interconnections for the transmission line, beam pipes, cryo-pipes and vacuum jackets; 3) installation of the skid containing the corrector magnets; 4) connection of the magnet cables to the electronics modules, 6) testing of the corrector supplies, instrumentation, and network readout, and 5) final alignment.
- System checkout proceeds in phases. 1) a re-verification of the electrical network, high-pot test, and beam vacuum tightness is performed after each half-cell is assembled; 2) the insulating vacuum is tested after installation of each vacuum break (every 8 magnets or 540 m), a cryogenic performance and current load test is performed after each 10-km magnet string is completed

A basic constraint on the installation is that it be consistent with the addition of the Stage-2 magnets at a later time. Since the second stage High Field Ring will modify tunnel layout, we must consider this upgrade while planning the Stage-1 work so that installed equipment will not make this upgrade too complicated. A tunnel cross section with both Low Field and High Field accelerators installed is shown in Figure 5.30.

### 5.1.8.1 *Tunnel Infrastructure Installation*

Before magnet installation a number of systems must be completed. Hangers must be mounted for the cable trays, transport trolley rail, and the helium gas return header. Alignment requirements for these hangers are in the 2-5 cm range and can be provided with the construction survey monuments at quad locations, and stretched strings or lasers for the alignment of intermediate brackets.

The baseline scenario uses manual labor and generic unit costs for bracket and piping installation. However, opportunity exists for optimizing the process. Repetitive bracket installation could take place with automatic drilling, installation, and bolting equipment. Long sections of pipes, trolley rail, and cable trays could be preassembled in the magnet factory and placed on

these brackets with a long vehicle and mechanical assists, thereby minimizing the number of in-tunnel pipe welds, trolley rail joints, etc.

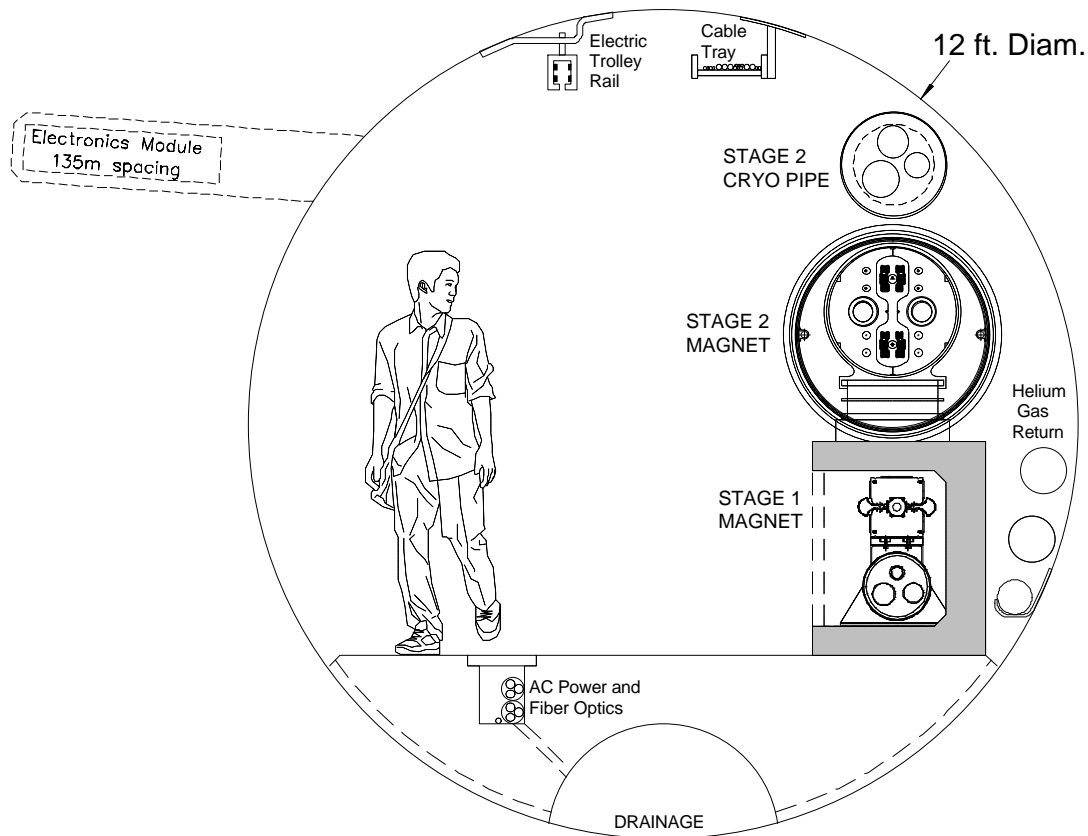


Figure 5.30. Tunnel cross-section after the Stage-2 upgrade. The evolution of the tunnel from Stage-1 to Stage-2 is shown in Figures 2.4 and 2.5.

Cable laying required in the tunnel is minimized as described in Section 5.2.3.2. Long-distance (10 km) power cable and optical fiber runs are laid in a trench in the floor by pulling a trailer with a large spool. Power and fiber connections to the electronics modules every are made by unspooling long vendor-supplied harnesses with prefabricated breakouts every 135 m. Waxed-wire fire safety cables are suspended from the cable tray near the top of the tunnel.

The time at which electronics modules are installed and commissioned is somewhat flexible. The modules should be functional by the time of final magnet checkout so that they can be used to monitor insulating and beam vacuum, temperature, etc. If they play an important role in tunnel communications and environmental monitoring they should be installed earlier. An early installation date encourages earlier system debugging, but an electronics design frozen several years before project completion will be painfully obsolete by the time of commissioning.

Prior to magnet installation, survey monuments must be embedded into the tunnel wall with positions known to sub-mm accuracy, as described in Section 7.7. Magnet support stands are pre-installed and aligned to the accuracy of  $\pm 1$  mm in both transverse planes.

### 5.1.8.2 Tunnel Transportation System

An electric trolley system with rubber-tired vehicles is chosen for transport of magnets and personnel. The system is similar to that recommended for the SSC [44] and also chosen for the LHC [45]. An overhead enclosed safety rail [46] operating at 400-750 VDC [47] provides power for magnet tractor/trailers, personnel transport vehicles, and temporary power for installation work lights, welding, etc.

The 30 ton magnet weight is less than the 35 ton LHC magnet so vehicle power requirements are similar. Drive requirements are 30 kW assuming a total vehicle weight of 50 tons, a rolling coefficient of friction of 0.02 [44], a drive train efficiency of 85% and a peak speed of 2.5 m/sec (9 km/h). Trolley power up to 100 kW is supplied at the 10 km alcoves, allowing up to three vehicles to operate simultaneously in each 10 km sector. Copper conductors  $\sim 1 \text{ cm}^2$  are required in the rail to limit line losses to  $<10\%$ . Details of the magnet transportation vehicles are discussed in the next section.

In addition to the overhead rail, limited battery power allows the vehicle to traverse unpowered regions such as splices and equipment bypasses. The battery is continuously recharged during normal operations. In emergency situations battery power is sufficient for the transport tractor to drop the magnet and travel 5 km to the personnel egress points.

Personnel transport vehicles similar to [44] will provide emergency egress, fire and ODH refuge, work break and sanitary facilities for installation crews.

### 5.1.8.3 Magnet Handling and Transportation Considerations

Because of the unprecedented magnet length and flexibility, careful attention must be devoted to their transportation from the factory to the place of installation in the tunnel. Magnets will be handled and transported using specially designed fixtures to prevent excessive stress concentrations and damage.

Allowable limits on local static deformation and torsion of the magnet are shown in Table 5.17. In the first three cases in the table, a force (or force couple) was applied to a single set of magnet support/adjusters while the magnet cross section was held fixed  $\pm 6 \text{ m}$  away at the position of the adjacent magnet supports.

Table 5.17. Limits of relative displacement of magnet parts over  $\pm 6\text{-m}$  length.

Mode	Allowable range	Limitation type
Horizontal	$\pm 3 \text{ mm}$	Relative displacement of upper and lower magnet halves is more than $100 \mu\text{m}$
Vertical	$\pm 4 \text{ mm}$	Stress in magnet structural elements exceeds safe fraction of yield limit
Twist	$\pm 16 \text{ mrad}$	Stress in magnet structural elements exceeds safe fraction of yield limit
Smooth Bend	$\sim 1 \text{ km}$ Radius	Stress in magnet structural elements exceeds safe fraction of yield limit

Taking into account its length, the magnet structure is quite flexible. The vertical sag can exceed the safe limits from the above table, just due to its own weight, if one of the supports is removed. On the other hand, a smooth continuous bend with 1 km radius of curvature produces a 50 cm sagitta in the magnet with acceptable internal stresses. To significantly reduce the risk of magnet damage during transportation, a 60 m long aluminum “lifting fixture” frame is used. The frame increases overall rigidity and protects the magnet from vertical bending damage. Figure 5.31 shows the frame moving inside the tunnel. Figure 5.32 shows the “A-Frame” structure of the beam that permits it to be either lifted or driven off of the magnet.

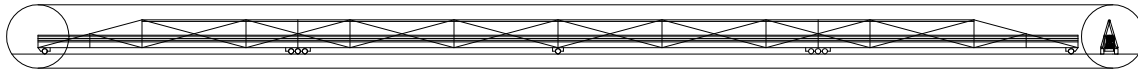


*Figure 5.31. Magnet transportation frame, which acts as a “lifting fixture” to uniformly support the magnet and prevent stress concentrations during transport and installation. The frame is stiff enough to allow the magnet to be picked up and supported at two points without damage. The major load is taken by the two sets of wheels at the 25% and 75% points, with other smaller wheels to damp oscillations.*

During transportation, dynamic loading effects have the potential to increase stress levels in the magnet. During transportation and installation, it is necessary to monitor and correct relative displacement of magnet parts to the limits well below those of Table 5.17. This is accomplished with an active shock absorber system. Several non-powered wheels installed along the frame use position controlled hydraulic cylinders to support the frame with the magnet inside during transportation. Inclinometers installed on the carts provide needed information to a feedback system about relative position of the neighboring carts. Accelerometers installed near critical points on the magnet detect any mechanical oscillations and slow down or stop transportation if any danger to magnet is suspected. Through the coordinated action of the cylinders it is possible to lower the magnet to its final destination in a controlled manner. This system is also effective at limiting vertical deflections when the transportation vehicle enters and exits the 4% slope of the installation ramp.

Two motorized trucks on both sides of the frame, each with engine power of 60 kW and a typical operating power of 15 kW, pull the frame during transportation from production facility to the designated location in the tunnel. An alternative (chosen by the SSC and LHC) is to use a general-purpose towing tractor pulling a passive magnet trailer. This allows the towing vehicle to be used as an egress vehicle if the personnel transporter fails.

An automatic guidance system is desirable to reduce the chances of pilot error on monotonous drives through the tunnel. The simplest system can use the overhead electric rail as a position reference. Another option, chosen by the LHC, is to use the magnetic field of a guide wire buried in a groove in the floor. Ultrasonic position detectors that sense nearby walls are commonly used on mobile vehicles in factory automation. These require no tunnel infrastructure and provide automatic shutdown if unexpected obstructions are encountered. These have been successfully tested in robotic tunnel guidance experiments undertaken as part of VLHC R&D at Fermilab [48].

#### 5.1.8.4 Initial Magnet Installation

The installation scheme shown in Figure 5.32 corresponds to the simplest case when magnet installation occurs with a clear space upstream or downstream of the installation point.

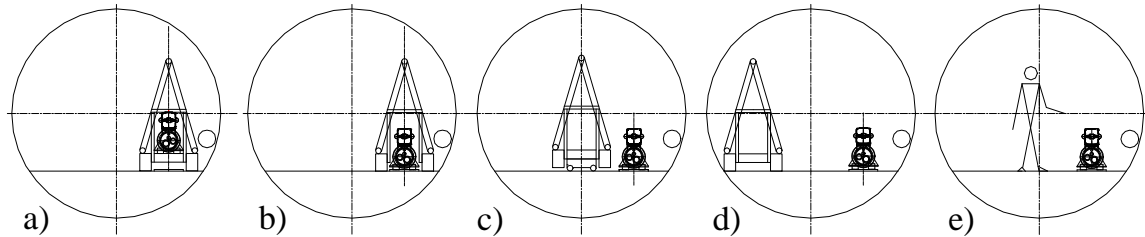


*Figure 5.32. Initial installation scheme that is possible when the upstream or downstream magnet slot is empty. Installation vehicle a) drives up to the location along the beam line, b) deposits the magnet on the pre-aligned stands, and c-d) departs by initially moving along the beam line, then moving if needed to the center lane to pass any pre-installed magnets. Final connections e) may be made by separate work crews working off-shift or in different sections of the tunnel.*

Magnets are driven to their location along the beam line and put on the support blocks without any transverse movement (Figure 5.32b). Unloaded frames are then backed out along the installation pathway (c). In this case, each next magnet can start its movement to the assembly place without waiting for the unloaded frame and the transport vehicles. Two magnet transport vehicles and an escape or a crew delivery vehicle can move in the tunnel simultaneously and independently. This scenario provides maximum flexibility for organizing optimal delivery traffic.

### 5.1.8.5 Magnet Interconnections

Three different types of interconnections are to be made after magnets are installed. First, the two 67-m magnets in each half-cell must be connected to form a common electrical, cryogenic and vacuum system. See the right-hand side of Figure 5.11. This is a “hard-welded” joint with no bellows in the vacuum shell, cryogenic piping, or beam pipes. There is a 1-m space available for this interconnection. Second, at the half-cell points (Figure 5.11) the superconducting transmission line dog-legs downward into the cryo service pipe enclosure to clear a 3.5-m space for conventional correction magnets. Finally, in the straight sections where special magnets are installed there is need for several modes of transmission line positioning. The interconnection scheme does not differ greatly among these cases (see Section 5.1.2.3).

The basic steps of this procedure are listed below:

- connection of the transmission line inner Invar pipes for both drive and return lines
- splicing of the superconducting cables
- installation of electrical insulation and performing a high-pot test
- connection of cryogenic piping
- installation of the 50 K screen and superinsulation
- sealing and leak checking the insulating vacuum.

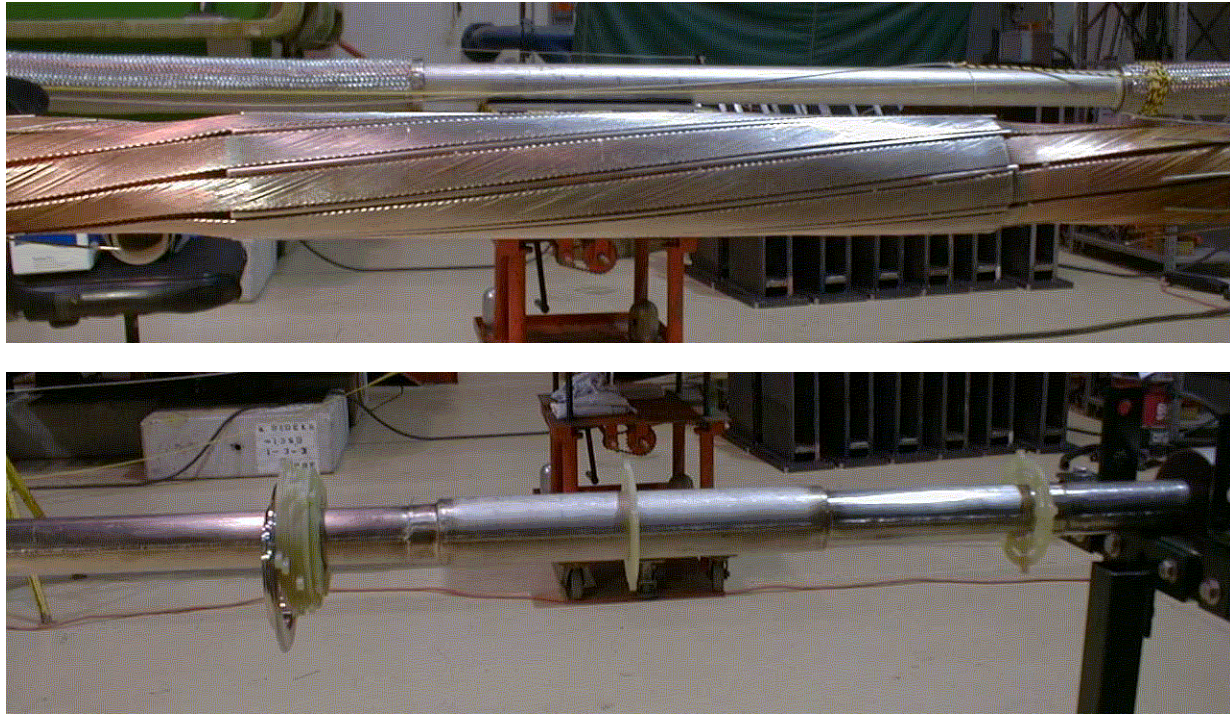


*Figure 5.33. Splice of 100-kA conductor on 17-m test loop. Top: soldered spiral-wrapped cables. Bottom: completed interconnection after weld and leak check complete.*

Automatic welding machines will produce high quality vacuum-tight connections of all helium pipes. An appropriate fixture for the 100-kA conductor splicing between the magnets must be designed and thoroughly tested to guarantee 100% reliability for these connections. The magnet interconnection appears to be the most labor-intensive procedure in the process of magnet installation, so R&D could profitably be devoted to making this procedure simple. A high voltage test (5 kV to ground) is to be made for each magnet before final closing of the external vacuum jackets of the interconnecting boxes.

#### 5.1.8.6 Corrector Magnet Skids

In the baseline scenario, a skid containing six corrector magnets is installed at the 3.5 m gap between half-cells (every other magnet or 135 m). These magnets are factory assembled and pre-aligned on a common support structure, with beam pipes, BPMs and bellows installed in the magnet gaps. All correctors and beam instrumentation will be electrically tested and cabled at the factory as described in Section 5.2.3.2. A description of the correctors can be found in Section 5.1.3. A total of 1568 corrector blocks will be transported and installed. A single magnet transport vehicle can carry 16 skids, so ~100 trips are required. A two-ton capacity fork lift or equivalent hydraulic fixture will be used to install the corrector magnet blocks on their support stands. The skids will be aligned via locating pins in the previously aligned laminations of the arc magnets. Then beam pipe interconnections can be made following by a vacuum leak test.

Depending on the number of cryogenic problems encountered it may be desirable to defer corrector and beam vacuum installation until cryogenic system testing is completed.

### 5.1.8.7 Magnet Replacement

A more complicated mechanical situation arises in the (hopefully rare) situation that a magnet needs to be replaced after installation, or is installed as the last magnet in an otherwise complete arc. In this case the magnet will be transported parallel to the magnets that have already been installed (Figure 5.34 a; installed magnets are not shown). Using hydraulic and control systems on the transportation trailers, the magnet will be lowered down to temporary support stands installed beneath the carts (b). After the frame is removed (c), the magnet is to be shifted horizontally and placed on the permanent stands with the use of a specially designed hydraulic pulling system connected to the permanent support blocks (d, e). Control equipment similar to that used during transportation will synchronize the system during this operation. This procedure will also be used to replace a Stage-1 magnet after Stage-2 installation is complete.

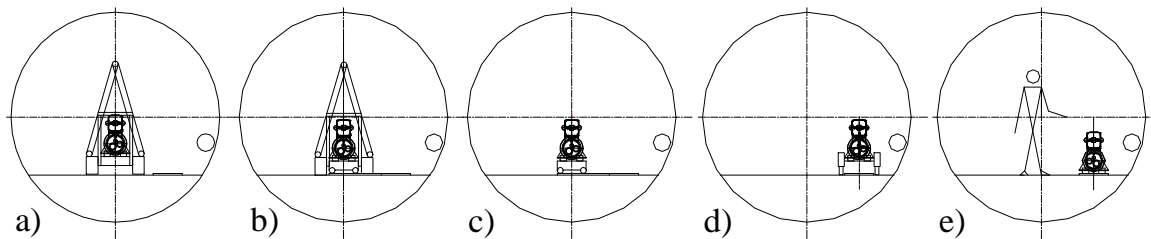


Figure 5.34. Magnet replacement scheme.

Magnet replacement will require the following work at the magnet interconnects:

- backfill the beam and insulating vacuum sectors with dry nitrogen and cut off beam pipes of the replaced magnet
- open the connection space
- remove super-insulation
- cut all the cryo-pipes and transmission lines of a the magnet to replace
- remove replaced magnet moving it horizontally out of the magnet string
- install new magnet following the repair scenario of magnet installation
- make interconnections as described above.

A reasonable goal for the magnet replacement procedure is to complete it during one 8-hour shift of multi-crew work. Pump-down and leak checking operations may extend this time. The overall magnet replacement time will be dominated by cryogenic warm-up and cool-down.

### 5.1.8.8 Arc Magnet Alignment

During installation, the 65-m magnet is bent in the horizontal plane to the radial position predefined by the pre-aligned support stands. It is assumed that the support stand rough alignment is done with the help of a semi-automated surveying system using available survey monuments in the tunnel.

Arc magnets are ready for final alignment after correction magnets are installed and vacuum pipe interconnections are made. Each magnet must be installed so that the magnet reference center is within  $\pm 0.25$  mm from the nominal orbit position. For each magnet, an

acceptable roll angle is less than 1 mrad rms or less per adjuster. Conventional optical techniques (theodolites and laser trackers) for alignment have angular errors in the range of 10 microns per meter, corresponding to  $\pm 300$  microns at the magnet ends from a setup at the center of the magnet. This would be marginally adequate to meet the magnet alignment specification of 250 microns rms over the length of the magnet. However this accuracy can be exceeded using the hydrostatic leveling and stretched wire techniques described below.

For each magnet there will be a support every 6 meters with horizontal, vertical and roll adjustment capability. The magnets will be built “laser straight” in the factory. The magnets will be installed in the tunnel with a 15.57-mm sagitta over the 65-meter length. The stiffness of the magnet will allow an independent range of motion of approximately  $\pm 3$  mm horizontally or vertically at each adjuster. Motions outside this range will require coordinated movements of nearby adjusters. The magnet position will be roughed in using optical techniques along the beam line relative to the internal tunnel network. At each of the support stands there will be a *hydrostatic leveling pot* for vertical alignment, a *capacitive stretched wire pick up* for horizontal alignment, and an *electronic gravity sensor* for roll. As the adjustment screws are turned there will be real time readout of both systems to allow for the positioning of each segment of the magnet. A  $\pm 3$  cm range of the adjusting screws will be sufficient to put in the sagitta and to compensate for installation errors in the magnet stands as well as drift and settling of the tunnel ( $\pm 1$  cm maximum) over a 20-year lifetime.

**Vertical alignment** can be made using a hydrostatic leveling technique, which makes use of fluid-filled containers with capacitive readouts. This technique allows vertical alignment within  $\pm 100$   $\mu\text{m}$  for each magnet. For larger scale, corrections taking into the account non-uniformity in the Earth’s gravitational field must be made. This will require careful study of the Geoid and the change in the density of the earth in the region of the machine. Corrections to the vertical can then be imposed on each magnet.

**Magnet roll** can be adjusted using a technique similar to the one used during leveling of the magnets. It can help to establish a real time display of the roll of the magnet at each adjustment station. Given a base support of 500 mm and a resolution of 2 microns for the hydrostatic levels a roll angle of  $\pm 4$  micro-radians is achievable. This exceeds the 1 mrad requirement for acceptable vertical closed-orbit distortion.

**Horizontal alignment** is done using the stretched wire technique. A small diameter (less than 1 mm) copper beryllium wire mechanically attached to both ends of the magnet forms the reference base. Two wires separated vertically can be used to increase the signal to noise ratio. Using capacitive pickup electrodes at each support stand, it will be possible to adjust the horizontal position of each magnet to the desired accuracy. Alignment of the entire 65-meter magnet to within  $\pm 100$  microns should be possible. To set the sagitta of 15.6 mm for the magnet all the adjustments must be made at the same time. Starting with optical tooling the rough sagitta can be set to an accuracy of  $\pm 300$  microns. Once this is done the stretched wire system can be installed. Each capacitive pick up will have a different offset from the magnet to account for the sagitta. The final adjustment will involve moving all adjusters at the same time.

A degree of automation is possible. The simplest approach is for the person at the central display of magnet alignment data to give directions to one or more workers with wrenches. A more sophisticated alternative is to manually place motorized wrenches at each of the adjusters, then run automated software procedures to bring the entire magnet into alignment. If these

systems were permanently installed and coupled with motorized adjustment stands they could be used as an active alignment that continually aligns the magnets as the machine runs. Beam position monitor information could also be used.

#### 5.1.8.9 *Straight Sections and Transfer Line Installation*

Special magnets of several types are to be installed in the ten straight sections and two beam injection lines (see Section 5.1.5). Straight section focusing quadrupoles and injection line dipole and Lambertson magnets are conventional magnets. The maximum weight of these magnets does not exceed 5 tons and their length is less than 6 meters, so they are installed on their support stands using conventional techniques.

Separation/recombination dipoles and the abort Lambertson use the transmission line for excitation. To minimize labor related to cryo interconnections, these magnets are assembled in the tunnel by installing steel magnet cores around preinstalled transmission line and vacuum pipes. Individual pieces have lengths up to 6 meters and weigh less than 5 tons. Dipole alignment is non-critical but the Lambertson septa must be accurately aligned.

Finally there are eight 10-meter, superconducting, high gradient, low-beta IR quadrupoles described in 5.1.4. Each quadrupole will weigh about 25 tons and is rigid enough to be transported to the place of installation using two high load trailers and two transport vehicles of the type used for the arc magnet transportation. The alignment requirement for these quadrupoles is  $\pm 100 \mu\text{m}$  so two adjustable support stands will be used. The alignment procedures are complicated by the presence of the detectors and could be similar to those used at the LHC.

Because sections that use special magnets are located closer to the Fermilab and Far Side sites than accelerator arcs, installation of these magnet can be done independently of the installation of arc magnets.

#### 5.1.8.10 *Installation Schedule*

The number and size of working crews needed to install the magnet in a 3-4 year term has been estimated. Several crews must work simultaneously to make the total installation time acceptable.

At least two access points at the opposite sides of the ring are required. The simplest magnet delivery scenario can be realized when assembly starts from the middle of the half-arcs connecting Fermilab site and Far End site and goes in four directions simultaneously. If magnet replacement is required after the magnet string is installed, a more complicated scheme must be used. In this case magnet traffic will go down the tunnel with already installed magnets, and additional measures must be taken to allow parallel work of an assembly crew. The magnet installation procedure in this case also is more complicated because it requires magnet movement across the tunnel.

Because of a high average magnet transportation distance inside the tunnel (about 30 km), only one magnet per day can be installed by each installation vehicle. Connection of the installed magnets in a string can be made simultaneously for several magnets.

### 5.1.8.11 *System Commissioning*

The described procedure will ensure interconnections of a high quality; nevertheless, after each 20-km magnet string assembly is completed, a cryo-test must be performed. This cryo-test will involve a pressure test, relief valve setting tests, magnet string cooling down, heat leak measurement, and transmission line current test. Cold vacuum leaks could be detected at this point. Cryogenic plant performance and magnet string quench tests will be also conducted.

A temporary installation of the 100-kA holding supply and current leads (Figure 5.42) easily fits in the underground caverns eventually intended for the Stage-2 dump resistors. The 2.5-V holding supply will ramp a 20-km magnet string to 100 kA in 40 minutes. This allows full-current testing of a complete quench protection cell of the accelerator.

The beam pipes are interconnected after the cryogenic test passes and the correction magnet block is installed. Because the system is not baked *in situ*, the static vacuum will improve steadily over time and it is desirable to have most of the system under vacuum for as long as possible before collider ring commissioning.

## 5.2 Accelerator Systems

The systems distributed around the ring circumference include cryogenics, arc instrumentation, corrector power supplies, and beam vacuum systems. The “once per turn” systems are located primarily in the straight sections on the Fermilab site. These include RF, injection, extraction, and once-per-turn instrumentation.

A completely conventional approach is taken to the standard utilities in the straight sections. Warm iron/copper magnets use LCW cooling and standard power supplies. Electronics and major power supplies are located in underground shielded instrumentation rooms that are accessible with beam on. A larger tunnel, conventional power systems, and generous cable trays provide the infrastructure for RF systems, injection and extraction kickers and Lamberts, beam crossovers, beam halo scraping, beam current and beam profile monitoring. Concentration of these major subsystems at the Fermilab site makes maintenance and accessibility requirements similar to other Fermilab accelerators. These systems are modeled on existing designs from recent projects for which the specifications and costs are well known.

Four distributed systems contain notable new features which will be described in some detail: the cryogenic system which is smaller and simpler than comparable systems, the beam stop which must deal with the large kinetic energy in the beam, the arc instrumentation which is distributed as electronics modules in “holes in the wall” at each quad location, and the beam damper system which is distributed around the ring circumference.

### 5.2.1 Cryogenic System

#### 5.2.1.1 *Cryogenic System Description*

The magnet’s superconducting transmission line is cooled by pressurized supercritical helium at 4.5-6.0 K. The heat load of the magnet system is removed by the sensible heat of the

supercritical helium stream. The fluid operates just outside the critical region expanding the helium stream as it passes through the transmission line, producing a large effective heat capacity. The tunnel cryogenics are an all-piping system with very simple topology. Figure 5.36 shows the temperature profile in the transmission line.

The Stage-1 cryogenic system is significantly simpler and lower-powered than the LHC or SSC systems. A rough comparison of the cryogenics of various machines, normalized to beam energy, is given in Table 5.18. For this comparison, the refrigeration for the SSC operating at  $L=10^{34}$  was crudely estimated by adding the synchrotron load scaled from the VLHC.

Table 5.18. Comparison of cryogenics per TeV beam energy for various machines.

		<b>Tevatron</b>	<b>HERA</b>	<b>LHC</b>	<b>SSC(<math>10^{33}</math>)</b>	<b>SSC(<math>10^{34}</math>)</b>	<b>VLHC-1</b>
<b>Refrigeration (4.5 K eqv.)/TeV</b>	kW/TeV	27	38	21	10	12	4
<b>Helium Inventory/TeV</b>	tons/TeV	4	21	14	16	16	4
<b>Cold Mass/TeV</b>	tons/TeV	600	5,000	5,143	5,000	5,000	286
<b>Magnetic Stored Energy/TeV</b>	MJ/TeV	400	1,000	1,629	600	600	171

As shown in Figure 5.35, cryogens are fed from six refrigerator plants spaced at 38-km intervals around the ring. For efficiency reasons, refrigeration is provided at two temperature levels. Refrigeration at a higher temperature range (40-70 K) provides cooling for a heat shield that is used to intercept much of the heat that would otherwise be absorbed by the lower temperature superconductor. Each plant provides refrigeration for an upstream and downstream magnet string 19-km long. Each string is sub-divided into two loops, referred to as “near” and “far” loops.

#### 5.2.1.1.1 Helium Distribution System

The helium distribution system is designed to distribute refrigeration to the magnet system with a minimal temperature variation. The distribution system consists of cryogenic valve boxes, transfer lines, and warm helium header.

##### *Cryogenic Valve Boxes*

Cryogenic valve boxes are used to redistribute the helium between the conductor loops for steady-state operation and perform various transient state operations. These boxes are located every 9.5 km and house the control valves and instrumentation required for each circuit. Boxes vary in configuration dependent upon location in the magnet string. These boxes are relatively simple devices mainly providing a transition for flow redistribution.

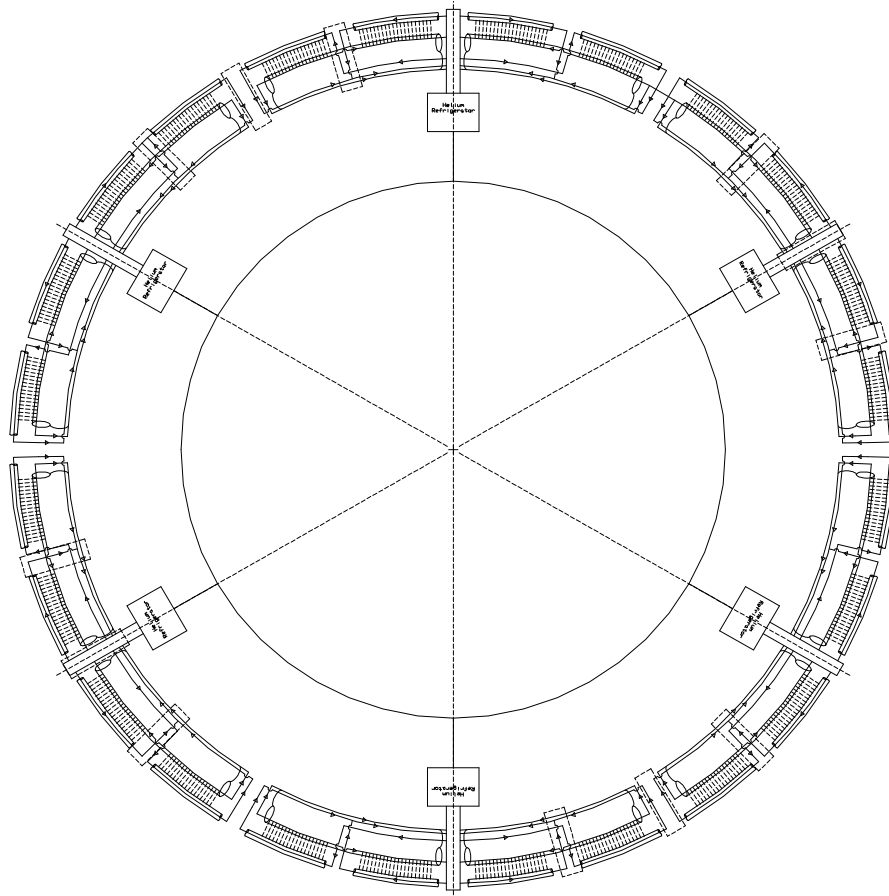


Figure 5.35. Cryogenic layout of the Stage-1 VLHC. Six plants are spaced at 38-km intervals around the ring. Each plant provides refrigeration equivalent to 9.6 kW at 4.5 K. Nominal operating wall power is 2 MW at each plant. One plant is on-site at Fermilab and has additional capacity for detectors, IRs, RF, and superconducting current leads.

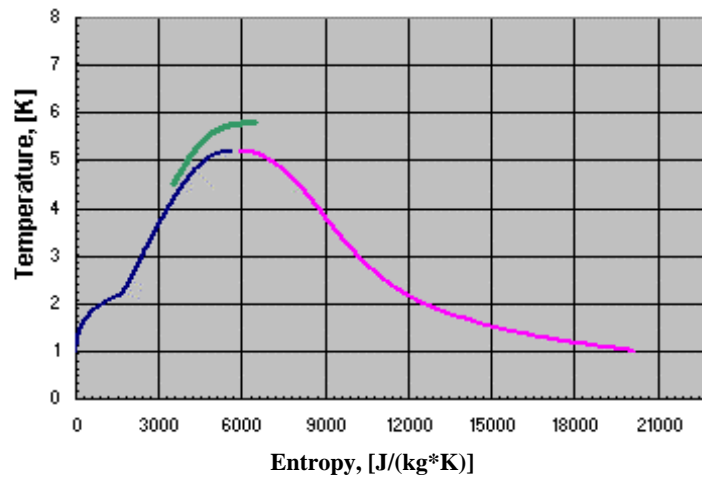


Figure 5.36. Temperature profile of the supercritical flow in the VLHC transmission line.

### *Cryogenic Transfer Lines Inside the Magnet*

Transfer lines are a part of the magnet assembly. A line contains five circuits: 4.5 K superconductor supply line (near loop only), 6.0 K superconductor return line, 40 K shield supply line, 70 K shield return line, and a vacuum circuit. Each section of transfer line is equal in length to a magnet (67.5 meters) and is attached to the magnet assembly as described in Section 5.1.2.3.

- The 70 K return line is a 0.102-m OD stainless steel pipe connected to an extruded aluminum shield that surrounds all the inner lines. The shield is wrapped with double-sided aluminized Mylar (dimpled and perforated). The longitudinal contraction of the line is compensated with guided formed bellows in the interconnects. During this shrinkage, the G-10 support structure is allowed to move within the vacuum space.
- The 40 K shield supply line is a 0.089-m OD stainless steel pipe supported on the G-10 spiders from the aluminum shield. Bellows are used at the end of each 67.5-m module to compensate for thermal contraction and expansion.
- The 4.5 K supply (near loop only) and 6.0 K superconductor return line are Invar tubes that are also anchored at the midpoint of the module. These lines are of concentric design. The 6.0 K helium flows between two concentric Invar tubes
- The 4.5 K supply line is suspended via G-10 spiders from a 6.0 K inner line.

#### *5.2.1.1.2 Helium Pressure Relief and Venting System*

Relief valves for each of the five circuits are located every 540 meters, as seen in Figure 5.37. These valves will vent into the warm helium header that is itself protected every 1 km at 3 MPa (30 bar) from over pressurizing. Each relief is conventional in nature and set to the MAWP of its given circuit. The primary need for these reliefs are for trapped volume and loss of insulating vacuum scenarios. The warm header is further protected at the refrigerator (above ground) at a set pressure of 0.2 MPa (2 bar), venting to the atmosphere.

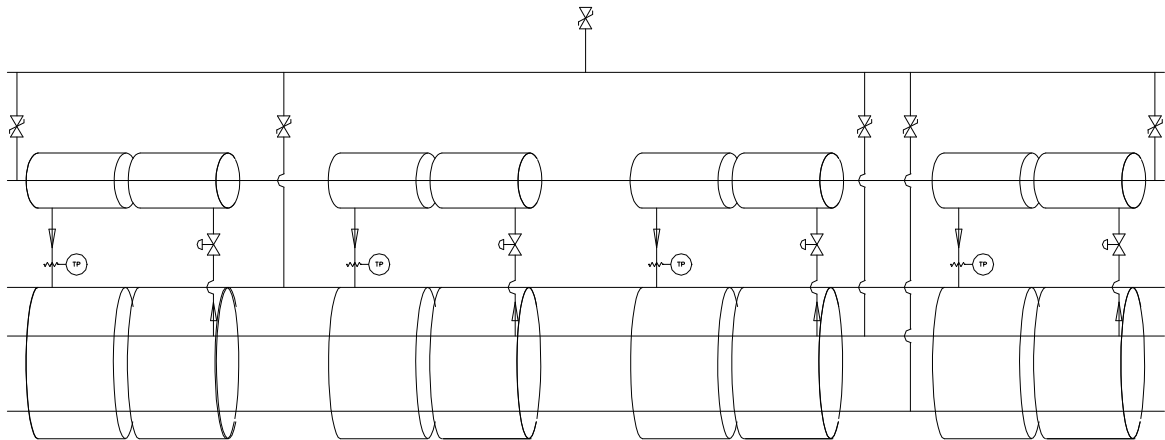


*Figure 5.37. Helium shield flow and pressure relief valves.*

Quench protection of the transmission line is discussed in Sections 5.1.2.2 and 5.2.2.3. The 100 kA transmission line conductor contains enough copper that it can be safely shut down with a 1 second time constant following a quench. A number of detailed quench simulations

have been performed. The peak temperature is  $\sim 250$  K. The worst-case peak pressure comes from a situation in which a mis-steered beam (kicker misfire) causes the beam to oscillate side-to-side in the beam pipe and scrape heavily in a series of locations separated by a half-betatron wavelength. In this case the peak temperature is unaffected, but a worst-case pressure occurs when the hydrodynamic shock waves from two adjacent quenches collide at the midpoint between quenches. The peak pressure is below the 4 MPa (40 Bar) pressure rating of the transmission line. Thus no helium needs to be vented anywhere, even for a long period following the quench. The pressure burst from the hydrodynamic shock wave, as registered on pressure sensors along the transmission line, should provide a convenient method of identifying where the quench occurred.

#### 5.2.1.1.3 Heat Shield Cooling System

Pressurized 40 K helium is used to intercept the radiation and conduction heat leak to the transmission line. Helium is supplied from the refrigerator at 1.7 MPa (17 bar) and returns at less than 70 K and 1.3 MPa (13 bar). Flow is supplied via a 0.089 m OD tube and distributed via a pair of 6 mm OD lines every 270 meters carrying 2.0 g/sec. This scheme provides shield cooling for every two magnets. Control valves and temperature sensors are included every 270 meters for heat shield flow control based on temperature requirements.

#### 5.2.1.1.4 Transmission Line Heat Load Estimates

Transmission line heat load estimates are divided into two components: the primary heat load on the 4.5 K system and the heat load to the 40 K shield system. The calculated heat loads are presented in Table 5.19.

Table 5.19. VLHC design study calculated transmission line heat loads.

		Primary 4.5K	Secondary 40K
<b>STATIC</b>			
	<i>Near Loop</i>		
	Mechanical Supports, [mW/m]	53	670
	Superinsulation, [mW/m]	15	864
	<i>Far Loop</i>		
	Mechanical Supports, [mW/m]	53	670
	Superinsulation, [mW/m]	13	864
<b>DYNAMIC</b>			
	Beam Loss, [mW/m]	2	1
	Superconductor Splice, [mW/m]	7	-

#### 5.2.1.1.5 Cryogenic Loads for On-Site Refrigeration Plant

The extra loads for the on-site refrigeration plant are summarized in Table 5.20. The total refrigeration power (4.5 K equivalent) is comparable to a single additional cryo plant.

Table 5.20. Extra loads for the on-site refrigeration plant.

	4.5 K (static)	4.5 K (dynamic)	40 K (shield)	Liquefaction (g/s)
Current Leads (Sec. 5.2.2.2)	-	-	-	15 g/s
IR Beam Debris (Sec. 5.1.4.2)	-	2.4 kW	0.5 kW	
IR Static Heat Load (rough est.)	0.5 kW	-	10 kW	
RF Cavities (Sec. 5.2.6)	0.48 kW	1.76 kW	-	
On-site Transfer Lines (6 km)	0.2 kW	-	12 kW	
<b>TOTAL</b>	1.2 kW	4.2 kW	25 kW	15 g/s

It is notable that most of the on-site cryogenic loads are dynamic and are not present during the injection cycle when the Tevatron is ramping. It is therefore plausible that most or all of the on-site cryogenic load could be serviced by load shifting from the existing Fermilab Central Helium Liquefier.

#### 5.2.1.1.6 Refrigeration System

The refrigeration system is composed of six 4.5 kW at 4.5 K capacity facilities equally spaced around the ring. Each plant will also provide 100 kW of 40 K refrigeration used in the shielding of the magnet system.

This provides approximately a 50% margin above predicted steady state requirements. This margin is required to ensure continued operation when the heat load increases either due to events such as a magnet quench or vacuum leak, or because refrigeration capacity falls below its intended design value (i.e. decreasing machine efficiency or inefficient heat transfer due to contamination). With this scheme, all six refrigerators must be operational for the accelerator to function. No plant redundancy is built into this design.

Figure 5.38 shows the refrigeration process schematic. The process helium is compressed from suction pressure of 0.101 MPa (1.01 bar) up to an intermediate pressure of 0.4 MPa (4.0 bar) by means of a first stage compressor discharging into a second stage, which compresses the helium to 1.85 MPa (18.5 bar). Turbo machinery is used for the refrigeration plants while positive displacement machines comprise the compressor system. There are two cold boxes: the upper and lower cold boxes. Each cold box contains five plate-and-fin type heat exchangers and three expanders. To avoid return helium gas instabilities due to the elevation change from the tunnel to the surface, the lower cold box will be located at the tunnel level. This requires a dedicated space of 432 m<sup>3</sup> (6 m along the beam by 6 m transverse by 12 m high) located near the accelerator tunnel.

These plants are well within existing commercial vendor capabilities. They are simpler but technologically similar to those of LEP, LHC, SNS, and HERA, and contain no nitrogen pre-cooling. The cold box configuration is a horizontal carbon steel shell enclosure housing all heat exchangers, piping, valves, cold ends of turbo expanders and vessels operating at cryogenic temperatures. The equipment within the cold box and the inner face of the vacuum jacket are

covered by multi layer aluminized Mylar. The cold boxes are designed to withstand the outside atmospheric pressure while they are evacuated and are also protected against overpressure by safety valves. All internal valves, filters, turbo expanders, bayonets and major pipe connections are fixed at the top plate and are accessible from a structural steel platform along the length of the cold box.

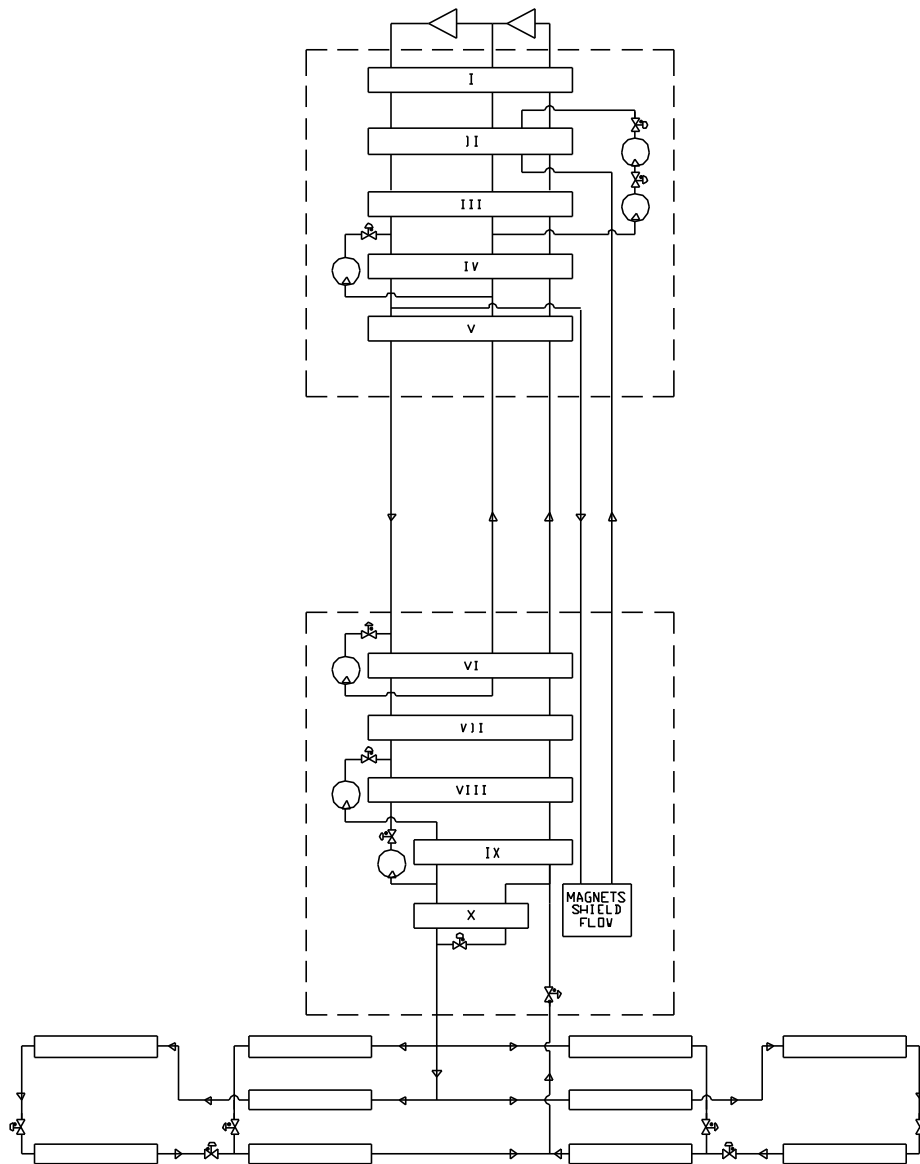


Figure 5.38. Refrigeration process flow and transmission line flow schematic. A split cold box similar to LEP is used to make the process insensitive to altitude changes between the tunnel and surface. The transmission line flows extend  $\pm 19$  km from the cryo plants. The flow is split into two parallel loops: the “near” loops that extend  $\pm 9.5$  km from the cryo plant, and the “far” loops that service magnets between 9.5 km and 19 km from the cryo plants.

The turbo expanders are self activated gas bearing type, superior in their performance to oil bearing turbines. Each turbo expander is a small single-stage centrifugal turbine braked by a direct-coupled, single stage centrifugal compressor. The turbine housing is vertically mounted

to a plate at the cold box top, projecting into its vacuum space. Within the cold box are brazed aluminum heat exchangers, pressure vessels containing an adsorbent to remove impurities and the cold end of gas-bearing turbo expanders. Part of the outer shell cover is flanged and has an O ring seal, and is removable for complete access to all cold box internal components and piping. Two panels will be mounted on the structural steel platform next to the cold box, one containing all instrument terminations and transmitters, and the other an assembly of purge and defrost valves. Provisions for purification of the process helium is provided at each plant as well as oil removal systems. A commercial control system package will permit the unattended operation of these plants.

Table 5.21. Predicted power requirements for ring cryogenics.

		Magnets				Shield
		Transmission Line		Current Return Bus		
		Near Loop	Far Loop	Near Loop	Far Loop	
Temp in	[K]	4.50	4.52	5.44	5.40	37.00
Press in	[bar]	4.00	3.80	2.00	2.50	17.00
Enthalpy in	[J/g]	12.09	12.09	33.92	27.18	207.28
Entropy in	[J/(g*K)]	3.52	3.56	8.19	6.69	14.76
Temp out	[K]	5.57	5.39	5.80	5.54	70.00
Press out	[bar]	2.80	2.50	1.90	2.10	13.00
Enthalpy out	[J/g]	26.40	26.66	37.79	34.24	381.66
Entropy out	[J/(g*K)]	6.44	6.59	8.96	8.18	18.71
Predicted heat load	[W/m]	0.044	0.044	0.024	0.022	1.534
Distance	[m]	19400	19400	19400	19400	38800
Design total heat	[kW]	0.85	0.85	0.47	0.43	60
Mass flow	[g/sec]	60	59	120	60	341
Design ideal power	[kW]	103	107	27	53	345

		Magnets	Shield
Predicted heat load	[kW]	2.6	60
Heat uncertainty factor	[-]	1.25	1.25
Design Heat Load	[kW]	3.2	74
Design mass flow	[g/sec]	120	348
Design ideal power	[kW]	291	345
4.5 K equiv design power	[kW]	4.43	5.26
Efficiency (fraction Carnot)	[-]	0.28	0.28
Nominal operating power	[kW]	1039	1233
Overcapacity factor	[-]	1.3	1.3
Installed operating power	(kW)	1351	1603

Operating wall plug power for one sector (MW)	2.0
Installed wall plug power for cryogenics for one sector (MW)	3.0
<b>Operating wall plug power for cryogenics for entire accelerator (MW)</b>	<b>11.8</b>
<b>Installed wall plug power for cryogenics for entire accelerator (MW)</b>	<b>17.7</b>

#### 5.2.1.1.7 Helium Compressor System

The compression package will consist of three oil flooded rotating screw compressors. One compressor will compress from 0.11 MPa (1.1 bar) to 0.4 MPa (4.0 bar), and the two other will compress in parallel from 0.4 MPa (4.0 bar) to 1.85 MPa (18.5 bar). The first stage compressor

is smaller than the two second stage machines. Each compressor skid contains the compressor, main drive motor, oil reservoir/separator vessel, and lubrication system mounted on a common rigid skid base. The base plate provided is suitable for installation on a flat pad without grouting. The helium enters the compressor and is compressed through the rotating screw compressor, also flooded with oil. The oil seals the rotor and absorbs some heat of compression. The compressed warm helium passes through a water-cooled heat exchanger and then into a bulk oil separator. The oil is also passed through a separate water-cooled heat exchanger. Each compressor is direct driven by an electric induction electric motor. The compressor assemblies are equipped with automatic inlet and outlet block valves and automatic recycle valves.

The high-pressure helium from the compressors passes through a skid mounted oil removal system. The oil removal system consists of three stages of coalescing filter housings followed by a vessel containing activated carbon. All entrained oil is filtered out of the gas stream by the three stages of filters. The small amount of oil in the vapor phase is removed by the activated carbon. The total amount of oil contained in the helium leaving the oil removal assembly is less than 10 ppb.

#### *5.2.1.1.8 Helium Liquid and Gas Storage and Inventory Management*

The inventory for the entire cryogenic system is estimated to be 75 tons of liquid helium, which is twenty times the Tevatron inventory. Each cryogenic plant will have three 37.8 m<sup>3</sup> liquid helium storage dewars, and fifteen gas tanks with a capacity of 113.6 m<sup>3</sup>. This will provide storage for 143 % of the total helium inventory. The gas storage serves as make-up/kick back during normal operations, and as a buffer/storage during quenches and warm up of a single loop. The liquid storage station will have pumps and heat exchangers necessary to liquefy/warm up cold gas during upset conditions. During the planned warm-up of the entire ring, the inventory will be liquefied into the dewars. In case of a sector warmup, the inventory can be distributed between five sector gas/liquid storage vessels via the cooldown header. The tunnel transfer line and the cooldown header can be used to hold up to 40% of inventory at pressure below the MAWP of any component in the system.

#### *5.2.1.1.9 Cryogenic Control System*

A well-proven process control system will be used. The cryogenic system in each sector will be controlled by a commercially available distributed control system (DCS). Commercial program logic controllers will be used for local control of the cryogenic hardware in the event that a high-speed network connection is unavailable. The cryogenic control system will provide full automation of any operation mode, including transient modes. The accelerator high-speed network will be used for communication and data exchange between sectors.

### *5.2.1.2 Design Operating Conditions*

#### *5.2.1.2.1 Steady State*

Helium is supplied from a refrigerator at 4.5 K, 0.4 MPa (4 bar) and returned at 5.8 K, 0.19 MPa (1.9 bar). Supercritical supply helium is fed from the helium plant to four parallel loops. Each loop is comprised of 9.5 km of magnet and transmission line. There are cryogenic connecting boxes at the beginning and end of each 9.5 km section. At the exit of the refrigerator

the helium process is split into four paths. There are upstream and downstream magnet strings that are mirror images of each other. The typical flow schematic of a magnet string is shown in Figure 5.39.

As helium enters the upstream or downstream magnet strings the flow is split into two parts: half enters the 4.5 K transmission line circuit (for the near loop) and half enters the 4.5 K current return circuit contained in the magnet (for the far loop). There is expected to be an approximately 1 K gradient across each loop. These loop flows are then re-distributed at valve boxes and become the return 6.0 K flow.

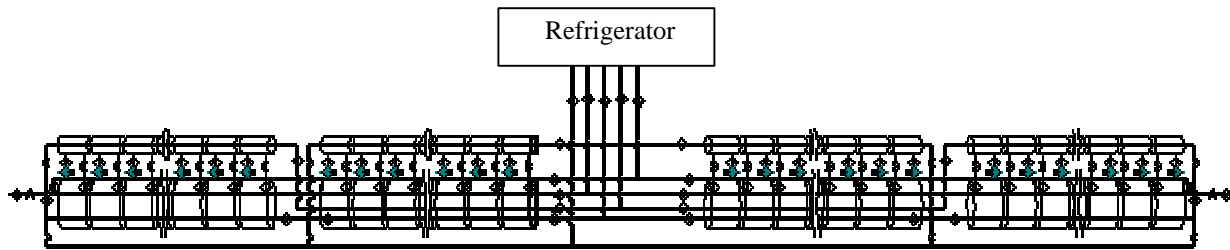


Figure 5.39. Flow schematic of the 38-km sector serviced by one cryogenic plant.

The cooling scheme relies on a balance between heat leak and pressure drop. Any scenario causing an upset in the heat load (i.e. vacuum degradation) can be compensated by increasing the helium flow rate and supply pressure for the proper loop. The refrigerator has been oversized by 50% to compensate for these types of upset conditions.

#### 5.2.1.2.2 System-Wide Purification

Purification of this machine will be done in two steps. First, each sector will be pumped and backfilled five times to 25 inches of mercury via pumpouts on every helium circuit at each valve box located every 10 km. This method has been proven to work in the Tevatron. Levels of contamination less than 100 ppmv are achieved with this first step by using roughing pumps. The second step is dilution purification. A purifier with a nitrogen cooled charcoal bed will be located at each refrigeration plant. The discharge gas of the compressor system will be circulated through this purifier and then will be distributed to the magnet/transmission line system. Contamination instrumentation, such as arc cells used on the Tevatron, will be used to monitor the ppmv levels in each sector. The system will be ready for cool down when contamination levels are < 5 ppm. It is estimated that the purification for a sector in the VLHC will be 72 hours.

#### 5.2.1.2.3 System-Wide Cool down

Cool down of the VLHC will be done in three stages. The first stage involves the cool down of the helium plants. The second stage is the cool down of the transmission line to 40 K. Finally the transmission line will be cooled to operating temperatures.

In the first stage, cooling is provided by turbines and should not take more than 24 hours per plant. In the second stage, the plant is set up in the liquefaction mode and 40 K gas at 0.4 MPa (4 bar) is sent via cool down valves located at each valve box back to the compressor suction warm gas header located in the tunnel. Gas flows out from the refrigerator through the

near loop transmission line, the 6.5 K return, the current return bus, and the shield circuits, and then returns via the warm header. When the temperature at the end of the “near” loop (measured at the valve box) is 70 K the flow is then re-directed to the “far” loop and into the return header. As the “far” loop temperature reaches 70 K the second cooldown stage can be started.

During the third cool down stage, the plant is re-tuned for an outlet temperature of 4.5 K. The flow pattern for the second stage is the same as the first stage. As the temperature for each loop is at 7 K the cool down valves can be closed and the flow will be looped back in refrigerator mode. Total cool down time is expected to be on the order of 10 days.

## 5.2.2 Magnet Power Supplies, Current Leads, and Quench Protection

Stage-1 power supplies are summarized in Table 5.22 below. The major item is the single 100 kA supply for the transmission line magnets. The Interaction Region power supplies, current leads and quench protection are discussed in Section 5.1.4. Total Stage-1 power supply requirements (both ramping and steady state) are about a third of the Fermilab Main Injector.

Table 5.22. Power supply, current leads and quench protection summary for the Stage-1 machine.

	Transmission Line Power Supply	IR Quadrupole Power Supplies (Sec. 5.1.4)	Straight section Warm Magnet Power Supplies	Corrector Magnets (warm copper)
Number	1	2	16 approx.	12,000
Location	FNAL	at Experiments	Straights	Quad locations
Voltage per supply	62	10 V typ.	1000 V typ.	100 Typ
Current per supply	100 kA	25 kA	200 A typ	2 A typ
Ramping MVA (tot)	6.2 MVA	1 MVA	-	-
DC Power (total)	0.4 MW	0.6 MW	7.4 MW	2.1 MW
LCW Consumption	-	-	150 liters/sec	(air cooled)
Quench Detection	1 Circuit at PS	2 circuits/quad	-	-
Quench Protection	Dumps @ 20 km	4 heaters/quad	-	-
SC Current leads	100 kA-pair	60 kA-pair	-	-
<b>Peak Ramping Supply Power</b>	<b>17.7 MW</b>			
<b>Total Power Supply Power in Collision</b>	<b>10.5 MW</b>			

### 5.2.2.1 Main Transmission Line Power Supply

The low inductance (3  $\mu\text{H}/\text{m}$ , 0.6 H ring total) and low stored energy (10 kJ/m, 3 GJ total) of the single-turn transmission line magnet allow the entire ring to be powered from a single supply [49]. See Figure 5.40. A voltage of  $\pm 62$  V ramps the machine up or down in 1000 seconds. The design current of 100 kA at flattop exceeds the 87.5 kA required for the transmission line magnet to reach its design field. The supply will be located on site at Fermilab in a shielded underground room approximately 25' x 50 ft in size. The ramping power and footprint of the power supply is comparable to one of the six Main Injector power supply buildings. Superconducting current leads will be located immediately adjacent to the supply to minimize

power loss in warm buswork. Superconducting buswork will carry the current through a short connecting conduit to the transmission line magnets in a manner identical to the MS6 test string [50].

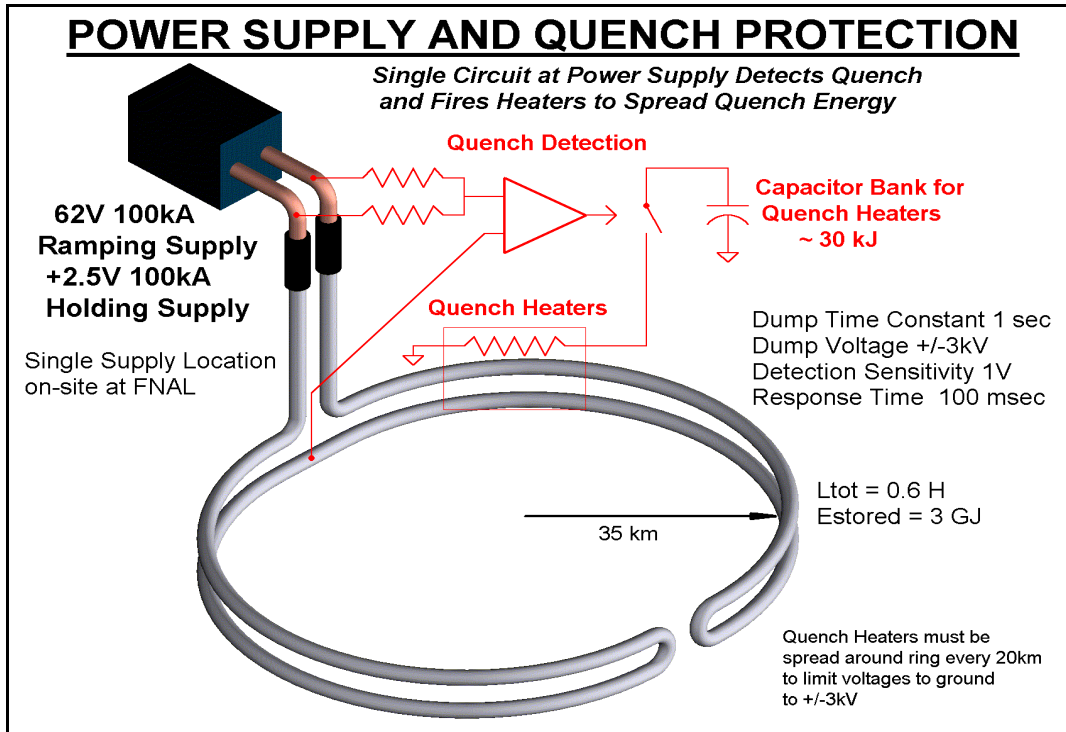


Figure 5.40. 100-kA power supply and quench protection for transmission line magnets.

The power supply is actually two supplies in series. The main ramping supply generates the positive or negative voltage to transfer the inductive energy into and out of the magnets. It is not used when the magnet is at constant current. The second “holding” supply maintains the current during long periods at flat top and injection, and provides only the voltage necessary to overcome resistive losses in the current leads, warm buswork, superconducting splices, and the shorting SCR switch across the ramping supply. This approach minimizes the cost of the ramping supply, simplifies the power distribution system, and moves the tightest regulation and ripple requirements to the precision holding supply.

The Main Ramping Supply design (Figure 5.41) is based on paralleling 8500 A modules of design similar to Main Injector supplies. This approach permits spare modules to be taken off line for repair, and allows the use of commercially available 10 kA DCCTs for current regulation. A 2-quadrant 12-phase SCR bridge returns inductive power to FNAL as the magnets ramp down. Ramping systems are designed to have rms power sized to be halfway between the peak (6.2 MVA) and the rms (3.1 MVA). This has proven to be a reliable design methodology for similar supplies at Fermilab. The rms feeder load of 4,800 KVA is less than one feeder cable for the source.

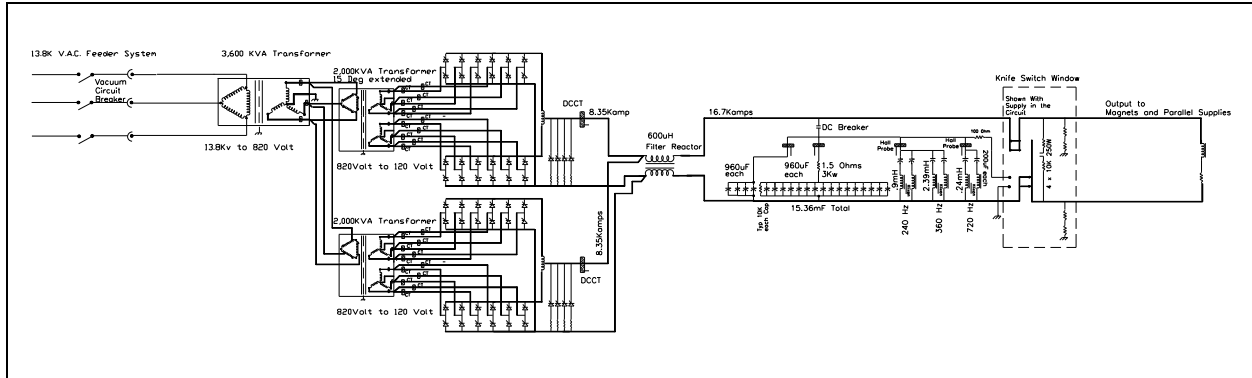


Figure 5.41. 100-kA ramping supply schematic (one 2 x 8.5-kA module shown).

The +2.5 V holding supply is essentially a copy of the 100 kA switching converter [51] constructed for the magnet string test. The device (Figure 5.42) consists of a 450 VDC, 500 kW bulk supply followed by ten 10 kA DC-DC converter modules in parallel. This two-stage regulation scheme provides immunity to variations in input line voltage. The modules use IGBT chopper bridges, tape-wound cores and Schottky power diodes.

The switching frequency is  $\sim 2$  kHz. To minimize output ripple the 10 modules are phased to switch sequentially. This pushes the fundamental ripple frequency up to 10x the switching frequency or  $\sim 20$  kHz. The switching will be phase locked to the revolution frequency so that beam emittance growth due to power supply ripple will be negligible. The control system for this switcher will be integrated into that of the main ramping supply to simplify regulation and load hand-off.

### 5.2.2.2 Current Leads

Superconducting current leads are required for both the main transmission line and for the IR quadrupoles. A single pair of 100 kA current leads is required for powering the transmission line. These could either be conventional copper leads identical to the leads developed for the MS6 transmission line test facility [50], or could be a specially built High-Temperature Superconductor (HTS) version using the 50 K transmission line shield flow as the inter-stage temperature. The cryogenic wall power associated with the conventional 100 kA leads is approximately 300 kW. This could be reduced by a factor of 4 with HTS leads [52]. Payback time for the electrical cost savings from HTS leads is approximately 3 years.

IR quadrupoles can use commercially available HTS leads similar to the LHC. The total requirement for current leads in the Stage-1 machine is about 150 kA-pair, or about  $1/12^{\text{th}}$  of the current leads required by the LHC.

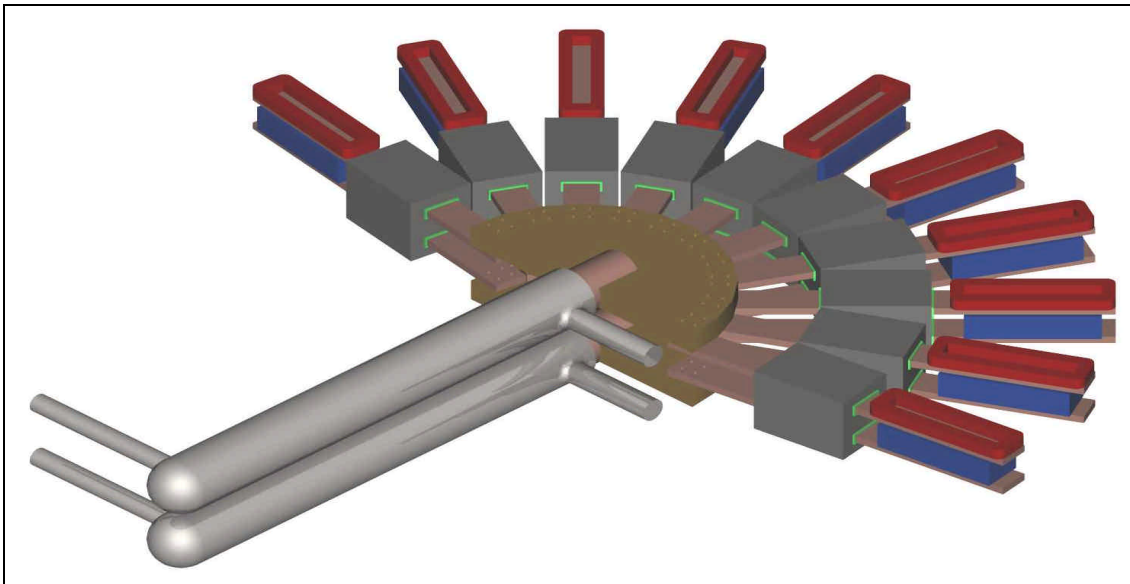


*Figure 5.42. 100-kA superconducting current leads and switching converters developed for the MS6 test string. A more compact arrangement of the leads and power converter will be small enough to be placed in the tunnel and used for partial-ring commissioning.*

### 5.2.2.3 Quench Protection

The only superconducting magnets of the Stage-1 collider are the transmission line magnets and the IR Quadrupoles. Protection of the IR quads with heaters is described in Section 5.1.4.

The low inductance and low stored energy of the transmission line magnet allows a simple and inexpensive quench protection system. The magnets themselves require no internal quench detection or protection circuitry. Ring-wide quench detection is performed by a single circuit

located at the power supply terminals. Quenches are detected by a voltage imbalance at the power supply (Figure 5.40). When a quench is detected, magnetic energy is extracted with a 1-second L/R time constant by cryogenic “dump resistors” spaced at 20 km intervals around the ring. This keeps the peak temperature and pressure in the quenched section of the conductor at acceptable levels as described in Section 5.1.2.2. Quench protection system parameters are given in Table 5.23. The theory of operation is explained in [53] and a detailed write-up is given in [54].

Table 5.23. Stage-1 quench detection and protection parameters.

Transmission Line Current	100 kA
Magnetic Stored Energy @100 kA	10 kJ/meter, 2100 MJ/ring
Magnet Inductance at low field	3 $\mu$ H/m 600 mH/ring
Energy Dump Time Constant	1 second
Peak Voltage To Ground during Dump	$\pm$ 3 kV
$I^2t$ during dump	$5 \times 10^9$ A <sup>2</sup> s
Peak Temperature of Conductor During Quench	250 K
Peak Pressure of Helium During Quench	35 Bar
Pressure relief during quench	Every 2 cells (500 m)
Effective Copper Cross Section of Conductor	3 cm <sup>2</sup>
Quench Detection Threshold	1 Volt
Quench Detection Method (primary)	Analog bucking with midpoint of current return bus
Quench Detection Method (backup)	Deviation from $V=LdI/dt$ at power supply terminals
Energy Dump Resistance	60 m $\Omega$ per location,
Dump Switch Locations	at cryoplants and midpoint of arc (20 km spacing)
Dump Switches	Quenched superconducting cables 65 m long
Superconducting Dump Switch Conductor	1:1 CuNi:NbTi “Switch Wire”
Cryogenic Dump Resistor Thermal Mass	65-m long, 3-cm ID, 5.5-cm OD Invar pipe
Final Dump Temperature after Dump from 100 kA	325 K
LHe Required for recovery after Dump from 100 kA	1600 liters (less if shield flow used for pre-cooling)

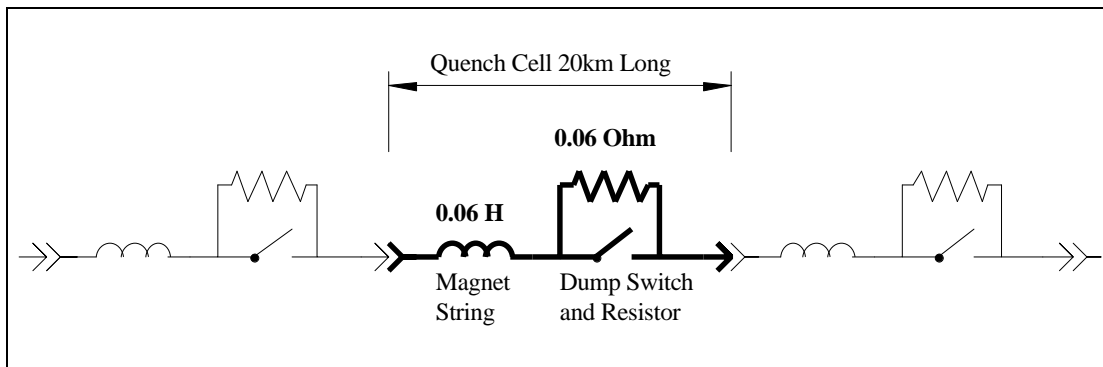


Figure 5.43. Quench protection cell of the transmission line magnet.

The “dump switches” are deliberately quenched sections of transmission line conductor built with Cu-Ni stabilized NbTi “switch wire”[55] which has a high normal state resistance. Current is transferred to a thick-walled Invar pipe that provides thermal mass. These dumps are efficiently recooled using helium from the cryogenic shield flows and transmission line flows, with the warm gas vented into the return header.

The protection circuit for the 100 kA current leads and power supply is integrated into the quench protection system. When an overtemperature or overvoltage is detected in the current leads, nearby copper buswork, or power supply components, the power supplies are shut off and a ring wide dump is forced. The required response time is equal to the thermal time constant of the leads or approximately 100 seconds.

It is instructive to compare this quench protection system to those of other accelerators. The LHC for example [56] requires a crate of quench detection electronics in the tunnel underneath each dipole in the tunnel. Each LHC magnet has more than 10 voltage taps and instrumentation feed-throughs. The LHC also requires a much larger array of energy dump resistors, dump switches, and current leads around the circumference of the ring. Despite the larger machine circumference, the quench protection system of the Stage-1 magnet is far simpler and should be more reliable.

#### 5.2.2.4 *Straight Section (Warm Magnet) Power Supplies*

The straight sections use warm iron/copper quadrupoles and a small number of other magnets. In each straight section all F and D quadrupoles are powered in series by a single supply. The IR straight sections have a larger number of independently programmable “tuning quads” but the total power and LCW usage is approximately the same as a normal straight section. The power supplies are located in shielded rooms (one per straight section) which contain ~500 kW of power supplies and are accessible with beam on. These are single quadrant supplies. Given the limited scope of these supplies it is desirable to make them fully redundant, especially those at the far side of the ring from FNAL. A detailed breakdown is given in [57].

Dipoles and quad correctors magnets identical to the arcs are provided at each quad location. Dipole magnets used to separate and cross over the beams are powered by the 100 kA transmission line and require no separate supplies.

#### 5.2.2.5 *Water Cooling (LCW) System*

The “on-site” and “far side” straight sections require LCW systems. No LCW system exists in the arcs. Major heat loads are the resistive magnets, power supplies, and the RF klystrons. Loads are detailed in [57] and summarized in Table 5.24. The overall scope of the onsite LCW system is comparable to the MI-60 LCW system of the Fermilab Main Injector. The far site LCW system is about half that size.

The layout of the LCW system is sketched in Figure 5.44. The on-site straight section is connected to the Main Ring LCW system and can use the FNAL infrastructure for filling and makeup. Existing (unused) Main Ring ponds exceed requirements for power dissipation. New ponds and purification systems are required at the far side sites. The vertical drop generates a 150 psi pressure head, which is overcome by locating the circulation pumps at tunnel elevation and pumping the return flow upwards. The beam stop and beam collimation cooling systems require separate pumped loops for radioactive water (RAW) which will be heat exchanged with the main cooling water flow to maintain isolation.

Table 5.24. LCW and power dissipation summary for Stage-1.

	Heat Load	Total Loads	Total kW	LCW Flow (l/min)
On-Site Straight Sections	Resistive Magnets	188	4480	3200
	Power Supply Cooling	22	500	600
	RF Klystrons	16	3760	6400
	RF Loads & Recirculators	16	5600	4500
	Beam Stop	1	500	600
	Total (on-site)	227	14840	15300
Far Side Straight Sections	Resistive Magnets	176	3320	3500
	Power Supply Cooling	9	550	600
	Beam Collimation	-	40	50
	Total (far side)	185	3910	4150
<b>LCW Systems Total</b>			<b>18750</b>	<b>19150</b>

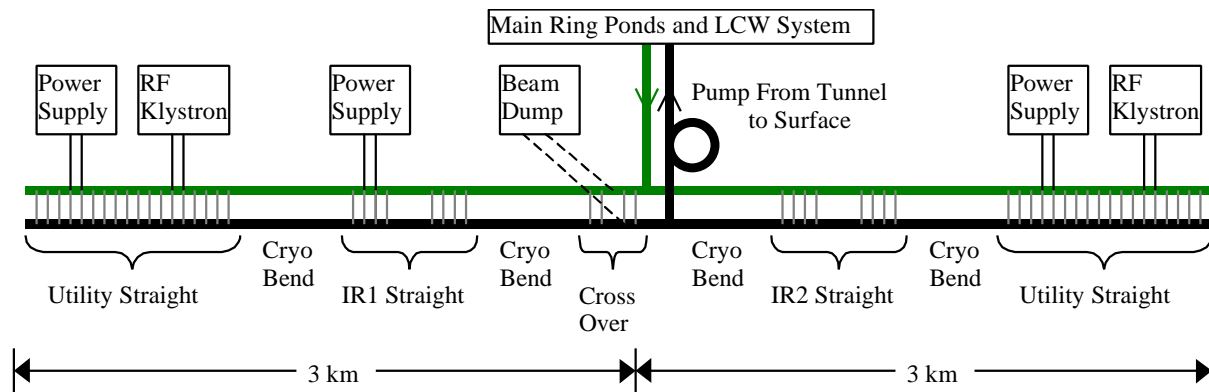


Figure 5.44. LCW system layout for on-site straight section. The far side LCW system is similar except that the RF loads are absent, the beam dump load is replaced by the smaller load from the beam collimation system, and an independent system of ponds and makeup water is needed.

## 5.2.3 Arc Instrumentation and Power Distribution

### 5.2.3.1 Reliability and Maintenance Considerations in the Arcs

The long arcs of bending magnets have specialized and limited requirements. The once-per-turn subsystems and their cabling, power and cooling requirements are absent. No LCW system is required. Only the repetitive instrumentation and corrector power supplies at each of the 1760 “half-cell locations” (every 135 m around the ring at the location of beta-max in each half-cell) are required. Infrastructure for power and communications occurs at alcoves at 10 km intervals.

Reliability is at a premium for the arc instrumentation due to the large size of the machine. Repair technicians at a centrally located facility require a 20 mile drive to reach the surface facility and begin access into the tunnel. Travel time will not be small compared to the 1.5 hour time needed to refill the machine and reaccelerate the beams. For this reason fully redundant capability is provided for all mission-critical subsystems in the arcs. Power distribution is provided to each module by two independent loop feeders with auto-resetting circuit breakers and remote disconnects. Two independent power supplies are provided for each corrector magnet and control function. Redundant network connections to each module are provided. The critical function of beam loss monitoring is provided by redundant sensors read out from alternate half-cell modules. The system design is such that even the failure of a handful of local electronics modules will not require immediate maintenance.

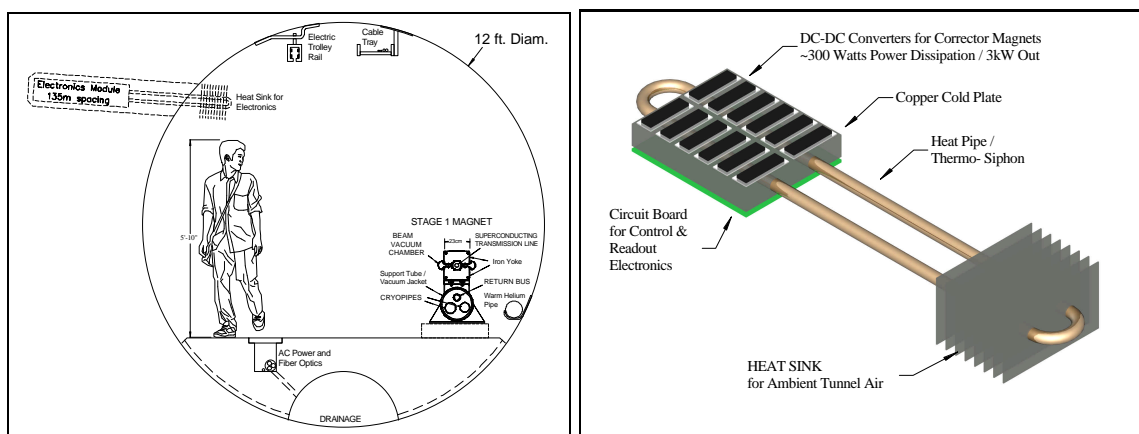


Figure 5.45. Electronics module at each half-cell location (every 135 m) contains beam instrumentation and DC-DC power converters for corrector supplies. Modules are in a radiation-shielded “hole in the wall” and dissipate their power in the ambient tunnel air via a heat pipe/thermosiphon and heat sink.

These electronics are located in a radiation-shielded modules buried in “holes-in-the-wall” at each half-cell location. All cables for instrumentation and corrector magnets are pre-assembled on the magnet and factory tested before installation. Cryogenic thermometry and a valve controller are used at every other half-cell location (270 m) to regulate the 50 K shield flow. Every 10 km there is a walk-in alcove associated with a tunnel egress point that contains conventional electronics racks and provides network connection, tunnel safety systems, bulk DC power for the instrumentation modules, and cryogenic instrumentation for the cooldown valve box. Average power dissipation is approximately 15 W per meter of tunnel, which can be air cooled.

### 5.2.3.2 Cabling in the Arcs

At the Fermilab Main Injector, the cable tray to each service building contains 316 cables with a total cable cross sectional area of  $180 \text{ cm}^2$  [58]. Over 95% of these cables service Beam Position Monitors (BPMs), Beam Loss Monitors (BLMs), ion pumps, corrector magnets, and temperature and vacuum monitoring. The superconducting Tevatron also has a large cable plant associated with quench protection and cryogenic monitoring and controls. The installation, termination, and testing of these cables are a significant cost and schedule item.

The Stage-1 design eliminates most cabling costs by multiplexing the signals to a local electronics module (Figure 5.45) at each half-cell boundary. Signals are digitized locally and sent to the control room via network fiberoptics. Instrumentation and corrector magnets are clustered at half-cell locations and cable runs are typically 5 meters. Cable harnesses are prefabricated by outside vendors and mounted on the magnets and tested in the factory.

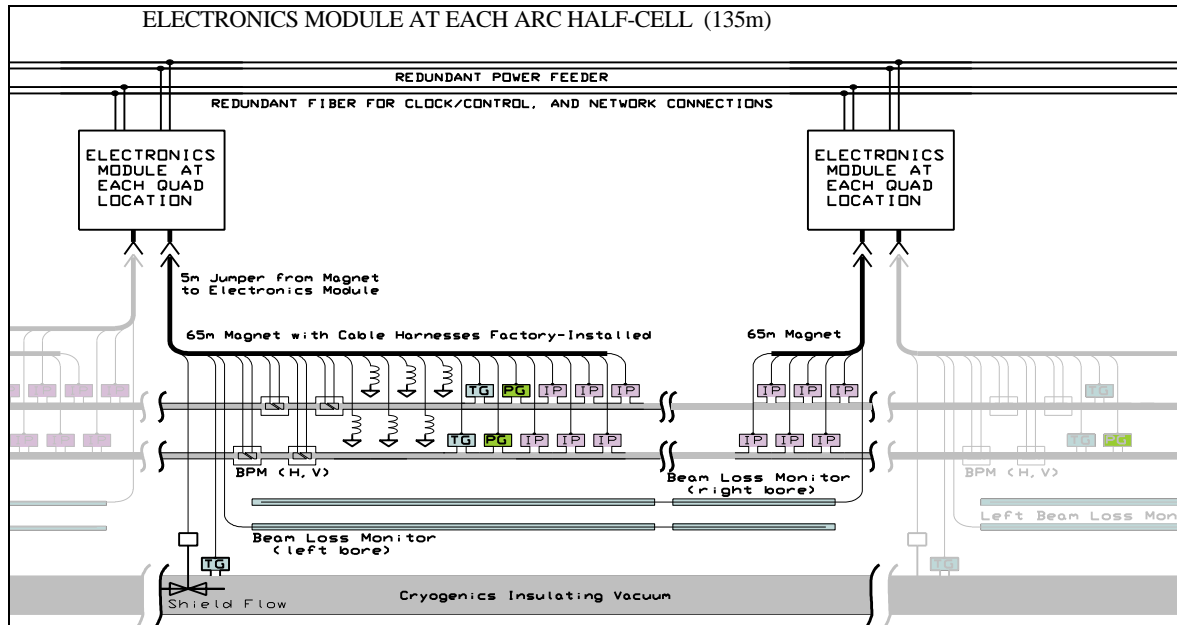


Figure 5.46. Cabling layout on the transmission line magnet. Cables and instrumentation are preinstalled and factory-tested on the 65-m magnets. Each magnet has a 5-m “extension cord” which jumpers to an electronics module located in a hole in the wall at each half-cell location (135-m spacing).

### 5.2.3.3 Corrector Power Supplies

The warm (air-cooled copper) correction magnets (Sec. 5.1.3) dominate the power consumption in the arcs. The electronics module at each half-cell location has 6-8 corrector magnet loads with a maximum installed power of approximately 1400 W. Average corrector power is < 1000 W in a realistic operating scenario. At maximum current approximately 90% of the power is dissipated in the magnets themselves with the remaining 10% (~150 W) in the power supply converters. Instrumentation and control power at each half-cell location is estimated to be ~100 W for a total of 250 W dissipated in the module. Power at this level can be passively carried away from the electronics (Figure 5.45) via a heat pipe [59] and removed by the tunnel airflow of ~1 m/sec.

### 5.2.3.4 Power Distribution in the Arcs

Redundant DC-DC power converters are provided both for module control power and for each trim magnet. Power can be drawn from either of two redundant 1 kV DC feeders that loop the ring (see Figure 5.47). Power supplies are connected in parallel at each load. Under normal

circumstances the load is shared and each power supply operates at < 50% of rated load, encouraging long lifetimes. Under failure conditions the load is taken over by a single supply which operates near its design rating (or less, if the corrector magnet setting is below 100%).

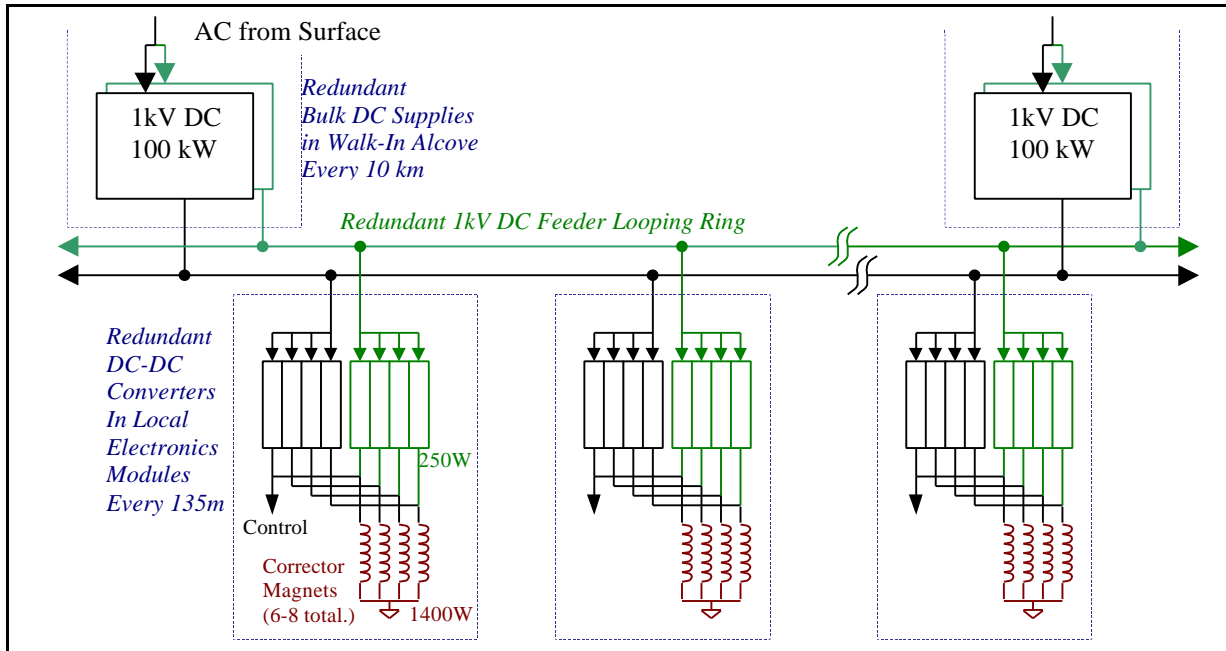


Figure 5.47. DC power distribution scheme in arcs. Redundant bulk DC supplies in walk-in alcoves every 10 km supply a redundant loop feeder. Each local electronics module contains two DC-DC converters for each load. Under normal conditions all supplies share loads and run at less than 50% of rated capacity. By means of auto-resetting circuit breakers (not shown), the system can tolerate short or open circuits on the loop feeders, a failure of one or both bulk supplies at any alcove, a failure of the AC surface feed to any single alcove, and individual failures on many corrector supplies.

Medium voltage 1 kV DC is chosen for power distribution to the electronics modules at each half-cell location. The DC is provided by 100 A bulk supplies every 10 km located in racks of electronics in walk-in alcoves. Two redundant bulk supplies are provided at each location, and two independent distribution loops are provided to route the power to the modules. Under normal conditions 25 A is sourced in either direction onto each of the 500 MCM loop feeders, and less than 3% of the power is lost in the distribution cabling. Under fault conditions one or both of the bulk supplies at one of the 10 km locations can fail, with the slack being taken up by adjacent supplies in the loop feeders. A short-circuit fault in one segment of the loop feeders can be tolerated by letting its circuit breaker trip and relying on the remaining loop feeder. Each module is protected with fault current limiting via automatically resetting “solid-state fuses” [60].

The advantages of DC power in this application are as follows. The main power consumption is due to corrector power supplies that naturally operate as DC-DC converters. These are more compact than line-transformer based supplies, an important consideration for the local electronics modules. Modern DC-DC converters [61] have the following parameters: power density 200 W/in<sup>3</sup>, efficiency ~90%, cost ~\$0.35/watt. In fact, essentially all modern AC devices (e.g., fluorescent light ballasts, computers, high current welders, motor controllers)

rectify the AC line power and then chop the signal using DC-DC techniques. Rectification at 60 Hz requires bulky capacitors and produces current spikes with power factor and noise problems that complicate AC distribution. DC power distribution makes the most efficient use of the copper in distribution cables, which is a major cost component in power distribution. DC power also simplifies the design of loop feeders, which may be powered from separate segments of the power grid without regard to the relative phase of the incoming AC power. Finally, by phase-locking the switching frequencies of the DC-DC converters to a frequency near the revolution frequency of the machine, the effects of power supply noise on emittance growth can be essentially eliminated as discussed in Section 5.2.2.1.

### 5.2.3.5 *Beam Position Monitors (BPMs)*

Both X and Y BPMs (Figure 5.48) will be provided every 135 m at the corrector region at each half-cell boundary (Figure 5.2). Although measurement of the second coordinate only improves the closed-orbit distortion by 10% [62], the added redundancy obtained by an independent readout of both coordinates will be beneficial given the small aperture and the travel distance to repair failed BPMs.

Button style beam pickups similar to those used on electron machines and the LHC are adequate. These devices are nonlinear outside the central 30% of their aperture. Given anticipated closed orbit distortions < 1 mm this is not a problem. In a few special locations near beam transfers where off-axis orbits must be measured, split-plate BPMs with better linearity will be used.

The BPM calibration offset can be verified *in situ* using the independently powered quadrupole correctors at each half-cell. The BPM can be accurately fiducialized to the warm iron of the corrector. At injection energy, the quad steering associated with a 1 mm orbit offset through the corrector generates an easily measured 3 mm orbit distortion as the corrector is powered.

BPM readouts using either AM/PM or Log Amp electronics are acceptable. In the case of Log-Amp readout both  $\log(A/B)$  and  $\log(A)+\log(B)$  would be digitized to provide both position and intensity readout. In the case of AM/PM conversion a separate channel (possibly a log amp) is required to provide intensity information. In either case an in-situ calibration is desirable. The calibration circuit injects equal signals of adjustable amplitude into both channels to accurately determine the zero-offset response at different input strengths. A recent example of log-amp readout made for the SLAC B-factory fit on a 2.7" x 4.7" board that also included calibration circuitry [63].

Digitization bandwidth is determined by the first turn and transient response desired. A digitization rate >25 MHz can be supported by the DMA channels of today's Digital Signal Processors (DSPs), with no external components other than the flash ADC. A 10-bit digitization of  $\log(A/B)$  would provide 20  $\mu\text{m}$  least count resolution. Power dissipation for four channels of 10-bit 40 MHz digitization would be 300 mW total [64].

The cable run from the BPM to the local electronics module is about 5 m. This is long enough that the signal must be terminated but short enough that normal RG-58 can be used. The cable runs are short enough that no cable trimming for phase matching is required if AM/PM electronics are selected.

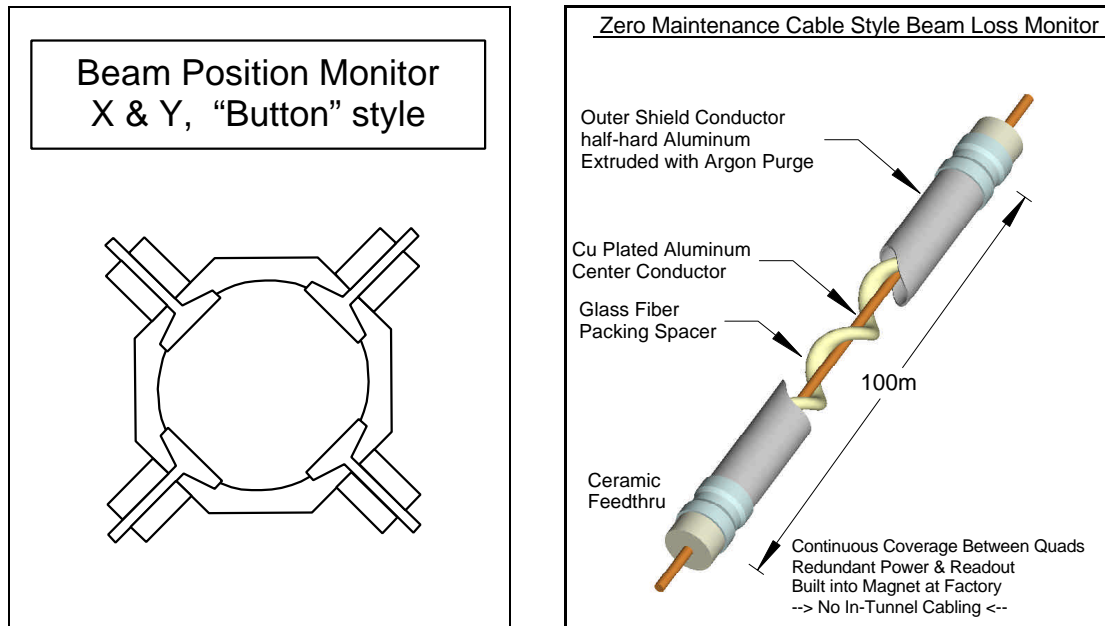


Figure 5.48. Beam Position Monitor (BPM) and Beam Loss Monitor (BLM) for Stage-1 magnets. The BPM is a capacitive “button” style typically found on small aperture beam pipes. The X and Y pickups are rotated by 45-degrees to avoid the synchrotron radiation (this is common at light sources). The BLM is a permanently sealed Argon filled cable-style ionization chamber. Two redundant BLMs run the full length of the magnet. It features all metal and ceramic construction similar to the Tevatron BLMs to allow the device to operate unattended for years (no gas bottle to change).

### 5.2.3.6 Beam Loss Monitors (BLMs)

The BLM function in the arcs is mission-critical in that no blind spots may exist which might allow chronic beam loss to go undetected. We therefore choose a cable style BLM. This is essentially a long ionization chamber that can provide complete coverage along the length of the magnet. The cable will be all metal/ceramic construction (Figure 5.48) so that no gas-bottle changing will be required. For redundancy, two independent cable BLMs are provided. Each runs the full length of the magnet but they are read out at alternate quad locations. This will provide complete BLM coverage even when the electronics module at a single location goes incommunicado. Separate BLMs on each side of the magnet provide some differential sensitivity to beam losses in each bore. Electronics required include a 2 kV/100  $\mu$ A Cockroft-Walton DC-DC converter module, an op-amp integrator, and a medium bandwidth  $\sim$ 100 kHz 14-bit ADC. Power dissipation should be  $<2$  W.

### 5.2.3.7 Ion Pump Power Supplies & Vacuum Gauges

Each 135 m half-cell contains 12 ion pumps (22.5 m pump spacing in each bore). These are powered and read out from the local electronics module. Each pump requires a 5 kV supply with a starting current of up to 30 mA but an operating current less than 0.1 mA. The power for all 12 pumps is provided by a single transformerless bulk supply (a 5-stage Cockroft-Walton converter operating from the 1 kV DC feeder). High voltage DC relays (Cotto 5501) isolate each pump and give the capability of providing the full starting current sequentially to each supply. Individual current readback on each pump is provided via an array of V/F converters

operating at HV with an optically isolated data link to the DSP. Vacuum gauge readout for the beam and insulating vacuum will also be incorporated into the local electronics module.

Failure of the bulk supply shuts down all ion pumps in a 135-m half-cell. Pumping from the NEG strip remains intact. This results in a 50x rise in the pressure of a single gas species ( $\text{CH}_4$ ) over the length of one half cell, equivalent to a 3% rise in the average pressure of  $\text{CH}_4$  in the ring and  $< 1\%$  drop in the overall beam lifetime. Redundancy in the ion pump power supplies is therefore unnecessary.

### 5.2.3.8 Network & Clock Connections

The electronics module at each quad location contains a DSP computer with an optical fiber connection running a network protocol stack. This CPU can store, average, spectrum analyze, and data-compress all digitized information before transmitting over a conventional fiber network. A separate dedicated fiber handles the FNAL-specific real time signals such as clock, event triggers, and beam abort heartbeat signals. These will be handled in hardware logic by a Programmable Logic Device (PLD) in the electronics module.

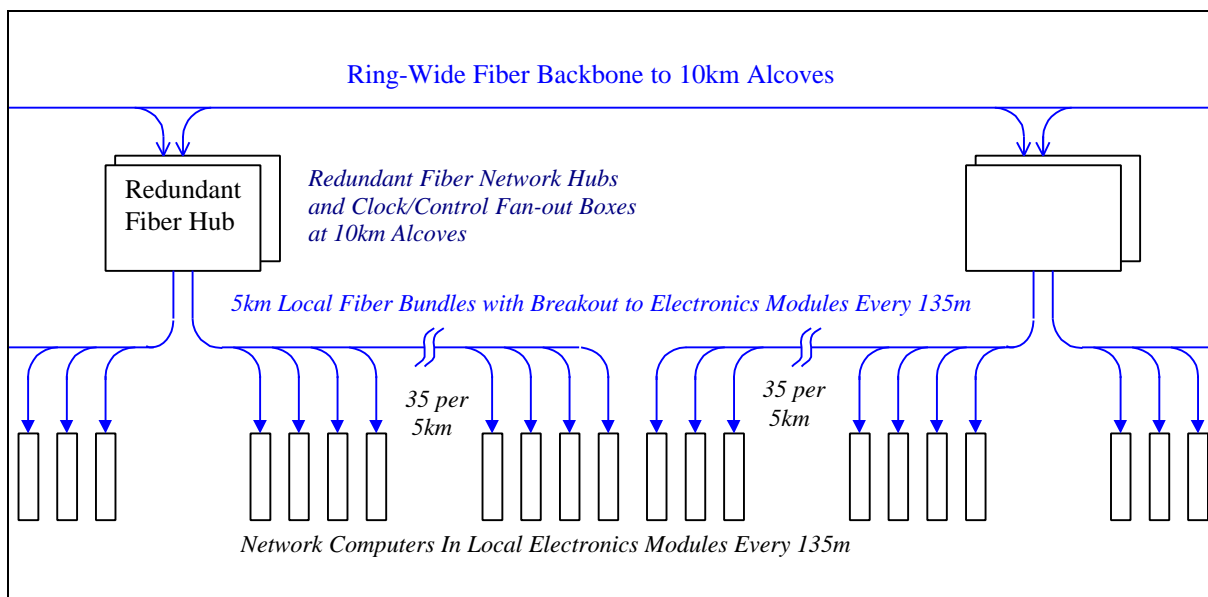


Figure 5.49. Fiberoptic clock and network connections in the tunnel, including redundant hubs and clock fanouts at 10-km alcoves.

A minimal set of fiber connection to each module consists of one network connection plus one dedicated fiber for delivering Fermilab-specific signals. For cost estimation purpose we have assumed four direct point-to-point fiber connections between each quad location and redundant network hubs at located in the 10-km alcoves. The fiber cable will be a pre-assembled harness 5-km long with 4-fiber breakouts at quad locations every 135 m. Installation will consist of laying the fiber harness in the cable tray immediately below the electronics modules (Figure 5.49) and plugging the breakout into each electronics module.

The long-haul fiber backbone interconnecting the 10-km alcoves around the ring will be buried with the power duct in the invert. This provides additional radiation shielding to compensate for the longer distance of the backbone fiber runs (see Section 5.3.3.2).

### 5.2.3.9 Local Electronics Module Miscellaneous Functions

The networked CPU in each electronics module allows additional features to be added at relatively low cost. In many cases this requires adding only an interface IC, transducer and software to the local electronics module. The engineering effort for this is not unreasonable given the large quantity of local electronics modules. Some possibilities are:

- Tunnel temperature, humidity, and airflow transducers
- Integrated radiation dose monitor for the electronics module (FET + resistor)
- Microphones for detecting quenches and water problems
- Speakers to communicate with tunnel crews
- RF modules to communicate with the cell phones and PDAs of tunnel crews
- Cryogenic sensors and valve controls (presently estimated as a separate system)
- Vacuum valve controls (presently estimated as a separate system).

## 5.2.4 Beam Vacuum System

The beam vacuum system is divided into two sections. In the 225 km of transmission line magnets an extruded-aluminum warm vacuum system similar to LEP and electron storage rings is used. In the 8 km of straight sections synchrotron radiation is absent and the vacuum system will be a conventional stainless steel system similar to those commonly used at Fermilab.

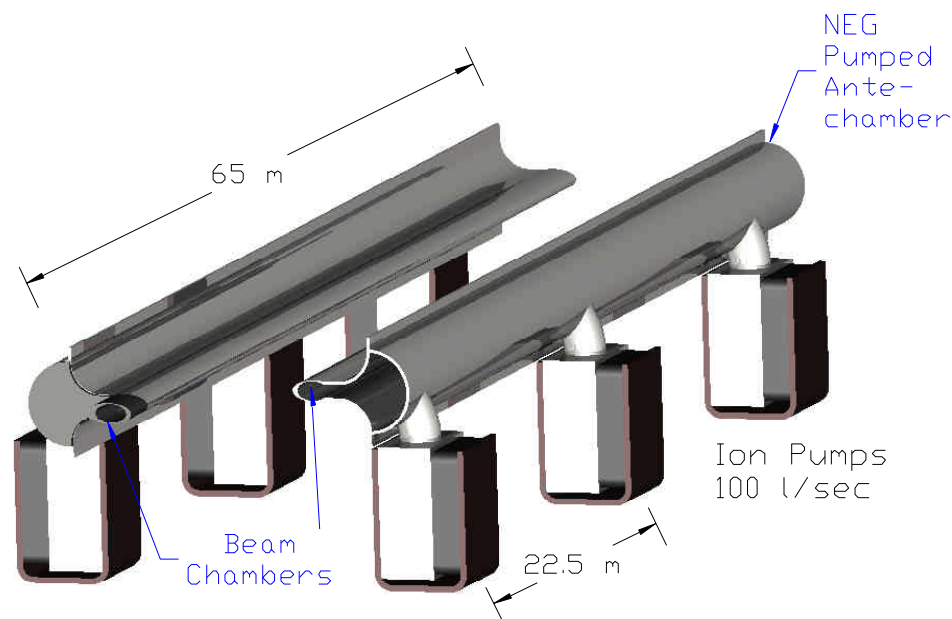


Figure 5.50. Extruded aluminum beam vacuum system in the transmission line magnets.

### 5.2.4.1 Arc Magnet Vacuum System

An extruded aluminum vacuum system (Figure 5.50) is used for the 225 km of arc magnets (450 km of beam pipe). The design of this system is driven by vacuum desorption from synchrotron radiation, the small aperture of the magnet gap, beam impedance and cost. Aluminum is chosen for reasons of economy and beam impedance. The system is pumped by a non-evaporable getter (NEG) strip located in an antechamber of the extrusion. Methane and noble gasses are pumped by 100 l/s sputter-ion pumps spaced every 22.5 m. The antechamber dimensions are chosen to provide adequate vacuum conductance to transport synchrotron-desorbed methane to the ion pumps. Pump power and vacuum gauges are discussed in 5.2.3.7.

The parameters and performance of this system have been analyzed in [65,66]. Inputs to the calculation included: 1) the measured synchrotron-induced desorption of major gas species from aluminum [67] as a function of the integrated dose of  $E_{\text{CRIT}} = 86$  eV photons, 2) the measured pumping speeds for NEG strip as a function of absorbed gas [68], 3) calculated conductances of the extrusion antechamber, 4) ion pump speeds for methane, and 5) scattering cross sections for the relevant gas species. This approach has given good agreement with the measured performance of LEP [69]. The result of the calculation (Figure 5.51) is that a beam-gas scattering lifetime greater than 200 hours will be achieved after approximately one week of operation. During the “beam cleaning” period the beam current will be increased from an initial 50 mA to the design value of 190 mA in five successive fills. The beam power scattered into the cryogenic system (Section 5.3.3) will not be a limiting factor during this time period.

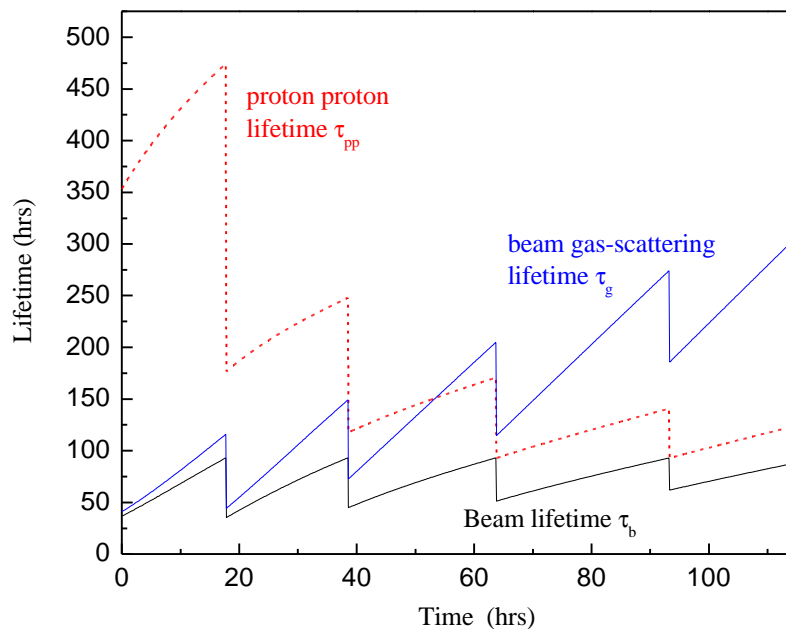


Figure 5.51. Beam scrubbing scenario for Stage-1 aluminum vacuum chamber. During the first 5 fills the beam current is increased from 50 mA to the design value of 190 mA. As synchrotron radiation desorption cleans the walls of the beam chamber, the vacuum lifetime increases to >200 hours.

Production of the aluminum vacuum system will be integrated into the magnet factory. Tunnel labor is minimized by pre-assembling 65 m lengths of extruded pipe which are installed in the magnets, cabled, and tested at the factory. Beam pipe extrusions 12 m in length will be

received, inspected, and cleaned using an environmentally safe alkaline cleaning procedure developed at the APS at Argonne and used on the Fermilab Recycler [70]. The sections will be welded together to form 65 m lengths that include the Ion Pumps, NEG strips, feed-throughs and end transition sections. The assembly will be sealed, pumped and baked at 200°C for 12 hours in a 65 m long vacuum oven similar to the one built for the Recycler beam pipes.

The vacuum pipe assembly is then snapped into the C-magnet gap (Figure 5.52) in such a way that the beam chamber is pre-loaded against the magnet laminations. The preload prevents any possible loss of vertical aperture inside the magnet. The beam pipe has to be deformed slightly to get it inside of the horizontally focussing gradient magnet. This has been analyzed [71] in ANSYS and stresses are acceptable even for annealed aluminum.

The design does not provide for an in-situ bakeout. After factory bakeout the magnets will be stored and transported with the beam pipes capped off and under vacuum, and the beam pipes will be let up to dry nitrogen and the caps cut off to make the field joints in the tunnel. Under these circumstances an in-situ bakeout gains about a factor of 2 in initial dynamic outgassing [72], and gains very little after the beam scrubbing has completed [73]. A similar conclusion has been reached at the ELETTRA light source [74]. Our R&D program should verify this.

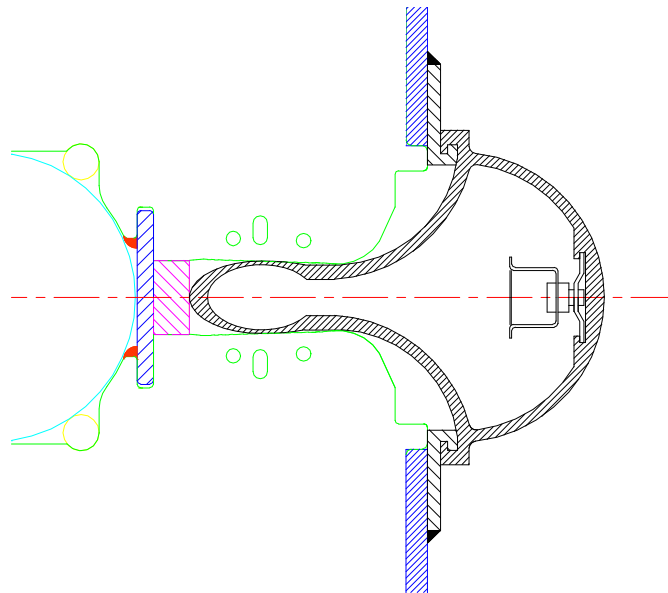


*Figure 5.52. Cross section of beam pipe extrusion inserted into the magnet. During insertion the beam pipe is elastically deformed to fit it into the gradient magnet.*

#### 5.2.4.2 Straight Section Vacuum System

Synchrotron radiation is absent or reduced in most of the 8 km of straight sections and the vacuum system will be a conventional baked stainless steel / ion pump system similar to those commonly used at Fermilab. The 10 cm aperture of the 135 m stainless steel pipes between quadrupole locations is large enough that the beam impedance, alignment, and vacuum conductance are not a problem. The reduced apertures at the quadrupoles and corrector locations will be handled with 30 cm funnel transitions, which may be copper-plated stainless, or aluminum.

### 5.2.5 Once-per-Turn Instrumentation

A number of standard instrumentation systems occur only once per ring. In general these can be copied from existing systems in the Tevatron and/or Main Injector. The 53 MHz bunch structure and modest beam currents ( $\sim 1/3$  of Tevatron fixed target) provide no special challenges. Readout electronics for these systems is located in shielded rooms at the Utility Straight Sections. A warm beam pipe is used everywhere except at the IR triplet and superconducting RF cavities, so the instrumentation interface is simple. Physical layout of these systems is not heavily constrained since quadrupole spacing is typically 150 m, the beam pipes are separated by  $\sim 45$  cm for much of the utility straight sections, and the transmission line and current return have been moved away from the beam to reduce fringe field. These are discussed more fully in [75].

Table 5.25. Once-per-turn instrumentation parameters.

FUNCTION	Occurrences	Readout Frequency	Comments
Tune Measurement	a few/ring	10 Hz	Use Arc Module DSPs for FFT?
Beam Current Toroids	1/ring		Also on injection lines
Sampled Bunch Display	1/ring	1 Hz	
Fast Bunch Integrator	1/ring	1 Hz	
Synchrotron Light Monitor	1/ring	1 Hz	
Ion Profile Monitor	2/ring	.1 Hz	Small beam size may be challenging
Flying Wires	1/ring	$\sim$ few per store	

### 5.2.6 Radio Frequency Systems

Either superconducting or warm copper cavities produce workable RF acceleration systems for the Stage-1 machine [76]. During the design study acceptable parameters and costs based on the B-factory RF systems were developed [77]. The system described here is based on superconducting RF (SCRF). The advantages of SCRF are a higher energy efficiency during the long periods at storage flattop, and more flexibility to produce RF overvoltage to control beam instabilities if this proves to be an advantage.

The RF system parameters and some RF relevant machine parameters are summarized in Table 5.26. The RF frequency is 371.7 MHz, the seventh harmonic of 53.1 MHz. Overall the VLHC RF system is similar to the LHC RF [78,79], but with somewhat relaxed requirements for higher-order mode damping due to lower total beam current. The superconducting cavities are manufactured using niobium on copper technology developed at CERN. As in the case of LHC, there will be separate RF systems for counter-rotating beams. The beam separation in LHC is 420 mm. If we just scale cryomodule dimensions with RF frequency, we get beam separation of 453 mm.

To minimize the effect of the transient beam loading, cavities with high stored energy are preferred. The LEPII RF system experience [80] and tests of LHC [79] and SOLEIL [81] cavities show that it is reasonable to expect operating gradients as high as 8 MV/m. For VLHC we chose a gradient of 7.75 MV/m (3.125 MV per cell). Sixteen single-cell superconducting cavities are needed for each beam in the Stage-1 machine and 64 cavities are needed for each beam in the Stage-2 machine. The low  $R/Q$  of the LHC cavity helps to increase its stored energy. Still, the large (10%) beam gap will produce a very strong periodic modulation of RF

phase of  $27^\circ$  for Stage-1 and  $10^\circ$  for Stage-2. This modulation is larger than at the LHC. A special RF feedback loop around the amplifier-cavity system assisted by the programmed phase modulation *a la* LHC [82] will be necessary to suppress this effect.

Table 5.26. Summary of RF system parameters.

	Stage-1		Stage-2	
	Acceleration	Storage	Acceleration	Storage
Beam current	190 mA		68.9 mA	
Beam energy	0.9 – 20 TeV	20 TeV	10 – 87.5 TeV	87.5 TeV
Acceleration time	1000 sec		2000 sec	
Acceleration per turn	14.8 MV		39.4 – 18.15 MV	
Acceleration power (both beams)	5.62 MW		4.134 MW	
Synch. rad. loss per turn		0.03 MeV		12.37 MeV
Total s.r. power (both beams)		13 kW		2.1 MW
Revolution frequency	1286.5 Hz			
Bunch length, rms	142 mm	66 mm	81.9 mm	33.7 mm
Synchrotron tune	0.00845	0.00179	.00280	.00189
Synchrotron frequency	10.87 Hz	2.30 Hz	3.60 Hz	2.43 Hz
Bunch frequency	53.1 MHz			
Number of buckets	41280			
Bunch spacing	5.646 m, 18.8 ns			
RF harmonic number	288960			
RF frequency (7×53.1)	371.7 MHz			
RF wavelength	80.65 cm			
RF voltage	50 MV	50 MV	50 MV	200 MV
Accelerating gradient	7.75 MV/m			
Voltage per cavity	3.125 MV			
$R/Q$	89 Ohm			
$Q$ factor at 8 MV/m	$2 \times 10^9$			
Number of cavities	32 (16+16)		128 (64+64)	
Cavities per cryostat	4			
RF cavity wall losses	55 W			
Cryostat static heat leak	60 W			
Total cryogenic heat load	2.24 kW		8.96 kW	
Beam power per cavity	176 kW	0.406 kW	42.4 kW peak	16.4 kW
Number of 500 kW klystrons	16 (8+8)		16 (8+8)	
Number of cavities per klystron	2		8	

Each cryomodule will accommodate four single-cell cavities with cell-to-cell distance of  $3\lambda/2$ . The overall length of the cryomodule is approximately 5.6 m. The static heat leak of the cryomodule is 60 W and the RF cavity wall losses are 55 W/cavity, which yields a total cryogenic load of 280 W per cryomodule. The overall cryogenic heat load (without losses in cryogen distribution system) is 2.24 kW for Stage-1 and 8.96 kW for Stage-2.

Due to the rather small RF power per cavity, we propose to use 500 kW klystrons with two cavities per klystron in Stage-1 and eight cavities per klystron in Stage-2. The number of klystrons required is 16 for each stage. A 500 kW CW klystron was jointly developed and constructed recently by CERN and SLAC for testing LHC cavities [83]. The klystron has a high

efficiency of 68% and thus the required AC power is 735 kW to generate RF output power of 500 kW. Then the maximum total wall-plug AC power for klystrons is 11.76 MW total for both beams.

The klystron collector cooling water flow of  $\geq 400$  l/min yields a total cooling water requirement of 6400 l/min. RF water loads will need an additional 4000 l/min (during beam deceleration only) and ferrite circulators will consume 480 l/min. Thus the total amount of de-ionized water required for the RF system is 10,880 l/min per ring.

To estimate the cost of Stage-1 cryomodules we will use the formula [84]

$$C = k \cdot (0.8)^{\log(L)} \sqrt{\frac{1300\text{MHz}}{f[\text{MHz}]}} \cdot L$$

Here  $L$  is the active length of accelerating structure;  $k = 200$  k\$/m is the cost factor. As one can see, the cryomodule cost scales approximately linearly with total length of the RF structure. The total cost of cryomodules for Stage-1 is then equal to 4.2 M\$. The RF chain cost (including klystrons, high voltage power supplies, low level electronics, and RF distribution) is \$1/W and totals to 8 M\$.

The VLHC RF system would greatly benefit from R&D on improving the technology of sputtering niobium on copper with the goal to decrease if not completely eliminate the phenomenon of the  $Q$  slope. Special efforts should be devoted to understanding the nature of this effect. Success of this R&D would allow an increase of the accelerating gradient without seriously increasing the cryogenic heat load. Also, an R&D program is required to develop RF controls for heavy beam loading. Careful analysis of transients during injection, acceleration and beam storing is necessary and may necessitate having an individual klystron for each cavity [79].

## 5.2.7 Beam Dampers

In the last 30 years high intensity storage rings have become absolutely dependent on beam damper circuits. The Tevatron in fixed-target mode, the Booster, and the LHC will not operate anywhere near design intensity without them. At synchrotron light sources and B-factories the beams are lost within milliseconds without dampers. It is thus not surprising that the VLHC requires damper circuits to reach design luminosity for both Stage-1 and Stage-2 operation. Fortunately this technology is well developed. One new element which does occur in the Stage-1 VLHC is the necessity to distribute the dampers for one type of instability (the coupled-bunch resistive-wall instability) around the large circumference of the ring. While this provides some level of redundancy (since the beam is stable even if one of the distributed circuits fails) it is a new element which will be described below. Other dampers are conventional.

### 5.2.7.1 Distributed Transverse Dampers for Resistive-Wall Stability

Growth of transverse motions of bunches in the LF ring will be suppressed with active feedback systems [85]. The strongest beam impedance arises from resistive-wall. At the frequency of the first lower-sideband coupled-bunch mode, which is  $(1-0.235)f_0 = 0.99$  kHz, the transverse beam impedance is  $(7.84+1.27j)10^{10}$  ohm/meter. This causes an exponential growth rate

of  $2.53 \times 10^3$  per second for a fully filled machine. Prompt cancellation of this growth is provided by six localized feedback stations spaced around the ring circumference. At each station, radial and axial damping are the same, and for each there are two feedback systems displaced azimuthally by  $270^\circ$  in betatron phase to address both ‘sine’ and ‘cosine’ phases of the oscillation; this makes the damping tolerant of tune changes that might be desired.

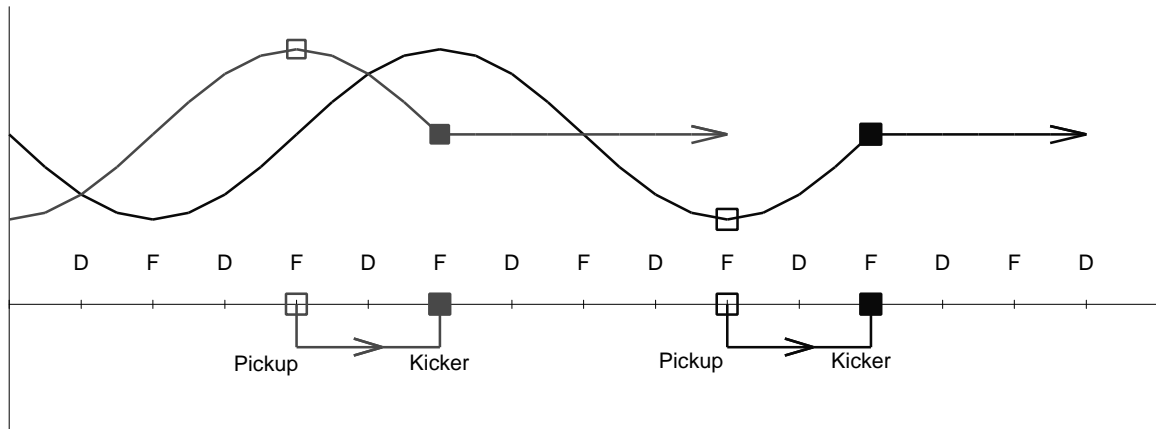


*Figure 5.53. Layout of pickup and kicker positions for the horizontal coordinate at one station. Incoming beams with sine-like or cosine-like oscillations have their positions sensed by pickups at cell boundaries (F- locations) and are kicked back towards the design orbit after one-quarter betatron oscillation. An identical set of vertical pickups and kickers operates at D-locations. Six identical stations are distributed around the ring, one at each Stage-1 cryoplant location.*

In localized feedback, a kicker is located downstream from the pickup by  $90^\circ$  in betatron phase (one lattice cell) and the signal is transmitted promptly from pickup to kicker through foam-insulated coax to minimize delay. Delay in the 271 meters of cable is 180 ns to which one adds about 50 ns for electronic processing and amplification. Although with this delay the signal from one bunch is delivered to the 12<sup>th</sup> following bunch, the phase delay at 1 kHz is a negligible 1.5 milliradian. For higher-frequency sidebands the phase delay increases, becoming a significant 1/8-oscillation at 550 kHz. The localized feedback systems will be used up to 500 kHz; at that frequency the impedance has become small enough to be controlled by a conventional one-turn bunch-by-bunch system that extends up to the needed 26.5 MHz bandwidth of coupled-bunch modes.

The hardware in a local feedback system consists of (1) a pair of capacitive pickup plates, (2) electronics and cable to the kicker, and (3) a 4-meter long stripline-pair kicker. The pickup strips are 25 cm long and connect to high-impedance amplifiers. The signals are then differenced and the unipolar pulses are stretched to half the interval between bunches to give a baseband signal for the kicker. At the lowest, strongest mode, the required feedback loop-gain is  $G = 0.287$  and to damp injection errors of 0.1 mm calls for a transverse kick of 83.3 kV. The kicker delivers this with a power input of 1.10 kW. Injection in bunch trains separated by 2 seconds produces unwanted transients, especially if there is closed-orbit offset. Bunch signals will be recorded and analyzed to generate a correction for the local closed-orbit corrector; this will zero the closed-orbit well before the second train of bunches is injected. After the ring is filled, additional rejection of very low frequency excursions will be made by the low-frequency

cutoff of the feedback electronics; this is possible with baseband operation as we have used here. For damping both radial and axial motions at 6 stations, 24 systems are required for each circulating beam.

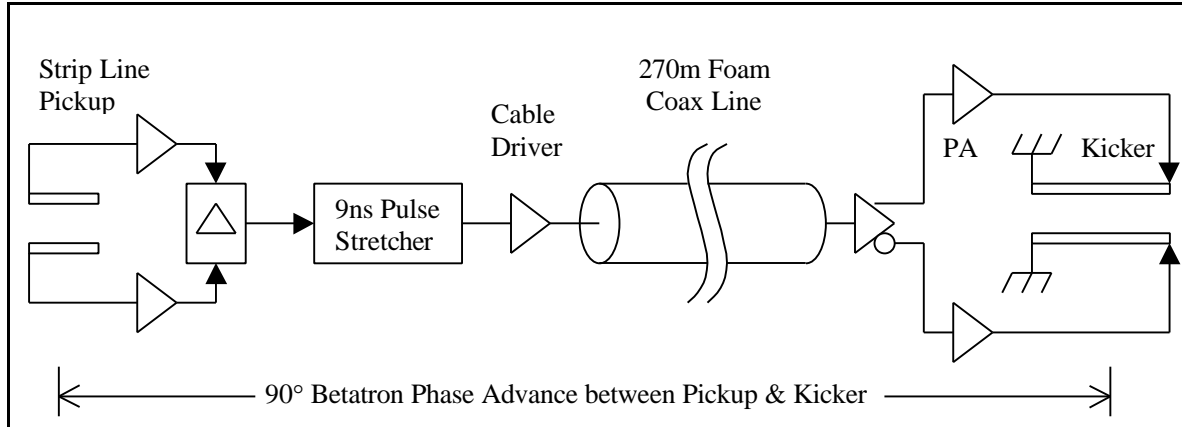


Figure 5.54. Electronic elements of the coupled-bunch feedback system.

Pickup and kicker are located at points of maximum betatron amplitude in slightly modified standard arc cells. The modifications (Section 3.2.1.4) involve removing 5 m of magnet iron at the boundaries of 8 successive half-cells. An additional quadrupole corrector is used at each location to repair damage to the  $\beta$ -functions caused by the missing focusing. The  $\sim 10\%$  dispersion wave generated by the missing bend automatically cancels outside the insertion by virtue of the  $360^\circ$  phase advance across the 8 half-cells. The damper system uses at most 6 of the 8 available free spaces. Placing the damper pickups and kickers where the dispersion is nonzero is not believed to cause difficulties although this will be the subject of continuing study.

At the coupled-bunch mode frequency of 500 kHz, the growth rate has been reduced to 57 per second or 0.044 per turn. This and all higher coupled-bunch modes are suppressed by the one-turn bunch-by-bunch feedback system that operates over the range  $53.1 \pm 26.5$  MHz. The kicker is a quarter-wavelength long at this frequency, 1.41 meter. The required kick for 0.1 mm excursion is 26.4 kV and power is 513 watt. Power amplifiers suitable for this application are commercially available. The pickup is the same length as the kicker and feedback gain is 0.108. Radial and axial systems are similar.

One can ask if electronic noise in these dampers will add emittance during a long collision time. Fortunately, although the loop gains are high, the small aperture and peak bunch current of 8.4 ampere make the pickup signal strong and large electronic gain is not needed. The peak current gives a pickup sensitivity  $IZ_L g / b \sqrt{2} = 2.6 \times 10^4$  volt/meter. Input thermal power with an amplifier noise figure of 1 dB is  $1.2kTB = 5.2 \times 10^{-21} B$ , where  $B$  is the bandwidth. Equating this to the pickup signal power with equivalent rms noise amplitude  $X_N$  gives  $\langle X_N^2 \rangle = 3.7 \times 10^{-28} B$ . The higher energy at collision reduces the gain to  $G = 0.013$ . The 12 feedback systems would then cause an emittance growth rate, without allowing for damping, of

$$\frac{de}{dt} = 12 \frac{f_0 g}{2b} \langle G^2 X_N^2 \rangle = 2.1 \times 10^{-17} \text{ m/sec}$$

Since the nominal emittance is  $1.7 \times 10^{-6}$ , this dilution rate is of no concern. It would actually be smaller because of damping by the feedback. The broadband system produces a similarly negligible emittance growth.

## 5.3 Radiation, Machine Protection, and Beam Abort

### 5.3.1 Overview

The 2.8 GJ of kinetic beam energy in the Stage-1 machine is approximately eight times that of the LHC. Under normal circumstances roughly 50% of this energy is gradually dissipated in beam-beam collisions at the IRs. A few percent of the energy is lost diffusely due to beam-gas collisions around the ring, intercepted by beam collimation inserts which scrape away beam halo particles, and dissipated in the RF loads as the beam is decelerated. Somewhere between 40% (intentional beam abort at the end of the store at normal operation) and 100% (unintentional beam abort at certain circumstances) of the beam energy can be deposited in the external beam absorbers.

A very small fraction of the machine circumference exceeds the limit ( $\sim 1$  W/m of beam losses) for normal “hands-on” maintenance [86]. These regions include the small-angle regions of the IRs, the beam collimation system, and a small region of arc magnets downstream of the beam collimation system. The average radiation load in these components is a few times higher than the LHC, and the shielding and handling requirements comparable. LHC experience will be useful in optimizing these designs.

Under accidental conditions there is enough energy to cause severe damage to the magnet and surrounding environment. This is not a new situation for high energy colliders. The ISR beams had enough energy to repeatedly burn holes in the machine [87]. The magnitude of the problem has increased however. The beam of the Stage-1 machine carries enough energy that in principle it could liquefy 400 liters of stainless steel (whereas the LHC beam can only liquefy 50 liters).

Under worst-case accident assumptions the beam will leave the machine and strike the tunnel wall. We have begun to study the mechanical and radiological consequences. See Section 5.3.3. A single shot beam accident releases beam energy equivalent to losing the Main Injector beam at one place for about 4 hours. This is not outside the scope of existing shielding requirements at Fermilab, and should not be major problem for a tunnel in deep bedrock.

Tunnel groundwater activation from single-pulse accidents appears not to be a concern. A preliminary calculation indicates that it would be possible to lose the beam in a single spot, immediately transfer the activation into the tunnel water sump pit, and pump out the activated water without violating applicable Federal guidelines. Another way of saying this is that you could dump the beam into the tunnel sump cistern and the water would still be safe to drink. (This is of course a very pessimistic scenario, since in reality it will take days or weeks for the groundwater to collect in the sump, by which time most of the radioactivity will have vanished).

Effective strategies have evolved to deal with machine protection issues culminating with the Tevatron, SSC, and LHC. These issues have been revisited for VLHC energies [88,89] and the results are summarized here.

A robust and redundant extraction system removes the beam whenever the position becomes unstable or anomalous losses are detected. This protects the machine from anything that happens “slowly” (in milliseconds to seconds) such as magnet quenches, RF or power supply failures, vacuum failures or corrector magnet trips. Such a system has prevented the Tevatron (so far) from having a hole burned through it. This is a standard feature, which continues to be essential at VLHC energies.

The one credible accident that occurs on a rapid time scale involves an abort kicker module misfire. The incompletely extracted beam will rattle around the machine and hit various well-defined limiting apertures such as extraction septa, IR quadrupoles, and beam collimators. The probability of this will be reduced in the LHC by replacing Thyratrons with solid-state kicker power supplies, and appropriate fail-safe logic which in principle prevents a single module misfiring. Since the probability of this cannot be reduced to zero, a set of “sacrificial collimators” are placed upstream of the vulnerable components. These are replaceable graphite structures that absorb and diffuse the beam energy. This strategy is essential at the SSC/LHC and will be necessary and sufficient for the VLHC.

Three qualitatively new features emerged while reviewing the machine protection situation at VLHC energies. First, the graphite core of the beam absorber may be damaged by a single pulse in the case of a sweeper magnet failure. The core must be protected (Section 5.3.2.2) with a replaceable sacrificial collimator immediately upstream. Secondly, in the case of a sweeper magnet failure the beam window in the extraction channel will have a hole melted in it. This is not a safety issue, but in this accident scenario the beam vacuum must be protected with an automatically closing gate valve and the window(s) must be replaced. Finally, the beam collimation system (Section 5.2.3.4) will require water cooling for the jaws of the secondary collimators.

## 5.3.2 Beam Abort System

### 5.3.2.1 *Extraction*

It turns out to be quite straight forward to kick the beams out of the machine towards absorbers. The magnet parameters and layout are discussed in Section 5.1.5.4.2. Like the Tevatron, SSC and LHC abort systems, we use fast kicker magnets to switch the circulating beam into the other aperture of Lambertson magnets. The circulating beam goes through the field-free hole in the Lambertson magnets, and the extracted beam is bent upward in the Lambertson magnets so as to clear the first quadrupole in the downstream half of the straight section. A full aperture extraction kick is used and the separation of the circulating and extracted beams is 25 mm at the entrance to the Lambertson magnets. Thus any beam which is circulating anywhere in the physical aperture will be extracted. Special large-aperture warm-iron-and-copper quadrupoles are used near the Lambertsons so that no aperture restriction is presented to the circulating beam.

Normally the beam extraction is synchronized with an “abort gap” in the beam that has a length equal to the rise time of the extraction kicker. During certain control system failures it may be necessary to unconditionally extract the beam. This sweeps the beam across the extraction septum, which must survive without damage. For the VLHC the stress on the extraction septum is roughly equal to the LHC (since the beam energy per unit time is similar) and does no damage.

The requirements for the reliability of a one-turn extraction mechanism are comparable to the SSC [90] and LHC [91]. The extraction kicker is broken into 10 independent modules, with any 7 out of 10 sufficient for a safe abort. Solid-state pulsers (as opposed to Thyratrons) will be used to minimize accidental prefires. Three Musketeer logic (“All-for-one, and one-for-all!”) guarantees that any single module firing will automatically trigger the rest of the modules.

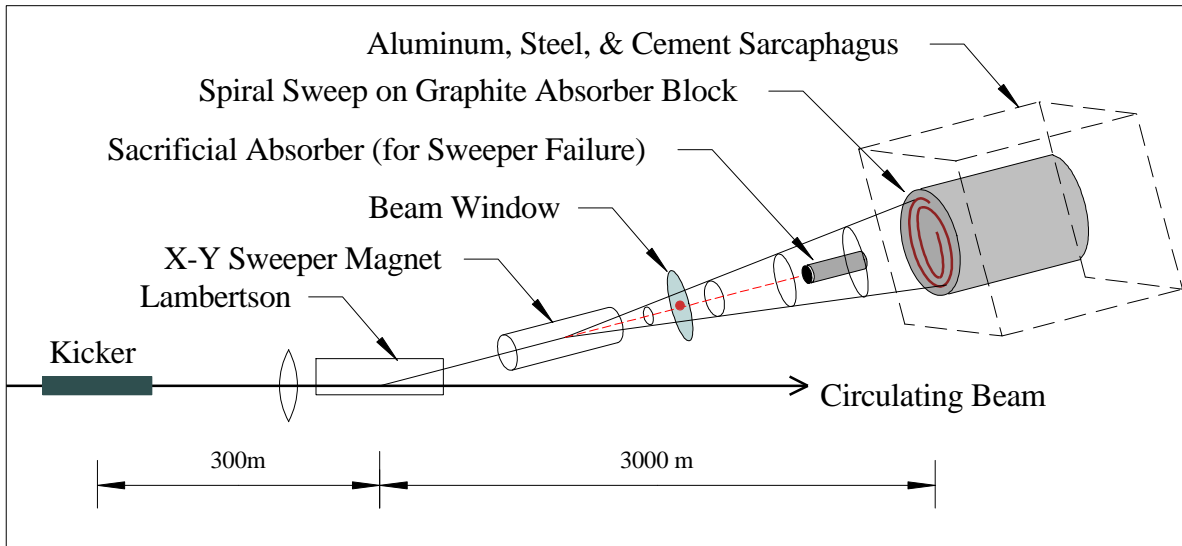


Figure 5.55. Schematic layout of beam abort channel including kickers, Lambertson septa, extraction beam sweeping, beam window, sacrificial rod, and graphite beam absorber. Under normal circumstances the extracted beam is swept in a spiral pattern to spread the energy across the graphite dump. If the sweeper magnet fails, the beam travels straight ahead into a sacrificial graphite rod, which takes the damage and must be replaced.

### 5.3.2.2 Beam Absorber

For TeV beams, the natural choice for the absorber is graphite, as at the Tevatron, SSC and LHC. The major difficulty lies in making the beams big enough that they will not crack a graphite absorber. A standard absorber consists of a graphite core, contained in an aluminum jacket with water cooling, followed by adequate steel and cement to protect ground water. The graphite core is rectangular, with dimensions  $10 \times 1.2 \times 1.2$  m. The thickness of steel shielding around the aluminum container is about 1.3 m on each side and extends about 3 m downstream. At present we consider a “4-in-1” design where extracted beams from both directions hit absorber cores in a common sarcophagus. The Stage-1 and Stage-2 machines share a common absorber for each direction (see Figure 2.2).

Activation and cooling water considerations are driven by the average beam power on the target. The 300 kW average power (Section 7.4.1) corresponds to one full-energy abort of both

beams every day and is equal to the 300 kW design value for the Main Injector beam absorber. The overall design is patterned on the Main Injector absorber that has proven satisfactory and meets ES&H requirements for this power level.

The graphite dimensions and beam size necessary to contain the showers without cracking the graphite were found by detailed simulations with the MARS14 code. The design goal was to keep the maximum temperature rise at the axis of the graphite core per spill below 1300-1500°C (from successful Tevatron dump experience and theoretical shock wave considerations). For a purely Gaussian beam with a spill that is stationary in transverse position, the beam sigma would need to be 19 cm in both x and y for the maximum temperature rise in the core of 1330°C. Expanding the beams to this size with defocusing quadrupoles is out of the question.

### 5.3.2.3 Beam Sweeping System

A spiral beam sweeping scheme similar to the SSC and LHC is adopted to spread the beam energy across the absorber core. The magnets are described in Section 5.1.5.4.2. A horizontal and a vertical sweeper, 90° out of phase, both oscillate with decaying amplitudes. Ideally the frequency should increase as the radius of the spiral decreases in order to keep the temperature rise constant. Since this is electrically difficult, a suitable compromise is to limit the inner radius of the spiral to half that of the outer radius and accept a factor of two higher temperature rise at the inner radius. An estimate indicates that an outer radius of 30 cm would be adequate to keep the temperature below 1500 °C. If the beam sigma was 0.5 cm in both planes, the frequency of these sweepers would be 9.7 kHz.

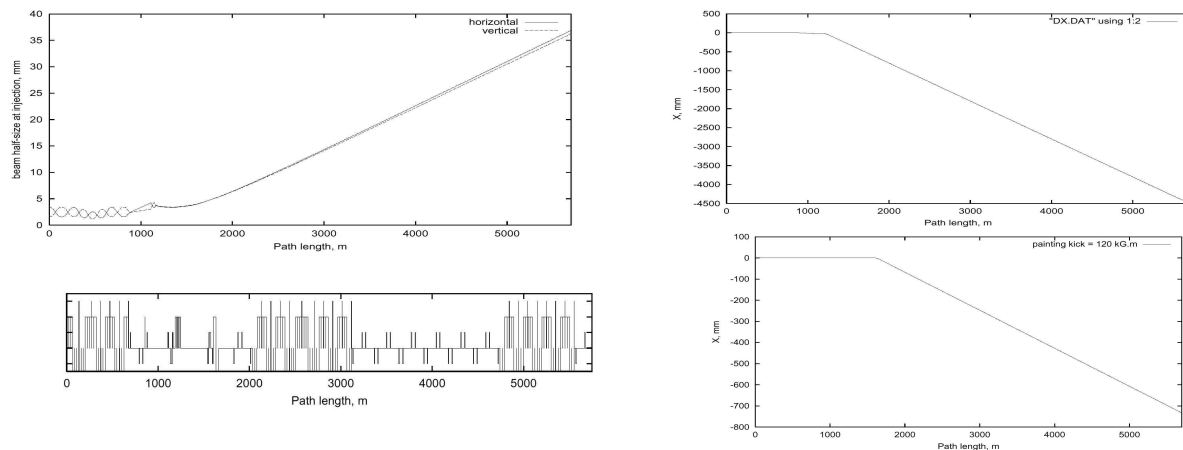


Figure 5.56. Beam sweeping system optics. Left: 3-sigma beam half-size at 1 TeV injection (beam size at 20 TeV is 4.5x smaller), and beam line layout. Right: beam displacement with respect to the direction of extraction straight section and maximum sweeping kick in the horizontal or vertical plane.

In the case of a failure of both coordinates of the sweeper system the beam would damage the graphite absorber core [92]. To prevent this, a sacrificial graphite rod 5 cm in diameter and 4 m long is positioned on the beam axis immediately upstream of the main absorber. See Figure 5.55. Normally the extracted beams will spiral around this rod without hitting it. If the beam is

extracted with all sweeping magnets off, the beam damage will be confined to the sacrificial rod. The rod will be housed in a metal box to prevent the spread of radioactive debris.

A beam window will not be protected in case of sweeping system (or defocusing quadrupole) failure, if the effective beam sigma on the window is less than 0.5 cm. The ring vacuum can be preserved by rapid-acting gate valves and/or multiple windows in series. Each window gets a small hole drilled in it when the sweepers fail, and pumping between the windows isolates ring vacuum until a slow gate valve closes. Alternatively, differential pumping with several wire meshes would do the same job. No personnel safety issues are involved.

### 5.3.3 Radiation and Beam Loss

#### 5.3.3.1 *Quenches from Beam Loss in Transmission Line Magnets*

The warm-iron design of the Transmission line magnet is less sensitive to radiation-induced quenches than ordinary superconducting magnets. To determine tolerable beam loss in the arcs, MARS14 simulations are done in the lattice both at injection (1 TeV,  $\sigma_{x,y} = 1.4$  mm,  $\alpha_{inc} = 0.7$  mrad) and top energy (20 TeV,  $\sigma_{x,y} = 0.3$  mm,  $\alpha_{inc} = 0.15$  mrad). Corresponding materials and magnetic field distributions have been implemented into a 3-D model. Inward and outward beam losses were considered both for inner and outer beam pipes (see Figure 5.57).

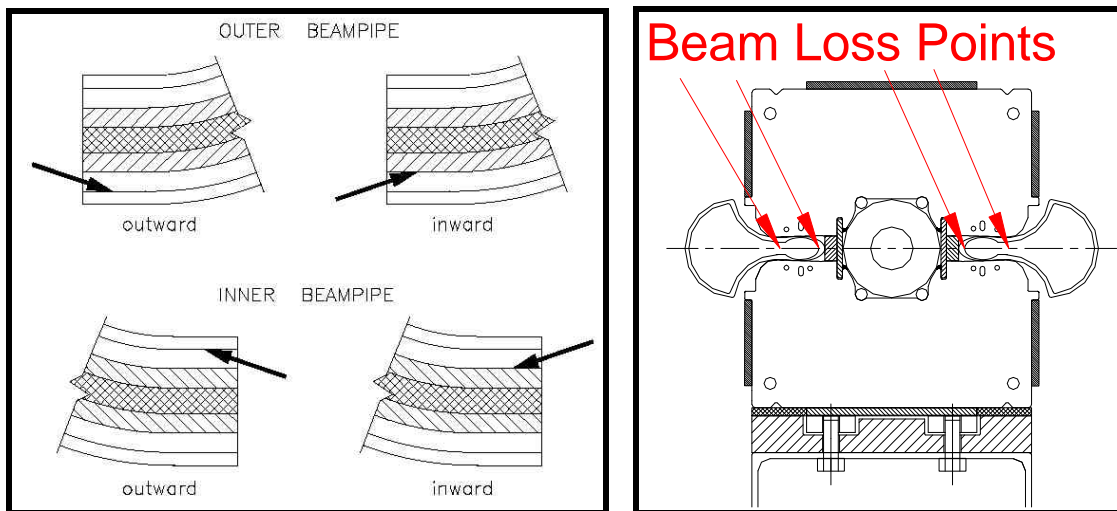


Figure 5.57. Beam loss geometries simulated in the Stage-1 VLHC magnets.

Simulations show that the superconductor in the transmission line magnets is rather well protected radially by warm iron. The energy deposition is diffuse and the peak temperature is relatively low at the hottest spot in the showers downstream of where the proton hits the beam pipe. Therefore, the tolerable beam loss is significantly higher than in a conventional cosine-theta type magnets. Table 5.27 shows fast (1 msec) and slow (0.1 sec) beam loss rates needed to initiate a SC magnet quench at injection and top energy in the Stage-1 ring. For comparison, the values for the Tevatron at 0.9 TeV are shown. This comparison assumes that the quench limits are the same in the VLHC conductor and the Tevatron dipoles. This assumption is

probably pessimistic since the braided cable of the VLHC can re-route the current around a quenched region on the magnet midplane, whereas a cosine-theta magnet cannot.

Table 5.27. Quench-inducing loss thresholds (protons per pulse) for the Stage-1 VLHC and Tevatron.

	Fast Loss (ppp)	Slow Loss (ppp)
0.9 TeV	$9 \times 10^8$	$3 \times 10^9$
20 TeV	$2.5 \times 10^7$	$7.5 \times 10^7$
Tevatron	$4 \times 10^7$	$3 \times 10^8$

### 5.3.3.2 Cryogenic Heat Load from Beam Losses

Heat load from beam-beam interaction debris in the IR quads is included explicitly in the discussion in Section 5.2.1. The distributed heat load from beam losses in the arcs is also a potential concern. At 20 TeV roughly 5% of the energy from beam losses is estimated to be absorbed in the cryogenic transmission line. If 1% per hour of the (3+3) GJ of beam energy were lost uniformly in the arcs, this amounts to a total heat load of 800 W (3.5 mW/m average). This is a 5% perturbation on the 5 K heat load. The collimation system (Section 5.3.4) is expected to localize essentially all beam halo losses into collimators in warm sections, thereby eliminating that heat load from the cryo system.

The collimation system will be ineffective against losses from inelastic beam-gas scattering. With the expected vacuum lifetime (Section 5.2.4.1) of >200 hours, the cryogenic heat load will be < 2 mW/m, less than 3% of the 4.5 K heat load. If continued R&D reduces the 4.5 K heat leak this will become an increasingly important part of the total.

### 5.3.3.3 Radiation Damage to Tunnel Electronics

Section 5.2.3 describes electronics housed in small enclosures (“holes in the wall”) at each half-cell location. This approach was studied at UNK [93] and the electronics was found to survive under rather conservative assumptions about their radiation hardness. A recent interesting development [94] is that modern CMOS is found to be intrinsically rad-hard due to the absence of long-term charge trapping at the gate oxide layer in sub-micron devices. The LHC is apparently contemplating placing unshielded electronics under each dipole, and is initiating a study of the radiation hardness of commercially available electronics [95]. Depending on LHC operational experience, the rather modest costs of the module enclosures might be saved by eliminating the enclosures.

Radiation damage to fiber optics placed in the tunnel was studied at the SSC [96]. It was found that placing the fibers into the trough in the invert guaranteed their survival even for upgrades to 10x the SSC luminosity. We have followed this approach (Section 5.2.3.8).

### 5.3.4 Beam Collimation System

Even in good operational conditions, a finite fraction of the beam will leave the stable central area of the accelerator aperture because of intra-beam scattering, small-angle beam-gas interactions along the circumference, collisions in the IPs, RF noise, ground motion and resonances excited by the accelerator imperfections. These continuously generate a beam halo. As a result of beam halo interactions with limiting apertures, hadronic and electromagnetic showers initiated in accelerator and detector components will cause accelerator related background in the detectors, magnet heating and accelerator and environmental irradiation. The design strategy of the VLHC is that the beam losses are controlled as much as possible by localizing them in a dedicated beam collimation system. This minimizes losses in cryogenic parts of the accelerator, and drastically reduces the source term for radiation hazard analysis in the rest of the lattice. The technology for these systems has been well developed for the Tevatron, SSC, and LHC.

For the VLHC a complete beam cleaning system which provides for both betatron and momentum scraping has been designed and simulated [97,98]. The three-stage beam collimation system consists of 5 mm thick primary tungsten collimators placed at  $7\sigma_{x,y}$  and 3 m long copper secondary collimators located in an optimal phase advance at  $9.2\sigma_{x,y}$  and aligned parallel to the circulating beam envelope. Two more supplementary collimators are placed in the next long straight section to decrease particle losses in the low- $\beta$  quadrupoles and in the accelerator arc. They are located at  $14\sigma_{x,y}$  to intercept only particles scattered out from the secondary collimators.

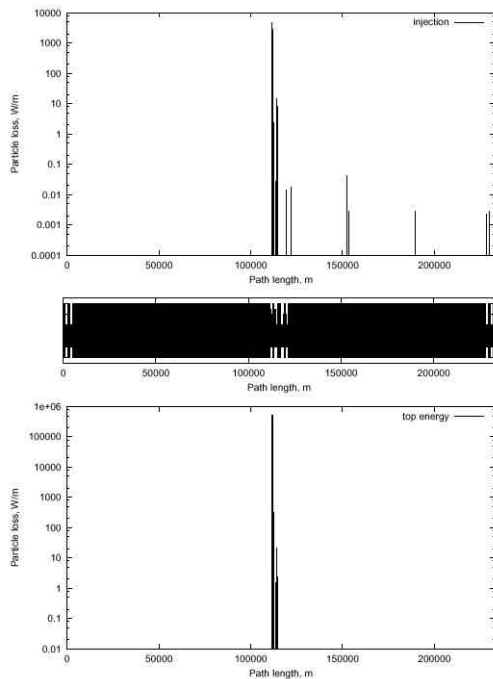


Figure 5.58. Beam loss distribution along the accelerator at injection (top) and at collisions (bottom).

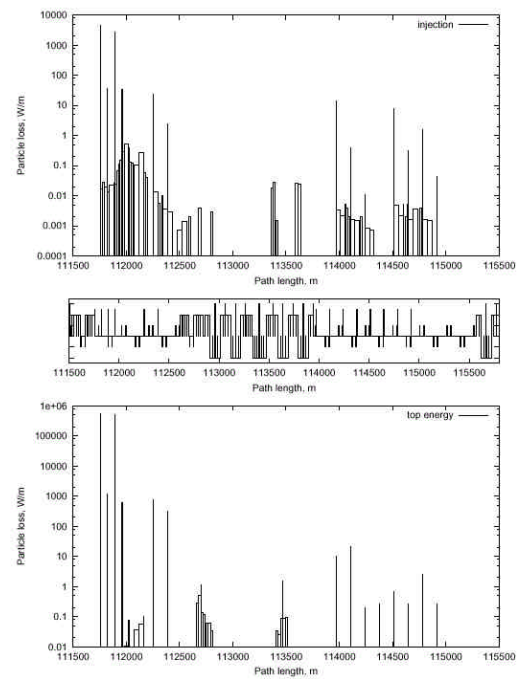


Figure 5.59. Beam loss distributions in the collimation section at injection (top) and at collisions (bottom).

Figure 5.58 shows that the simulated performance of the system meets the goal of essentially eliminating losses away from the cleaning insert. The main reason for this excellent performance is that the system uses a lattice insert specifically designed for this purpose, rather than something that has been retrofit into an existing machine such as the Tevatron. The maximum beam loss in the arc section behind the collimation region (Figure 5.59) is 1 W/m in two 21.5-m long dipoles and one 6-m long quadrupole, and 0.2 W/m in two 21.9-m long gradient magnets.

The beam cleaning system was designed with the goal of reducing losses and detector backgrounds near the high luminosity insertions. Without the supplementary collimators, about 61 W of beam power ( $2 \times 10^7$  protons/sec) are lost upstream of the detectors. Including the supplementary collimators in our calculations, however,  $6 \times 10^4$  particles are lost in the collimators, and we did not see any losses in the vicinity of interaction point. Further investigations should be done to determine ultimate particle backgrounds in the IP with the collimation system.

The primary collimation insert will be located in a far side straight section conjugate to the one of the on-site Utility Straight Sections. Secondary collimators will be located in this section as well as in special locations near the IRs. The secondary collimator will absorb approximately 20 kW of beam power and will require water cooling, probably through an isolated RAW (radioactive water) loop heat exchanged with the LCW flow. Shielding of the collimators will require approximately 1 m of radial iron followed by 50 cm of radial concrete over a length of ~15 m along the beam line to allow free passage of rad-trained personnel. This will require locally enlarging the tunnel cross section but should not require a bypass tunnel.

### 5.3.5 IR Protection

A sophisticated system must be designed to protect the IR SC magnets, particularly from kicker misfires. As in the LHC [99], it will consist of a front collimator, inner and intermediate absorbers in the inner triplet, and of a neutral beam dump and several collimators in the outer triplet. The similarity of the Stage-1 IR layout to the LHC makes it likely that a similar protection layout would be workable. The length of these sacrificial collimators will need to be increased due to the increased energy and decreased beam spot size of the VLHC beams.

### 5.3.6 Worst-Case Beam Accidents

Work has begun on understanding the implications of a “worst-case” beam accident in the VLHC. The assumption is that some unspecified agent causes the beam to be kicked out of the machine with a rise time fast compared to the revolution frequency, so that the normal beam abort does not have time to act. This agent is also assumed to possess a “kicker flat top” accurate enough (<1%) that the beam is effectively held in one place for the duration of the accident. Under these assumptions the beam will rapidly melt a hole in the magnet and impact the tunnel wall at near grazing incidence (3-5 mrad).

A preliminary observation is that the nearby cryogenic piping would rupture due to the rapid temperature rise. This would also be true of the Tevatron, HERA, and the LHC so it is important to keep this mysterious agent out of these machines as well. The cryo piping is contained inside carbon-steel structures (vacuum jackets and magnet iron) which would limit

collateral damage. It would probably not even be noticed from the outside of the magnet. This is not our biggest problem.

A second observation is that the “beam drilling” scenario (in which a stable beam vaporizes a small channel deep into the target) is impossible at grazing incidence, even if the beam were perfectly extracted on a fixed trajectory. This beam drilling scenario is expected when the beam is normally incident onto a semi-infinite slab of material such as a beam absorber block. However at grazing incidence, the imbalance of the mechanical forces near the beam impact point (due to local heating of the rock) will cause a rock chip to “spall” out from the tunnel wall. This spalling behavior has been observed during rock excavation tests with electron beams [100] and follows this simple mechanical model. This spalling effectively sweeps fresh material across the beam and guarantees that non-vaporized material will be available to initiate the shower, even if the beam is perfectly extracted. Thus the pattern of energy deposition can be calculated accurately enough by assuming that the shower initiates at a more-or-less fixed position near the point of grazing incidence.

A MARS calculation has been performed (Figure 5.60) to evaluate the energy deposition under the assumption that both the rock and beam position remain fixed. The simulation indicates that a region 8 meters long and about 15 cm in radius are heated to the melting point of dolomite. Obviously it will splatter to the floor. The next step in the calculation (in progress) is to use ANSYS to evaluate the thermal stresses in the surrounding rock and estimate the amount of rock that breaks off from thermal stress. The rise time of the heat pulse (1 machine revolution or about 0.8 msec) allows the mechanical stresses to relieve themselves on the scale of a couple of meters, so a static mechanical analysis is approximately valid.

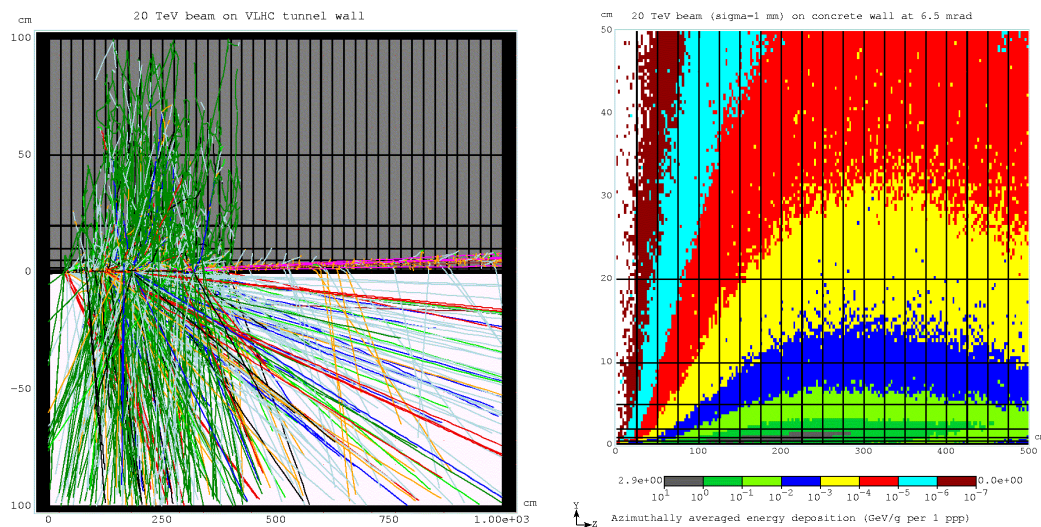


Figure 5.60. Stage-1 VLHC beam at 6.5 mrad grazing incidence on tunnel wall. The left picture shows particle tracks; the right picture is a map of energy deposition.

A more realistic situation in which the beam angle sweeps by even a few milliradians during extraction changes the situation significantly. In this case the heating is distributed into a large enough rock mass that the only a very small region (of order a centimeter wide) approaches the melting point. The picture becomes that of a destroyed magnet, a centimeter-wide

scar on the tunnel wall, and an amount of residual radiation comparable to that of a 4-hour continuous beam loss at the Fermilab Main Injector.

### **5.3.7 General ES&H Considerations**

#### *5.3.7.1. Introduction*

The VLHC with its two stages present a number of important considerations in the general area of environment, safety, and health. It is the intent of this section to identify the character of these challenges in a general way. Some of the considerations which must be taken into account are very similar to those that have been encountered and solved during the construction and operation of other facilities at Fermilab and at similar laboratories elsewhere in the United States and worldwide. Other novel issues have not been encountered on the same scale and require particular attention to assure their timely resolution in a manner that is cost-effective and that meets the approval of the public. In this section, both the conventional and the novel issues are discussed. With adequate planning in the conceptual design stages, these problems can be adequately addressed in a manner that merits the support of the Laboratory, the Department of Energy, and the public.

#### *5.3.7.2. Procedural/Regulatory Matters*

The actual design, construction, and operation of the VLHC will have to meet a number of procedural/regulatory milestones to assure timely and continued support by the public and by the Department of Energy. ES&H requirements are currently set forth as a part of Fermilab's Work Smart Standards, incorporated in the contract between the Universities Research Association and DOE. Currently, the Work Smart Standards are reviewed annually to assure that they adequately address the hazards of the laboratory, including those of any new facility. If changes are necessary they are negotiated and the URA-DOE contract is revised accordingly. These standards include listings of applicable Federal and State Regulations as well as internally developed policies and national standards [101]. Of course, the contract under which Fermilab might operate in the future is likely to change in ways that could modify the applicable requirements.

##### *A. Environmental Protection Procedural/Regulatory Matters*

All DOE activities are subject to the requirements of DOE's regulations for implementing the National Environmental Policy Act (NEPA) [102]. A new project of this magnitude will be the subject of an Environmental Assessment (EA). A review will be done of all possible impacts of this project on the environment and the public. The required analysis is broad in scope and includes societal impacts along with those topics that are more generally associated with environmental protection such as the discharges of pollutants, effects upon wetlands and floodplains, and exposures of people to chemicals and radioactive materials. It will include a review of the alternatives of carrying out the project elsewhere or not at all. This process is centered on the production of a comprehensive document but also includes the participation of the public by methods that will be chosen by DOE. A likely result will conclude that the preparation of an Environmental Impact Statement (EIS) is necessary since the VLHC extends

far beyond the present boundary of the Fermilab site. The EIS process is generally considered to be an arduous one, but one that can be followed to a successful conclusion. The preparation of an EIS is certain to be a large task having significant cost, customarily accomplished using external resources. Regardless of the eventual path of the NEPA process, project funds cannot be issued to support a Congressional "line item" project beyond the early conceptual stage prior to the successful completion of the NEPA process. It is thus crucial that this process be conducted in a manner that is honest and which comprehensively addresses the potential concerns of members of the public. A good working relationship with the Department of Energy is also a necessity to a successful result.

Other procedural requirements apply in the area of environmental protection. These will be more certainly identified as a part of the NEPA process but early planning may well serve to avert problems later. DOE facilities are generally subject to Federal and State environmental protection regulations promulgated chiefly by the U. S. Environmental Protection Agency (USEPA) and the Illinois Environmental Protection Agency (IEPA). Some of the Federal and State permits apply during the construction stages, others apply during operations, and some apply during both stages. Permits are likely to be required to cover such topics as storm water discharges, discharges of cooling water, wetlands mitigation, releases of air pollutants for both non-radioactive pollutants and for radionuclides, and construction in any floodplains. Archaeological sites might need further investigation and study prior to the commencement of construction. The preparation of the applications for these permits and approvals is generally straightforward. Early coordination with the project design team should greatly facilitate completion of the associated milestones. The VLHC is likely to be initially viewed by the public and by Federal and State regulators as a poorly understood, esoteric technology. In recognition of this and also because it will have an impact beyond the geographical boundaries of the present Fermilab site, early coordination with the Federal and State regulatory agencies is recommended as a vehicle to promote enhanced understanding of the nature and impact of the facility.

#### *B. Safety and Health Procedural/Regulatory Matters*

In accordance with Fermilab's Work Smart Standards, the Laboratory will be required to prepare an assessment of the ES&H issues associated with this project in the form of a Safety Assessment Document (SAD). Given the size, scope and cost of the VLHC, the preparation of a Preliminary Safety Assessment Document (PSAD) is needed. The purpose of the PSAD is to identify the relevant ES&H issues at an early stage and propose how they might be mitigated. A final Safety Assessment Document (SAD), then, documents the resolution of all the pertinent issues raised by the PSAD. Environmental issues are customarily integrated into the PSAD/SAD process to promote program cohesiveness. It is nearly certain that DOE will choose to review these safety documents by utilizing an external review team. Just prior to facility operation, a readiness review will be conducted in similar fashion using an external review team. Unlike NEPA assessment activities, PSAD/SAD activities generally begin after funds are issued. Nevertheless, careful consideration of PSAD/SAD in the design can only result in beneficial results. Efforts should be taken at early stages to promote consistency between the conclusions of the NEPA assessment and the safety and health documentation.

DOE is presently "self-regulating" in the areas of industrial safety and occupational radiation protection. There is a possibility that during the development of the next accelerator

facility, DOE activities might become subject to "external" regulation in these areas, as well as in occupational radiation protection. It is difficult at this time to anticipate the form such external regulation might take or which agencies might be involved.

#### 5.3.7.3. *Occupational Safety During Construction*

The VLHC requires a large amount of tunneling in bedrock units, most of it horizontal or nearly so, and other tunnels with slopes. In addition to the safety requirements pertaining to construction activities, Federal regulations pertaining to underground operations (e.g., "mining" activities) come into play. Solutions to these issues are being developed to address challenges of this type encountered in the excavation for the NuMI project. These include the standard concerns about tunneling safety and material movement as the tunneling proceeds. Tunnel Boring Machines (TBMs) will be used for most of the tunnel. For some portions of the underground facility the drill and blast method will most economical. Both methods have associated occupational safety considerations. Provisions for emergency response including underground rescues will be needed. Egress issues relevant to protection of the construction workers will be of paramount importance.

It is clear that stringent measures must be taken to prevent flooding both during the construction period and thereafter. This problem must be addressed in harmony with the related environmental protection concerns (see Section 5.3.7.4). Downward slopes in the bedrock units will require attention to the prevention of uncontrolled movements of heavy objects downhill. While such control measures are well within those encountered in mining operations elsewhere, they are novel at accelerator laboratories.

During project construction, industrial radiography, a tool commonly used in general industry, is likely to be employed to assure the quality of pipe welds. Such radiographic operations, which typically use radioactive sources of high activity and relatively hazardous compared with the sources commonly used in particle physics experiments, would need to be conducted in compliance with the pertinent requirements of the State of Illinois in order to control the hazard to personnel. In the course of construction, other radiation-generating devices such as soil density gauges and media water-content probes might also need to be used. Standard procedures pertaining to such activities should be applied.

#### 5.3.7.4. *Environmental Protection During the Construction*

A small portion of the VLHC will be located near the surface, in the glacial till, while most of it will be located deep underground in various rock strata. For the portions near the surface, construction may proceed by cut and fill techniques similar to those employed to build most of the present facilities at Fermilab. Erosion control measures similar to those in practice for a number of years will be employed in accordance with good engineering practice and Federal and State regulations. Dust from any spoil piles must be kept under control. Likewise, a storm water management plan will need to be developed. Noise from construction activities is not expected to be significantly larger than that associated with normal civil construction activities in the vicinity of Fermilab. The NEPA process will result in a determination of the impact of the project on wetlands and or floodplains. It may be necessary for compensatory man-made wetlands to be created.

Tunneling in the bedrock units will result in the removal of a considerable volume of rock. The management of the spoil is a major issue that must be addressed and provisions for its proper stockpiling provided. In particular, concerns about dust may be more severe for this material, largely pulverized rock. The duration of this storage may be temporary for the spoil that is of marketable quality and longer for that reused at Fermilab or disposed. This should be carefully planned in accordance with Fermilab's longstanding tradition of placing high importance on aesthetic issues. The management of spoil materials will need especially vigorous attention off site. The placement of such a project in any aquifers results in the need to protect drinking water resources from contamination during construction. Also, the "de-watering" of tunnels, as the construction proceeds will require measures to prevent the depletion of wells and also to manage effectively any additional water discharges from this source.

The storm water management plan will need to take into account any releases of groundwater generated in the course of "de-watering" the tunnel. Careful hydrogeologic studies need to be performed to understand the interplay of the construction of the project with the various aquifers. This must be done to establish with certainty that the construction activities will not cause significant perturbations of the local individual and municipal water supplies. The exact depth of the various aquifers is not known in detail at all locations and accurate measurements will be needed. The results can be used to plan a strategy for preventing the tunnel from serving as a possible path of cross-contamination from one aquifer to another. During construction activities, precautions are needed to guarantee that spills of chemicals, including lubricants and fuels from the construction equipment, are captured before they enter the groundwater.

Tunneling activities can generate considerable noise and vibration. For blasting techniques, quantitative standards apply to the amplitude of the vibrations that are allowable at the surface. Noise exposure, both occupational and to the public at the site boundary and at off site locations will be an issue that needs to be addressed.

### 5.3.7.5. *Occupational Safety During the Operations*

#### A. *"Ordinary" Occupational Safety Hazards*

In this section, the focus is on the issues that have been successfully addressed before, at Fermilab and elsewhere by well-known techniques.

- The facility will use high current electrical circuits on a large scale. Present techniques in managing power distribution and providing means to effectively lock out supplies should be adequate to address the electrical hazard.
- Radio-Frequency (RF) generation and distribution equipment will be used extensively. Present techniques for controlling possible exposures to non-ionizing radiation should be sufficient.
- Large amounts of cables, transformers and electrical switchgear will be installed underground. Current methods for addressing fire protection concerns should be adequate.
- Long tunnels will be present. There is a need to adequately address Life Safety Code/fire protection issues to assure adequate provisions for egress and adequate means of prevention of and response to fires.

- There will be movements and alignment of large, heavy components. There is a need to include considerations in the design related to ease of movement of equipment to facilitate the prevention of injuries.

#### *B. Novel Occupational Safety Hazards*

This section is directed to those occupational safety hazards that are not generally encountered at accelerator facilities. These will require consideration in the early planning stages in order to be addressed in an efficient manner.

- The VLHC requires the extensive use of superconducting materials and cryogenics. While these technologies are relatively new, a number of accelerators worldwide have developed techniques adequate for addressing them. Provisions will need to be made for the safe release of cryogenics to the surface both during normal operations and in the event of quenches. Current accelerator facilities have developed mechanisms for using skilled engineers to independently review such systems for safety during the design and commissioning stages. The result has been the development of a number of standard engineering practices to mitigate both direct cryogenic hazards and the accompanying oxygen deficiency hazards (ODH).
- As during construction, the strong desire to minimize the number of exit points will render adequate design and engineering with respect to the Life Safety Code imperative. It is likely that special means of communication underground will need to be provided, "refuge" locations incorporated into the design, and adequate means of transport of personnel, both healthy and injured, to the surface established. These provisions will need to incorporate recommendations of a qualified fire protection professional at the time of the development of the conceptual design in order to assure adequate allowances for their costs. Later involvement of fire protection engineering will also be needed as the detailed design proceeds.

#### *5.3.7.6. Ionizing Radiation Safety During Operations*

##### *A. Prompt Radiation Shielding*

The siting of the VLHC deep underground will provide adequate passive shielding to attenuate prompt radiation to levels acceptable to the members of the public. The shielding of proton accelerators needs to attenuate the neutrons produced at large angles. At the forward angles, given the copious production of muons, and the increased importance of range-energy straggling at high energies [103], the shielding requirements must be well-understand at the earliest possible stage in the design and in the NEPA process.

Current Department of Energy requirements are not well matched to discussions of radiation fields that exist beyond the boundaries of DOE sites. DOE has specified the annual limits on the radiation dose equivalent that can be received by occupational workers and members of the public (see Regulation 10 CFR 835) [101,104]. These limits, in all situations expressed to date, pertain to the dose equivalent delivered to people or to locations where people could reasonably be. For individual members of the public, the primary limit is 100 mrem (1 mSv) in a year, not including man-made, medical, or enhanced natural radioactivity. Special reporting requirements apply when the annual dose equivalent received by an individual exceeds 10 mrem (0.1 mSv) in a year. DOE has expressed the view that non-occupational annual doses to

members of the public are not expected to exceed a few mrem in a year. In light of public concerns about radiation exposures, any new facility should be designed to keep the dose that could be reasonably received by actual members of the public to as small a value as possible.

*B. Residual Radioactivity of Components*

In the high-energy region, most, but not all, of the radiation effects scale roughly with the beam power. In particular the effects of high residual activity levels should be carefully taken into account at early stages of design of beam cleaning and abort systems and other locations of possible high beam loss. Doses that might be received by workers are an important subject that must be assessed as a part of the NEPA process. The need to minimize the generation of radioactive wastes and to eliminate the creation of wastes that contain materials that are toxic or hazardous, and which contain radioactive waste, is an important concern.

*C. Airborne Radioactivity*

Federal Regulations promulgated by the USEPA have established an annual limit on dose equivalent of 10 mrem (100  $\mu$ Sv) to any member of the public that can be received as a result of operations of DOE facilities such as accelerators [105]. Further, the same regulations impose stringent continuous monitoring requirements if the annual dose equivalent to any member of the public is to exceed 0.1 mrem (1  $\mu$ Sv) in one year. In addition, if the level of 0.1 mrem in one year is to be exceeded, then an application for approval to construct and a notification of startup must both, in proper sequence, be submitted to the USEPA. Given the extent of the VLHC beyond the present boundaries of the Fermilab site, careful attention must be paid to the production of airborne radioactivity.

*D. Radioactivity in Soil and Groundwater*

The VLHC siting requires that the production of radioactivity in hydrogeologic units be given careful attention. Before the exact footprint of any chosen facility is irrevocably determined, detailed hydrogeologic studies should be conducted to determine the relevant parameters precisely, as they are known to vary significant in the vicinity of the Fermilab site. It is clear that protection of groundwater against contamination with radioactivity merits early, detailed attention in project design to assure satisfaction of likely public concerns. It may well be that the most prudent choice of design objectives might be far below present regulatory standards for drinking water.

*5.3.7.7. Non-Radiological Environmental Protection Issues  
During Operations*

Operations of the facility should be planned in a way that incorporates proper measures to control the generation of non-radioactive wastes. Further, there is a need to address potential spills of hazardous or toxic materials in a way that fully protects members of the public and of environmental resources. The detailed attention to these issues will be required as part of the NEPA process and the designs should provide information of the quality needed to support all required permit applications to State and Federal environmental regulatory agencies. In any enclosures located deep underground the cross-contamination of the various aquifers must be

prevented and any de-watering operations must assure that local community or individual drinking water supplies are not perturbed.

### 5.3.7.8. *Summary*

The construction and operation of the VLHC present a number of ES&H challenges. Many of these have been encountered, and effectively addressed, at other accelerator facilities. Some of the problems are common to other recent projects undertaken at Fermilab and elsewhere that have resulted in the need to develop new methods to address them. Given the scale of the VLHC some of these issues may have a greater importance than found in the present experience. With adequate planning in the design stages, these problems can be adequately addressed in a manner that merits the support of the Laboratory, the Department of Energy, and the public.

## References

- [1] R.R. Wilson, Proceedings of Snowmass 1982.
- [2] E. Malamud, ed., "The Pipetron: a Low-Field Approach to a Very Large Hadron Collider," Snowmass '96 (a.k.a. pink book).
- [3] G.W. Foster, "Transmission Line Magnet Status Report," VLHC Information Packet for HEPAP Subpanel, Fermilab 1998.
- [4] G.W. Foster, V.S. Kashikhin, E. Malamud, P. Mazur, H. Piekarz, J. Fuerst, R. Rabehl, P. Schlabach, J. Volk, "The 100 kA VLHC Transmission Line Magnet Superconducting Cable Test Facility," MT-16, *IEEE Trans. of Applied Superconductivity*, Vol.10, No.1, March 2000, pp.318-321.
- [5] R. Walker, "50 m Invar Thermal Cycling Report," TD-01-037, 2001.
- [6] N. Shatil, "Quench Simulation of VLHC Transmission Line Magnet (Final Report)," TD-01-025, 2001.
- [7] J. DiMarco, G.W. Foster, V. Kashikhin, A. Makarov, P. Schlabach, "Measurements of a Crenellated Iron Pole Tip for the VLHC Transmission Line Magnet," PAC 99, pp. 3327 – 3329.
- [8] G.W. Foster, V.S. Kashikhin, I. Novitski, "Design of a 2 Tesla Transmission Line Magnet for the VLHC," MT-16, *IEEE Trans. of Applied Superconductivity*, Vol.10, No.1, March 2000, pp.202-205.
- [9] G.W. Foster, V.S. Kashikhin, V.V. Kashikhin, "Pole Profile Optimization of VLHC Transmission Line Magnet," EPAC 98.
- [10] G.W. Foster, "Experience with Permanent Magnets in the 8-GeV Line and the Recycler Ring," EPAC '98.
- [11] V.S. Kashikhin, "Corrector wires in holes-in-the-poles for transmission line magnets," TD-01-038, 2001.
- [12] V. Tsvetkov, "Transmission Line Magnet Mechanics," TD-01-039, 2001.
- [13] V. Tsvetkov, "Alignment of the Transmission Line Magnet in the tunnel," TD-01-040, 2001.
- [14] V.S. Kashikhin, "Mechanical model 2 test results," TD-01-041, 2001.
- [15] V.S. Kashikhin, "Transmission Line Magnet for VLHC. Magnetic Forces and Magnet Deflection," TD-01-042, 2001.
- [16] M. McAshan, "Cryogenic System for the 3 TeV Injector Study," Fermilab VLHCPUB-87,1997.
- [17] ULTEM 2300 is a 40% glass-filled polyetherimide marketed by GE plastics. It was developed for use in SSC quadrupole support posts at BNL. See J. Sondericker et al., *Advances in Cryogenic Engineering*, Vol. 40, pp. 1099-1105, Plenum Press, New York (1994).
- [18] G.W. Foster, "Mechanical Load Cycling Tests of the Transmission Line Spiders," TD-01-043, 2001.
- [19] I. Novitski, "Analysis of the spider support," TD-01-044, 2001.
- [20] E.C. Quimby et al., "VJR/VJRR Design, Construction, Installation, and Performance," *ACE*, vol. 43, New York, 1998.

- [21] G. Grygiel et al., "Status of the TTF Cryogenic System," *ACE* vol.41, New York, 1996.
- [22] K. Hosoyama et al., "Development of a High Performance Transfer Line System," *ACE* vol. 45, 2000.
- [23] M. Chorowski, "Risk analysis of the LHC cryogenic system," *ACE* 2000.
- [24] V. Parma et al., "The Insulation Vacuum Barrier for the Large Hadron Collider Magnet Cryostats," ICEC 18.
- [25] B. Jenny et al., "A Composite Vacuum Barrier for the LHC Short Straight Section," *ACE* vol.41, New York 1996.
- [26] "Technical Specification for a Compound Cryogenic Helium Distribution Line for the Large Hadron Collider (LHC)," IT-2399/lhc/lhc, Geneva, Switzerland, December 1997.
- [27] R.C. Niemann, "Model SSC Dipole Magnet Cryostat Assembly at Fermilab," Supercollider 1, New York 1989.
- [28] N. Andreev, "Compact superconducting correctors with cold ferromagnetic screens," TD-01-046, 2001.
- [29] G. Ambrosio et al., "Preliminary Proposal of a Nb<sub>3</sub>Sn Quadruple Model for the Low-Beta Insertions of the LHC," INFN Report, INFN/TC-95/25, Sept. 13, 1995.
- [30] R. Scanlan, "Conductor Development Program," Low Temperature Superconducting Workshop, Santa Rosa, CA, Nov. 8-10, 2000.
- [31] M. Canali, L. Rossi, "DYNQUE: a computer code for quench simulation in adiabatic multicoin superconducting solenoids," INFN Report, INFN/TC-93/06, 1993.
- [32] L. Imbasciati, G. Ambrosio, P. Bauer, V. Kashikhin, A. Zlobin, "Quench Protection of the Common Coil Racetrack (CCRT-1): Results of Adiabatic Model Calculations," TD-00-056, FNAL (Sept. 2000).
- [33] G. Ambrosio, G. Bellomo and L. Rossi, "A 300 T/m Nb<sub>3</sub>Sn Quadrupole for the Low-beta Insertions of the LHC," *Proc. of EPAC96*, Sitges (Barcelona), p. 2290.
- [34] Nikolai Mokhov, private communication.
- [35] Bill Turner, private communication.
- [36] V.V. Kashikhin, I. Terechkine, "Superconducting straight section quadrupole magnet for low-field VLHC," FNAL, TD-01-008, Feb. 2001.
- [37] Conceptual Design of the Superconducting Super Collider. SSC-SR-2020, DE93 007234.
- [38] J. Volk, "Injection transfer line magnets," TD Note TD-01-027, FNAL, 2001.
- [39] J. Carson, R. Bossert, "A Proposed Production Procedure for Stage 1 Transmission Line Magnets," TD-01-028, 2001.
- [40] J. Carson, R. Bossert, "Throughput for Stage 1 Transmission Line Factory," TD-01-029, 2001.
- [41] P. Schlabach, "Magnetic Measurements During Production of VLHC Low Field Combined Function Magnets," TD-01-007, 2001.
- [42] G. Ganetis et al., "Field Measuring Probe for SSC Magnets," Particle Accelerator Conference, 1987.
- [43] L. Walkiers, "Measurements for the Acceptance Tests of the LHC Superconducting Magnets," Eleventh International Magnet Measurement Workshop, 1999.
- [44] Brown & Root, Installation & Transport Proposal for the SSC.
- [45] Supply of Cryo-Magnet Transport Vehicles and Unloading Equipment for the LHC Tunnel, LHC-HMU-CI-0001.
- [46] An example of a commercial safety rail can be found at <http://www.vahleinc.com/pdf/Catalog4C.pdf>.
- [47] Examples of tram systems and drive components operating in this voltage range can be found at [http://w4.siemens.de/ts/products\\_solutions/light\\_rail\\_tram](http://w4.siemens.de/ts/products_solutions/light_rail_tram).
- [48] G.W. Foster, PAC 2001 invited talk.
- [49] S. Hays, "100 kA Power Supply Options for the VLHC," TD-01-047, 2001.
- [50] H. Piekarz et al., "Summary of Transmission Line Magnet R&D Activities at MS-6," TD-01-048, 2001.
- [51] G.W. Foster, S. Hays, H. Pfeffer, "Design of a Compact 100 kA Switching Power Supply for Superconducting Magnet Tests," TD-01-045, 2001.

- [52] J. G. Weisand (ed.), *Handbook of Cryogenic Engineering*, p. 411.
- [53] K. Koepke, P. Mazur, A. Zlobin, Snowmass '96.
- [54] G.W. Foster, H. Piekarz, "Quench Protection of the Transmission Line Magnet," TD-01-049, 2001.
- [55] Switch wire is used on persistent-current MRI magnets. Commercial sources include SW-18 and SW-1 from Supercon Inc, Shrewsbury, MA, and Oxford Instruments, [www.oxinst.com](http://www.oxinst.com).
- [56] See the LHC PAC '99 papers. See also the proceeding of the workshop on powering the LHC, <http://lhcp.web.cern.ch/lhcp/TCC/PLANNING/TCC/Power2000/welcome.htm>.
- [57] I. Terechkine, "LCW and power summary for the VLHC-1 Straight Sections," TD-01-050, 2001.
- [58] Fermilab Main Injector Technical Design Report, Table 3.9.1.
- [59] Typical laptop computers have heat pipes in them. See <http://www.thermacore.com/papers.htm>.
- [60] Auto-resetting fuses are sold (for example) by: <http://www.circuitprotection.com>.
- [61] Specifications quoted are single-quadrant DC-DC converters from Vicor, Inc. [www.vicor.com](http://www.vicor.com).
- [62] Fermilab Main Injector Note MI-75.
- [63] Medvenko & Smith, Beam Instrumentation Workshop 2000, p.503.
- [64] Specifications quoted are from <http://products.analog.com/products/info.asp?product=AD9203>.
- [65] W. Turner, "Beam Tube Vacuum in Low Field and High Field Very Large Hadron Collider," LBNL-39482, UC414, presented at the Snowmass Conference, CO, October 1996.
- [66] M. Pivi and W.C. Turner, "Beam Tube Vacuum in a Very Large Hadron Collider Stage 1," Version 2.1, 12 April 2001.
- [67] J. Gomez-Goni, O. Gröbner and A.G. Mathewson, "Exposure of a baked Al lined stainless steel chamber to photons," CERN, Vacuum Technical Note 94-10 pg. 9, AT-VA/JGG.
- [68] C. Benvenuti, "Molecular Surface pumping: the getter pumps," CAS CERN Accelerator School - Vacuum Technology, CERN Yellow Book, pg. 48.
- [69] J.C. Billy, J.P. Bojon, O. Gröbner, N. Hilleret, M. Jimenez, I. Laugier, P. Strubin, "The LEP Vacuum System: a Summary of 10 Years of Successful Operation," Proc. EPAC 2000.
- [70] G.P. Jackson, ed., "The Fermilab Recycler Technical Design Report", FNAL-TM-1991.
- [71] I. Novitski, "Vacuum pipe stresses in the low field VLHC", TD-01-051, 2001.
- [72] A. Chao and M. Tigner, *Handbook of Accelerator Physics and Engineering*, pg.225.
- [73] Oswald Gröbner pvt. comm.
- [74] A. Gambitta et al., "Experience with Aluminum Vacuum Chambers at ELETTRA," EPAC 2000, Vienna, Austria; and J. Miertusova et al., "How to Save Money Designing a Vacuum System for a Third Generation Synchrotron Light Source," EPAC 1996.
- [75] Bob Goodwin, Peter Lucas, Elliott McCrory and Mike Shea, "Thoughts on Controls/Instrumentation for 3 TeV booster/VLHC," <http://fnalpubs.fnal.gov/archive/vlhc/VLHCPub-14.html>, July 1997.
- [76] V. Shiltsev, "Summary of the Working Group II: RF, Instabilities and Feedback Systems," VLHC Accelerator Technology Workshop, TJNAF, Feb.1999. [http://www.vlhc.org/tjef/wg2\\_summary.pdf](http://www.vlhc.org/tjef/wg2_summary.pdf).
- [77] A. Jackson, contribution to the VLHC Design Study, unpublished.
- [78] The LHC Study Group, "The Large Hadron Collider – Conceptual Design Report," CERN/AC/95-05 (LHC),1995.
- [79] D. Boussard and T. Linnecar, "The LHC Superconducting RF System," *Proceedings of the 1999 Cryogenic Engineering and International Cryogenic Material Conference (CEC-ICM'99)*, 12-16 July 1999, Montreal, Canada.
- [80] P. Brown et al., "Performance of the LEP200 Superconducting RF System," *Proceedings of the 9th Workshop on RF Superconductivity*, 1-5 November 1999, Santa Fe, NM, USA.
- [81] P. Bosland et al., "Completion of the SOLEIL Cryomodule," *Proceedings of the 9th Workshop on RF Superconductivity*, 1-5 November 1999, Santa Fe, NM, USA.

- [82] D. Boussard, "RF Power Requirements for a High Intensity Proton Collider," *Proceedings of the 1991 Particle Accelerator Conference*, pp. 2447-2449.
- [83] H. Frischholz, W.R. Fowkes and C. Pearson, "Design and Construction of a 500 kW CW, 400 MHz Klystron to be Used as RF Power Source for LHC/RF Component Tests," *Proceedings of the 1997 Particle Accelerator Conference*, pp. 2911-2913.
- [84] H. Padamsee, "SRF for Muon Colliders," *Proceedings of the 9th Workshop on RF Superconductivity*, 1-5 November 1999, Santa Fe, NM, USA.
- [85] G. Lambertson, "Active feedback systems for Stage-1 VLHC," TD-01-052, 2001.
- [86] N.V. Mokhov and W. Chou, ed., "Beam Halo and Scraping," *Proc. of ICFA Workshop*, Lake Como, Wisconsin (1999).
- [87] Bryant & Johnsen, *Circular Accelerators and Storage Rings*, p. 308.
- [88] A.I. Drozhdin and N.V. Mokhov, "Energy Deposition Issues in the Very Large Hadron Collider," Workshop on VLHC, Fontana, Wisconsin, February 22-25, 1999.
- [89] A.I. Drozhdin, N.V. Mokhov, C.T. Murphy, S. Pruss, "Beam Abort For a 50X50 TeV Hadron Collider", <http://fnalpubs.fnal.gov/archive/vlhc/VLHCPub-51.ps>.
- [90] I.S. Baishev, A.I. Drozhdin, N.V. Mokhov, B. Parker, R.D. Richardson, J. Zhou, "Dealing with Abort Kicker Prefire in the Superconducting Super Collider," PAC 93, Washington, DC, May 1993.
- [91] *The Large Hadron Collider*, Conceptual Design, CERN/AC/95-05(LHC) October 20, 1995.
- [92] D.C. Wilson, C.A. Wingate, J.C. Goldstein, R.P. Godwin, N.V. Mokhov, "Hydrodynamic Calculations of 20-TeV Beam Interactions with the SSC BEAM Dump," *Proc. of IEEE Particle Accelerator Conference*, p. 3090. (1993). A legendary SSC video contains a visualization of the extracted SSC beam drilling a hole in the absorber block when the sweeping magnet system fails.
- [93] N. Mokhov, pvt. comm.
- [94] R. Yarema, pvt. comm.
- [95] LHC Talk at Beam Instrumentation Workshop '00.
- [96] S. Hunt, S. Crivello, N. Mokhov, "Radiation Effects on Optical Fiber Links at the SSC," *Nucl. Instr. Meth. in Phys. Research*, **A352** (1994) 329-243.
- [97] A.I. Drozhdin and N.V. Mokhov, "The VLHC Beam Collimation System," TD-01-053, 2001.
- [98] A.I. Drozhdin, N.V. Mokhov and A.A. Sery, "The Very Large Hadron Collider Beam Collimation System," Workshop on VLHC, Fontana, Wisconsin, February 22-25, 1999.
- [99] N.V. Mokhov and J.B. Strait, "Towards the Optimal LHC Interaction Region: Beam-Induced Energy Deposition," *Proc. of IEEE Particle Accelerator Conference*, p. 124 (1997).
- [100] Electron Beam Tunnel Boring papers from LBL, circa 1975.
- [101] "Fermilab Work Smart Standards Set," Fermi National Accelerator Laboratory, <http://www-lib.fnal.gov/library/protect/worksmart.html>, November 15, 1999.
- [102] *United States Code of Federal Regulations, Title 10, Part 1021*, "Department of Energy National Environmental Policy Act Implementation Procedures," 1997.
- [103] A. Van Ginneken, P. Yurista, and C. Yamaguchi, "Shielding calculations for multi-TeV hadron colliders," Fermilab Report FN-447 (1987).
- [104] U. S. Department of Energy, "Radiation Protection of the Public and the Environment," DOE Order 5400.5, January 7, 1993.
- [105] *United States Code of Federal Regulations, Title 40, Part 61, Subpart H*, "National Emissions Standard for Hazardous Air Pollutants (NESHAP) for the Emission of Radionuclides other than Radon from Department of Energy Facilities," 1989.